NAS12-567

Final Technical Report

STUDY OF A MULTIPATH REJECTION TECHNIQUE APPLIED TO AIRCRAFT NAVIGATION BY SATELLITE

By R. Wachsman, H. Salwen, L. Klein, and R. Zaorski

15 March 1969

Prepared under Contract NAS12-567

for

National Aeronautics and Space Administration
Electronics Research Center
GS/Guidance Laboratory
Cambridge, Massachusetts 02139

ADVANCED COMMUNICATIONS INFORMATION MANAGEMENT

RESEARCH • DEVELOPMENT • ENGINEERING

ADCOM

A TELEDYNE COMPANY

Final Technical Report

STUDY OF A MULTIPATH REJECTION TECHNIQUE APPLIED TO AIRCRAFT NAVIGATION BY SATELLITE

By R. Wachsman, H. Salwen
L. Klein, and R. Zaorski

15 March 1969

Prepared under Contract NAS12-567 by

ADCOM
A Teledyne Company
Cambridge, Massachusetts 02139

For

National Aeronautics & Space Administration
Electronics Research Center
GS/Guidance Laboratory
Cambridge, Massachusetts 02139

G-106F

TABLE OF CONTENTS

TABLE OF CONTENTS (Continued)

TABLE OF CONTENTS (Continued)

TABLE OF CONTENTS (Continued)

LIST OF ILLUSTRATIONS

LIST OF ILLUSTRATION (Continued)

LIST OF TABLES

1. INTRODUCTION

This document constitutes the Final Report prepared by ADCOM, a Teledyne Company, for NASA Electronics Research Center, Cambridge, Massachusetts, under contract NAS12-567. The report presents work performed by ADCOM during the period 15 May 1968 to 15 February 1969.

1.1 Object of the Program

The object of the program conducted during the period 15 May 1968 to 15 February 1969 was to investigate the effects of multipath interference on a NAV/SAT ranging receiver for the case where the range modulation signal consists of a BINOR ranging code directly phase modulating a 1.6 GHz carrier, and to design an alternate ranging modulation and receiver which is capable of improved (and optimized) performance. Finally, the suitability of the steerable null technique developed during Part I of this contract (and reported in the Interim-Scientific Report dated April 15, 1968) to multipath rejection in the 1.6 GHz multipath channel was to be investigated. In particular, the following tasks were specified:

Task I - Modify the multipath channel characterization for application to satellite-to-aircraft links operating at 1540 - 1660 MHz. Diffuse scattering of the multipath return and the effect of L-band antenna characteristics shall be included.

Task II - Refine the performance analysis of BINOR code acquisition and ranging to include the effects of carrier and clock jitter and the presence of multipath on acquisition speed and ranging accuracy.

Task III - a. Design a signal for NAV/SAT application which is optimized with respect to acquisition speed, ranging accuracy, performance in the presence of multipath, hardware complexity and reliability.

b. The basic format of the signal is a carrier (1.6 GHz) which is phase modulated by a subcarrier (320 kHz) which, in turn, is modulated by the sum or hard limited sum (BINOR) of range ambiguity resolving square waves.

c. The parameters to be optimized are: deviation of the subcarrier on the carrier; method of modulation and modulation index for the combined range ambiguity resolving square waves; ratios among square wave frequencies; and the method of combining the square waves.

Task IV - Design a receiver for reception and demodulation of the signal derived in Task III. Perform a digital computer simulation of a phase model of the receiver reception process to verify the optimization procedure of Task III, to demonstrate feasibility of the receiver, and to establish a trade-off between hardware complexity and system performance.

Task V - Modify the multipath rejection technique and simulator constructed under Item 2 so that it represents the multipath channel in the 1540-1660 MHz region and employs the signal process derived under Task III.

1.2 Organization of the Report and Summary of Results

The organization of the report follows the order of the task statements presented above.

Section 2 treats the problem of characterizing the multipath channel in the 1.6 GHz NAV/SAT link. This problem has been conveniently divided into three parts, which are:

1) The physics and geometry of multipath scattering at 1.6 GHz off the ocean in the NAV/SAT link.

2) Characterization of the received multipath signal including definitions of, and bounds on, the multipath signal parameters.

3) L-band Antenna characterization in order to estimate the minimum antenna multipath-suppression factor that can be obtained for grazing angles near 10^{o}.

The physics and geometry of the multipath scattering in the NAV/SAT link are discussed and the characteristics of the multipath interference for both specular and diffuse scattering are presented as well as the conditions under which each prevails. These characteristics include the relative received multipath power, the relative specular multipath time delay and the time delay spread for diffuse multipath, the relative specular multipath carrier doppler frequency, the fading bandwidth of the received diffuse multipath signal, the angles of arrival of the direct-path and multipath signals, and the size of the scattering region for pure specular and pure diffuse scattering. In addition, the direct-path carrier doppler frequency is computed. An interesting phenomenon concerning the dependence of the relative specular multipath carrier doppler frequency on aircraft altitude fluctuations is also discussed. The effects of these small unavoidable altitude fluctuations is shown to predominate over the effects of the horizontal aircraft motion under certain frequently encountered conditions. This fact has apparently been overlooked by some investigators. A discussion of the validity of certain results for diffuse scattering which have appeared in the literature is also presented.

The received multipath signal is expressed in a form which is both suitable for computing its effects on the performance of the NAV-SAT receiver and which contains all the essential characteristics derived from the physics and geometry considerations.

Finally, the characteristics of aircraft-mounted L-band antennas is presented. Envisioned for the NAV/SAT application are three antennas. One on the top of the aircraft for communicating with satellites at high elevation angles, and two side-mounted antennas (one on each side of the aircraft) for communicating with satellites at low elevation angles. What is desired for the side-mounted antennas is a relative multipath suppression of at least 6 dB for even the lowest grazing angles which are being considered (i. e., 10^{o}) and including a possible aircraft roll or banking angle of up to 10^{o}.

The analysis of the BINOR acquisition and ranging is refined in Section 3, to include the effects of carrier and clock jitter and the presence of multipath on acquisition speed and ranging accuracy in the proposed NAV/SAT ranging system.

To this end, calculations for the probability of correct acquisition of the BINOR code are made for three cases. In each subsequent case additional factors are included in the calculation. The three cases are:

a) Case where effects of multipath, carrier and clock loop phase jitter, and video filtering of the BINOR code in the receiver are neglected.

b) Case where effects of multipath are neglected but effects of carrier and clock loop phase jitter, and video filtering of the BINOR code in the receiver are included.

c) Case where multipath effects as well as the other effects are included.

The third case is, of course, the most complex, and is best understood in terms of the modifications required in the results of the first two cases.

From the analyses conducted in Section 3, the following conclusions are drawn:

1) The presence of a small multipath interference will not cause a drastic reduction in the total probability of correct BINOR acquisition if

a) at least a 6 dB aircraft antenna discrimination against the multipath is maintained

b) aircraft speeds are on the order of 600 mph or more so that the frequency spreading of the diffuse multipath component is on the order of 50 Hz or more

c) the grazing angle exceeds 10^{o} and the rms displacement of the sea surface exceeds 10 cm, so that the average relative specular multipath power is no larger than approximately 0. 065.

For the vast majority of the time the grazing angle exceeds 20° and the aircraft antenna multipath discrimination exceeds 6 dB. The specular multipath component is then negligible, and the frequency spreading of the diffuse multipath component is more on the order of 100 to 200 Hz. The effects of the multipath in this case becomes almost entirely negligible during BINOR acquisition.

For grazing angles close to 10°, specular multipath may become a problem for calm seas at 1.6 GHz. However, the probability of correct BINOR acquisition is still on the order of 98% on the average for $\ell = 5$. Analyses of additional worst-case possibilities that may occur in the presence of specular multipath indicate that it is very unlikely that the probability of correct BINOR acquisition (with $\ell = 4$) will fall below 95% at the worst-case SNR used in all of the calculations.

Ranging accuracy is shown to be a function of the rms phase jitter in the clock loop. This phase jitter is shown to result from the presence of Gaussian noise and multipath components in the loop noise bandwidth. During the ranging measurement, in the present system, the multipath becomes an important consideration. This is so because the BINOR is removed and only square-wave clock is transmitted. This increases the signal and multipath powers in the clock loop to the point where the multipath, rather than the noise, becomes the limiting factor. This appears to be especially true when specular multipath is present. However, the differential doppler offset between the direct-path and multipath carrier frequencies may be sufficiently high compared to the clock loop noise bandwidth to cause considerable suppression of the specular multipath clock component. This would substantially reduce the limiting effects of the specular multipath component on ranging accuracy. The diffuse multipath component causes an increase in rms range error of approximately 50% over that caused by front-end noise alone. The effect of the diffuse component is reduced only when the fading bandwidth is much smaller than the differential doppler which is unlikely in the present application.

In Section 4, the optimum modulation and receiver design problem is presented. The discussion begins with an investigation of the possible modulation methods by which the ambiguity resolving square waves may be applied to the 320 kHz subcarrier. Low deviation PM is selected. Then the optimum method for encoding these square waves is considered. The BINOR technique (hard limited sum of square waves) is rejected in favor of a simple sum of square waves. Optimum deviations for the square waves on the subcarrier and the subcarrier on to the carrier are selected. Then, a description of the ambiguity resolving procedure is presented. The discussion concludes with a hardware design exercise. This effort results in a detailed block diagram of a range data demodulation and measurement system appropriate to the optimized ranging modulation.

The ranging modulation which has been designed for NAV/SAT applications provides the following characteristics:

1) No sequencing is required at the satellite transmitter. All modulation functions are carried simultaneously.

2) Signal format provides for convenient generation at the satellite.

3) Ranging accuracy on the order of 10 ft.

4) 99.9% prob. of correct amb. resolution in 1 sec.

5) Carrier suppression of only 2 dB by modulation.

6) Carrier and clock jitter have negligible effect on ambiguity resolution process.

7) Improved performance in the presence of diffuse multipath because all data is averaged over the entire acquisition interval.

8) Receiver demodulator complexity comparable to that required for the BINOR (when range measurement phase meter and system reference generator are included in the comparison).

9) Receiver hardware lends itself readily to medium or large-scale integration.

and finally,

10) The signal format can provide simultaneous data transmission capability employing straightforward communication transmission and reception concepts and implementations.

These characteristics are desirable for the NAV/SAT application. It is therefore recommended that the modulation technique be given further consideration. In particular, modulation deviations may be readjusted to reduce ranging accuracy (which is 3 times better than required) in trade for shorter acquisition time and/or higher probability of acquisition and/or higher carrier component power. It is noted, however, that these alterations are not necessary for successful implementation of the modulation technique. Further analysis of the demodulation and measurement technique will yield improvements in implementation beyond those presented in the section. Again, it is noted that the complexity of the implementation presented is on a par with other proposed systems. It is further recommended that the communication capabilities of the signal format be investigated in more detail to determine the optimum modulation method and maximum data rate capability.

A digital computer simulation of the receiver digital-divide-down carrier acquisition aiding PLL is presented in Section 5. Analysis of the signal format derived in Task III and the corresponding demodulator permitted optimization of the signal modulation parameters to be achieved without the aid of computer simulation. However, it became apparent that the time required for carrier acquisition in the present NAV/SAT receiver configuration represented a serious drawback on overall acquisition speed. Consequently, a digital-divide-down carrier acquisition aiding PLL was proposed as a technique for reducing this contribution to the overall acquisition time. The difficulties involved in analyzing the operation of this acquisition aiding PLL at low input SNR led naturally to the use of digital computer simulation as an

aid in the design of this loop. The results of this analysis indicated that a first order loop performs better in the acquisition mode than a second order loop. Criteria for the selection of the digital-divide-down ratio and the loop gain were developed in terms of the expected maximum carrier frequency offset and the expected minimum SNR. Acquisition times on the order of 10 milliseconds or less were consistently obtained in the computer simulation for input SNR down to -10 dB in a 20 kHz IF bandpass filter. It was also found that the loop would acquire for input SNR's down to -30 dB.

Finally, in Section 6, the feasibility of steerable null control for the rejection of diffuse multipath is investigated. A simulation experiment was also performed to investigate the ability of the steerable null control system to reduce the effects of coherently fading diffuse multipath interference. ADCOM's conclusions concerning the effectiveness of the steerable null control system for combatting multipath interference at 1.6 GHz in a NAV/SAT applications are summarized as follows:

1) Since diffuse multipath interference arises from scattering off a much larger area of the sea surface than for the case of specular scattering, the multipath interference in the diffuse case arrives at the aircraft from a range of different directions centered on the specular direction. Consequently, placing a sharp null in the direction of the specular point will not eliminate all of the multipath interference. In addition, slight variations of antenna gains with directions of arrival of the diffuse multipath components will preclude the possibility of achieving the required amplitude gain balancing necessary for achieving a true null. At best, only the coherently fading diffuse multipath component can be nulled, with the incoherently fading diffuse multipath interference being simply reduced somewhat.

2) The presence of incoherently fading diffuse multipath interference interferes with proper operation of the steerable null control system and may prevent the null from being placed on the direction of arrival of the coherently fading diffuse multipath component.

3) Steerable null control at 1.6 GHz does not work as well at low grazing angles as at intermediate grazing angles (i.e., around 30^{o}), even for the case of specular scattering. For the 1.6 GHz NAV/SAT channel grazing angles as low as 10^{o} are being considered.

4) Steerable null control may not be needed at 1.6 GHz, since antennas can be built at these frequencies which may adequately discriminate against the multipath if the angular separation between the directions of arrival of the direct path and multipath signals at the aircraft is greater than about 20^{o}.

A modification of the steerable null simulator (constructed previously under this contract) was made to simulate the randomly fluctuating carrier phase of a coherently fading diffuse multipath component. The results indicated that the steerable null system could work well under such circumstances in that the rapidly fluctuating multipath carrier phase prevented the phase of the multipath carrier from dwelling too long in a region where operation of the steerable null control system became ineffective.

Since the steerable null system would not be used for the situation where incoherently fading diffuse multipath interference was dominant, the simulator was not modified to simulate this kind of multipath interference. Such an effort could not be justified in light of the theoretical considerations itemized above. These considerations are based on the results derived and presented in Section 2 of this report concerning the characteristics of multipath at 1.6 GHz.

2. MULTIPATH CHANNEL CHARACTERIZATION

2.1 Summary

The problem of characterizing the multipath channel in the 1.6 GHz NAV/SAT link is conveniently divided into three parts. These are:

1) The physics and geometry of multipath scattering at 1.6 GHz off the ocean in the NAV/SAT link.

2) Characterization of the received multipath signal including definitions of, and bounds on, the multipath signal parameters.

3) L-band Antenna characterization in order to estimate the minimum antenna multipath-suppression factor that can be obtained for grazing angles near 10°.

The physics and geometry of the multipath scattering in the NAV/SAT link are discussed in Section 2.2. The characteristics of the multipath interference for both specular and diffuse scattering are presented as well as the conditions under which each prevails. These characteristics include the relative received multipath power, the relative specular multipath time delay and the time delay spread for diffuse multipath, the relative specular multipath carrier doppler frequency, the fading bandwidth of the received diffuse multipath signal, the angles of arrival of the direct-path and multipath signals, and the size of the scattering region for pure specular and pure diffuse scattering. In addition, the direct-path carrier doppler frequency is computed. An interesting phenomenon concerning the dependence of the relative specular multipath carrier doppler frequency on aircraft altitude fluctuations is also discussed. The effects of these small unavoidable altitude fluctuations is shown to predominate over the effects of the horizontal aircraft motion under certain frequently encountered conditions. This fact has apparently been overlooked by some investigators. A discussion of the validity of certain results for diffuse scattering which have appeared in the literature is also presented.

The characterization of the received multipath signal is discussed in Section 2.3. The received multipath signal is expressed in a form which is both suitable for computing its effects on the performance of the NAV/SAT receiver and which contains all the essential characteristics derived from the physics and geometry considerations.

Finally, the characteristics of aircraft-mounted L-band antennas is presented. Envisioned for the NAV/SAT application are three antennas. One on the top of the aircraft for communicating with satellites at high elevation angles, and two side-mounted antennas (one on each side of the aircraft) for communicating with satellites at low elevation angles. What is desired for the side-mounted antennas is a relative multipath suppression

of at least 6 dB for even the lowest grazing angles which are being considered (i.e., 10^{o}) and including a possible aircraft roll or banking angle of up to 10^{o}.

2.2 Physics and Geometry of Multipath Scattering in the NAV/SAT Link

2.2.1 Scattering Geometry of the NAV/SAT Link

The geometry of the NAV/SAT configuration is shown in Fig. 1. For the case of specular scattering there is a single multipath ray as indicated. The ray which reaches the airplane P from the satellite S is the one which scatters off the earth at point M. At point M, the angle of incidence equals the angle of reflection. This point is referred to as the "specular point". The size of the "specular point" is equal essentially to the area of the first Fresnel zone. The concept of the first Fresnel zone is useful for situations in which it is small in size compared to the distances from it to the observer and from it to the source, and for which the source illuminates the first Fresnel zone uniformly. This is the case for the NAV/SAT application.

When the scattering off the ocean is diffuse, the airplane P receives multipath radiation from the satellite S which has been scattered off the ocean from an area centered approximately at the specular point M and which is considerably larger than the first Fresnel zone. The sizes of the first Fresnel zone and the diffuse scattering region will be estimated, for grazing angles between 10° and 20°, in Section **2.2.2.5.**

From the geometry of Fig. 1 several important parameters of the multipath channel may be defined and calculated approximately as functions of the aircraft altitude, h, and the angle, α, subtended between the aircraft and the satellite as measured from the earth center. This angle α may in turn be determined from the latitude and longitude separations between the aircraft and satellite by the spherical trigonometric relationship

$$\cos \alpha = \cos \Delta\alpha_{\text{long.}} \cos \Delta\alpha_{\text{lat.}} \qquad (1)$$

This is further illustrated by Fig. 2.

The multipath channel parameters of interest here are:

1) The relative specular multipath time delay, τ_{ms}, given by

$$\tau_{ms} = \frac{1}{c} (R_m - R_d) \qquad (2)$$

where c is the velocity of light, and R_m and R_d are the path lengths of the multipath and the direct path respectively.

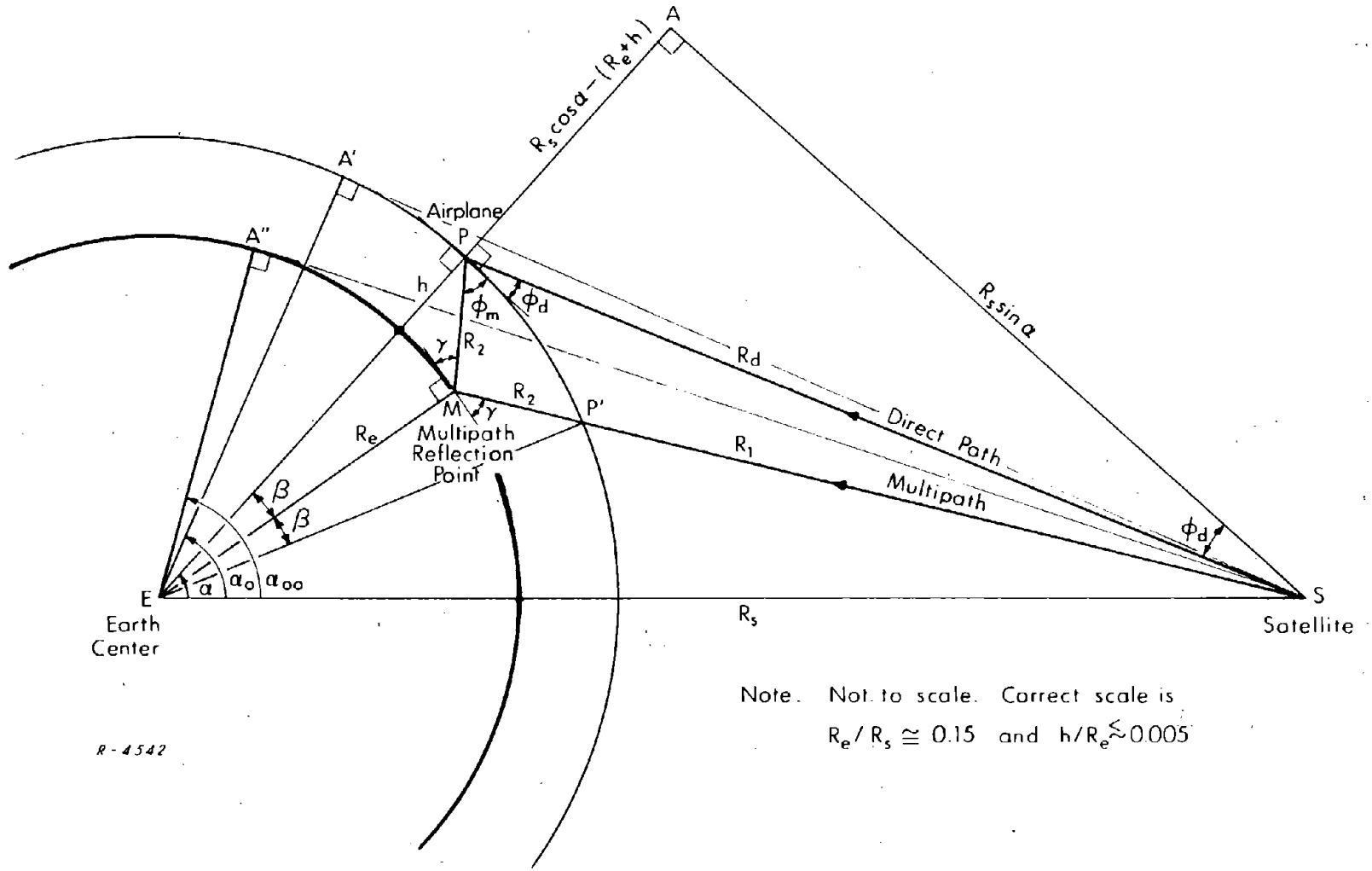

Fig. 1 AC-Satellite Link Multipath Geometry

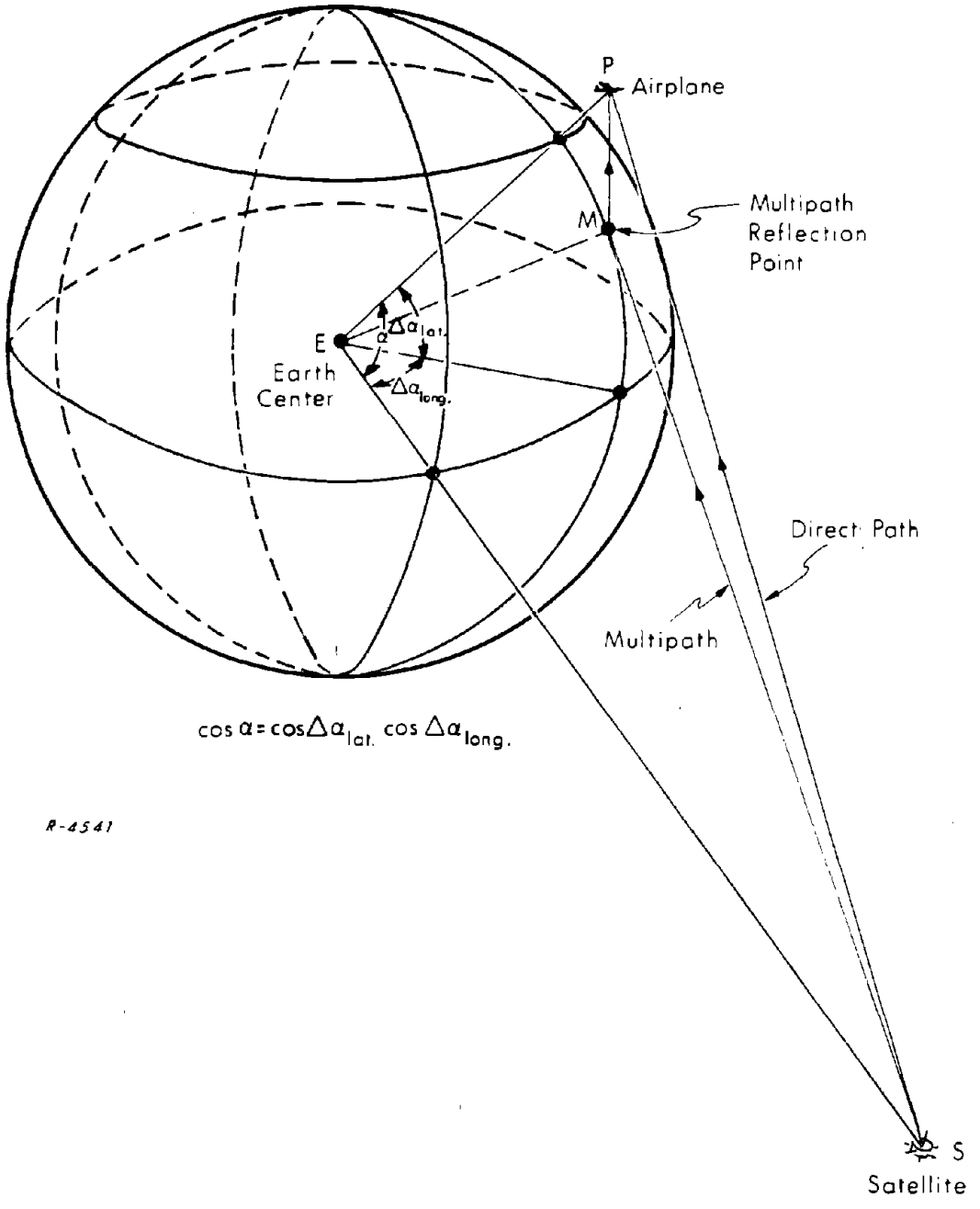

Fig. 2 Multipath Geometry Relating Satellite-Aircraft Angle, α, to Aircraft Latitude, $\Delta\alpha_{lat}$, and Aircraft-Satellite Longitudinal Separation, $\Delta\alpha_{long}$

2) The grazing angle γ.

3) The angles of arrival of the direct-path and multipath signals at the aircraft ϕ_d and ϕ_m as measured with respect to the horizontal at the aircraft. The angle ϕ_d is also referred to as the satellite elevation angle. The complement of this angle, $\pi/2-\phi_d$, is referred to as the aspect angle. The directivity angle, δ, is defined as the sum $\phi_m+\phi_d$, and is the angular separation between the directions of arrival of the desired direct-path signal and the interfering multipath signal.

4) The relative multipath and direct-path carrier doppler frequencies.

Of particular interest is the range of grazing angles between 10° and 20°. The minimum expected grazing angle is 10°, and for grazing angles above 20° the multipath problem is not as severe as for angles less than about 20°. This is so for several reasons based on characteristics of the aircraft-to-satellite link and the navigation system implementation. These are, in order of importance:

1) The L-band antenna directivity can significantly suppress the multipath signal as a result of the larger directivity angles.

2) Specular multipath interference, which may present a problem at lower grazing angles, is entirely negligible for grazing angles above about 20° at 1.6 GHz and for normal ocean conditions.

3) The fading bandwidth, which is a measure of the spectral spreading of the diffuse multipath signal, is larger at higher grazing angles. A large fading bandwidth may reduce the effects of the multipath in the narrow bandwidths of the carrier and clock PLL's and in the integrate and dump BINOR code acquisition filters. This is so when it corresponds to a frequency spreading of the multipath power at these particular frequencies into a bandwidth which is larger than the corresponding filter noise bandwidth.

For the grazing angles in this range, and for aircraft altitudes less than about 20 miles, it is a good approximation to assume that the direct-path ray S-P and the multipath ray segment S-M are parallel as indicated in Fig. 3, and that effects of the earth's curvature between the scattering point M and the point on the earth's surface directly under the aircraft are negligible. In this case, the angles γ, ϕ_d, and ϕ_m are <u>all equal</u>, and given by

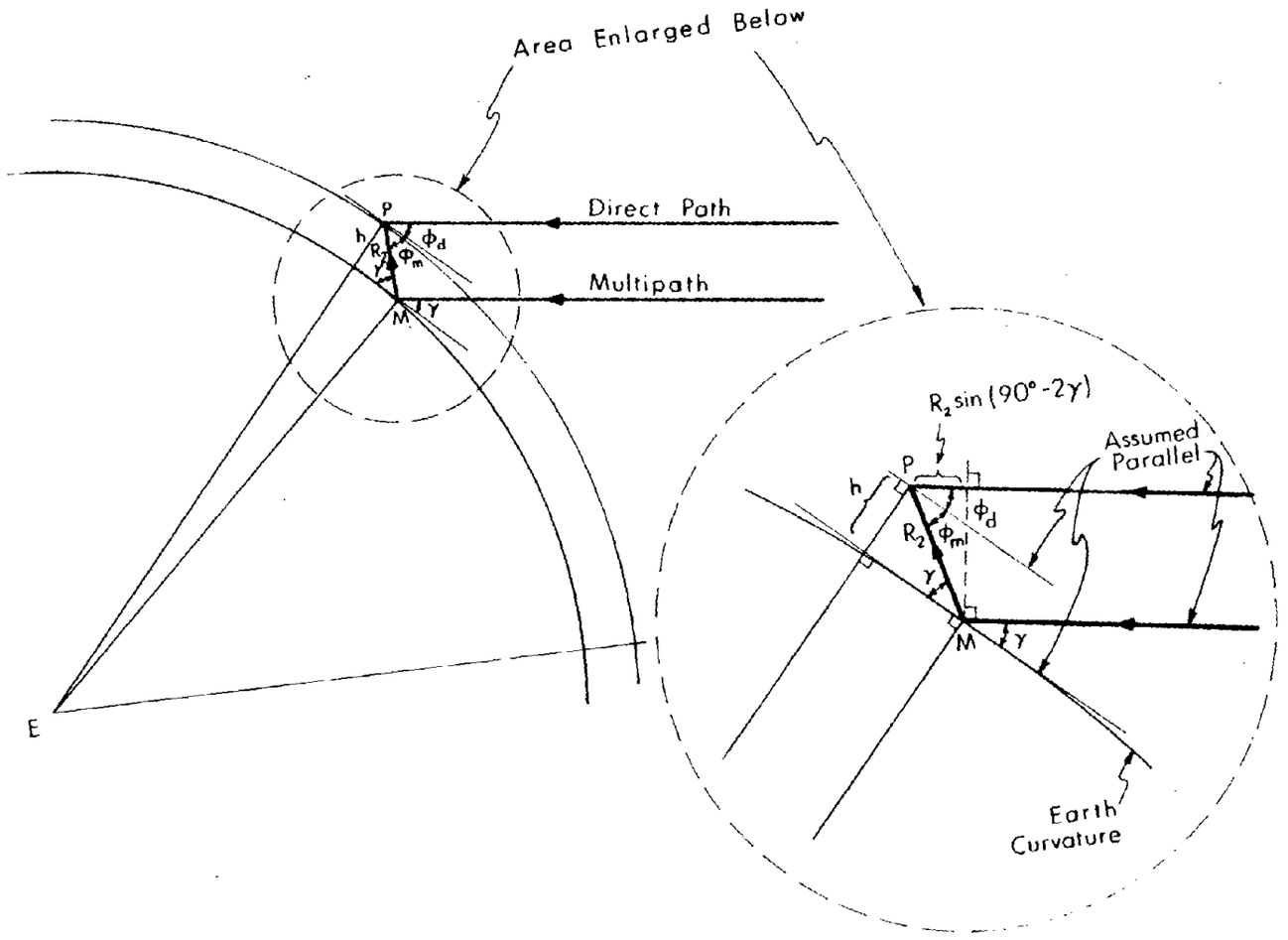

Fig. 3 AC-Satellite Link Multipath Geometry Approximation

$$\cot \phi_d = \cot \phi_m = \cot \gamma = \frac{R_s \sin \alpha}{R_s \cos \alpha - (R_e + h)} \tag{3}$$

where R_s and R_e are the synchronous satellite orbit radius and the earth radius respectively, and h is the aircraft altitude. The angle α was defined above and in Figs. 1 and 2. Dividing numerator and denominator of Eq. (3) by R_s permits cot γ to be written in a normalized form as

$$\cot \gamma = \frac{\sin \alpha}{(\cos \alpha - \cos \alpha_o)} \tag{4}$$

where

$$\cos \alpha_o \equiv \frac{R_e}{R_s} \left(1 + \frac{h}{R_e}\right) \approx \frac{R_e}{R_s} \tag{5}$$

if $h/R_e << 1$. with $R_e \cong 3,960$ miles, $R_s \cong 26,260$ miles (for synchronous equatorial orbit), and with $h_{max} = 20$ miles,

$$\frac{R_e}{R_s} \cong 0.1508 \text{ and } \frac{h}{R_e} \leq 0.00505 \tag{6}$$

In terms of the grazing angle, γ, the relative specular multipath time delay, τ_{ms}, is

$$\tau_{ms} \cong \frac{2h}{c} \sin \gamma = \frac{2h}{c} \frac{1}{\sqrt{1 + \cot^2 \gamma}} \tag{7}$$

A curve of sin γ as a function of α is plotted* in Fig. 4 for γ between 10° and 30°.

The differential carrier doppler, f_{ms}, is another important parameter of the multipath signal, and is given by

* In addition to the approximations of parallel rays and locally flat earth used to derive Eqs. (3) and (7), the approximation indicated in Eq. (4) has also been made.

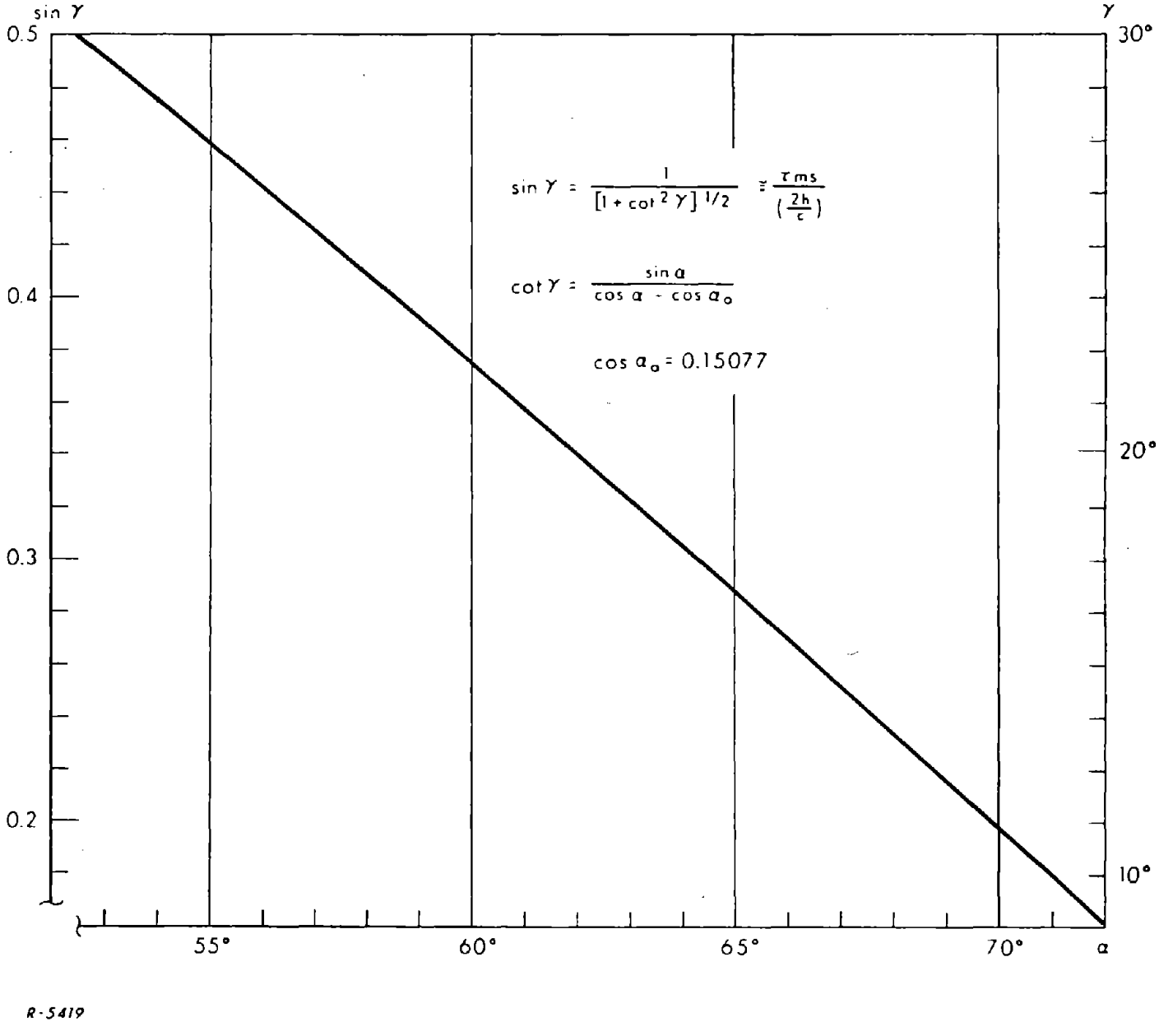

Fig. 4 Sin γ as a Function of the Angle α for $10° < \gamma < 30°$

$$f_{ms} = -f_c \frac{d\tau_{ms}}{dt}$$

$$= -f_c \left\{ \frac{\partial \tau_{ms}}{\partial h} \frac{dh}{dt} + \frac{\partial \tau_{ms}}{\partial \alpha} \frac{d\alpha}{dt} \right\} \tag{8}$$

where f_c is the carrier frequency (1.6 GHz). From Eqs. (4) and (7), this is approximately given by* †

$$f_{ms} \cong \left(\frac{2f_c}{c}\right) \sin\gamma \left\{ -\nu_h + \left(\frac{h}{R_e}\right) \cos^2\gamma \, (\cot\alpha + \cot\gamma) \, \nu_\alpha \right\} \tag{9}$$

where ν_h and ν_α are the vertical and horizontal (in plane) aircraft velocity components given by

$$\nu_h = \frac{dh}{dt} \quad \text{and} \quad \nu_\alpha = \frac{1}{(R_e + h)} \frac{d\alpha}{dt} \approx \frac{1}{R_e} \frac{d\alpha}{dt} \tag{10}$$

The horizontal component of velocity which is perpendicular to the plane containing the aircraft P, satellite S, and earth center E does not contribute to the differential doppler frequency.

An interesting phenomenon concering the differential doppler, which has apparently been overlooked by some authors, is the relative effect that a small unavoidable vertical component of aircraft velocity can have on the value of $f_{dop.}$ even for nominally "constant altitude" flight. This is particularly true at lower aircraft altitudes and for intermediate grazing angles where the ratio (h/R_e) is small and cot γ is not too large, so that the factor multiplying ν_α in Eq. (9) is much less than 1. To illustrate this point further, the ratio of ν_α to ν_h required for the effects of vertical and horizontal (ν_α) aircraft velocities on f_{ms} to be equal, $(\nu_\alpha/\nu_h)_o$, is plotted as a function of α for aircraft altitudes of 5, 10, 15, and 20 miles in Fig. 5. From Eq. (9), the ratio $(\nu_\alpha/\nu_h)_o$ is, of course,

$$\left(\frac{\nu_\alpha}{\nu_h}\right)_o = \frac{1}{\left(\frac{h}{R_e}\right) \cos^2\gamma \, (\cot\alpha + \cot\gamma)} \tag{11}$$

---

* In addition to the approximations of parallel rays and locally flat earth used to derive Eqs. (3) and (7), the approximation indicated in Eq. (4) has also been made.

† Added in proof: See Addendum for a revised derivation of f_{ms}.

From the curves in Fig. 5, it is seen that this ratio will always exceed approximately 32 if the grazing is always greater than 10° ($\alpha \leq 72°$) and the aircraft altitude is always less than 20 miles. For aircraft altitudes less than 15 miles and for grazing angles greater than 20° ($\alpha \leq 64°$), a much more frequently encountered condition, this ratio will be greater than 80. What this means is that for aircraft flying at 600 mph and having a v_a component of 200 mph or less, the vertical aircraft velocity would have to be much less than about 6 mph for grazing angles of 10° and aircraft altitudes of 20 miles, and much less than about 2.5 mph for grazing angles in excess of 20° and aircraft altitudes less than 15 miles, in order for the relative multipath carrier doppler frequency, f_{ms}, to be determined primarily by the v_a contribution. Consequently, since aircraft vertical velocities cannot be held to less than plus or minus several mph, the random or uncontrollable vertical aircraft motion will have a pronounced effect on f_{ms}. Therefore a minimum differential or relative multipath doppler offset cannot be counted on, but only a range of values for f_{ms} may be estimated, with f_{ms} likely to be anywhere in that range with approximately equal probability. The range, of course, corresponds to the uncertainty in aircraft vertical velocity, and is centered on the more deterministic contribution to f_{ms} from v_a.

Finally, the direct-path carrier doppler may be determined from the geometry of Fig. 1. This is given by

$$f_d = -f_c \frac{d\tau_d}{dt} = -f_c \frac{1}{c} \frac{dR_d}{dt} \tag{12}$$

where R_d is the direct-path distance and τ_d is the direct-path transmission time delay. R_d is given by (see Fig. 1)

$$R_d = \left\{ R_s^2 + (R_e + h)^2 - 2 R_s (R_e + h) \cos \alpha \right\}^{1/2} \tag{13}$$

so that

$$\frac{dR_d}{dt} = \frac{\partial R_d}{\partial h} v_h + \frac{\partial R_d}{\partial \alpha} \frac{1}{(R_e + h)} v_a \tag{14}$$

$$\cong \frac{R_s}{R_d} (\cos \alpha - \cos \alpha_o) \left\{ -v_h + \frac{\sin \alpha}{(\cos \alpha - \cos \alpha_o)} v_a \right\} \tag{15}$$

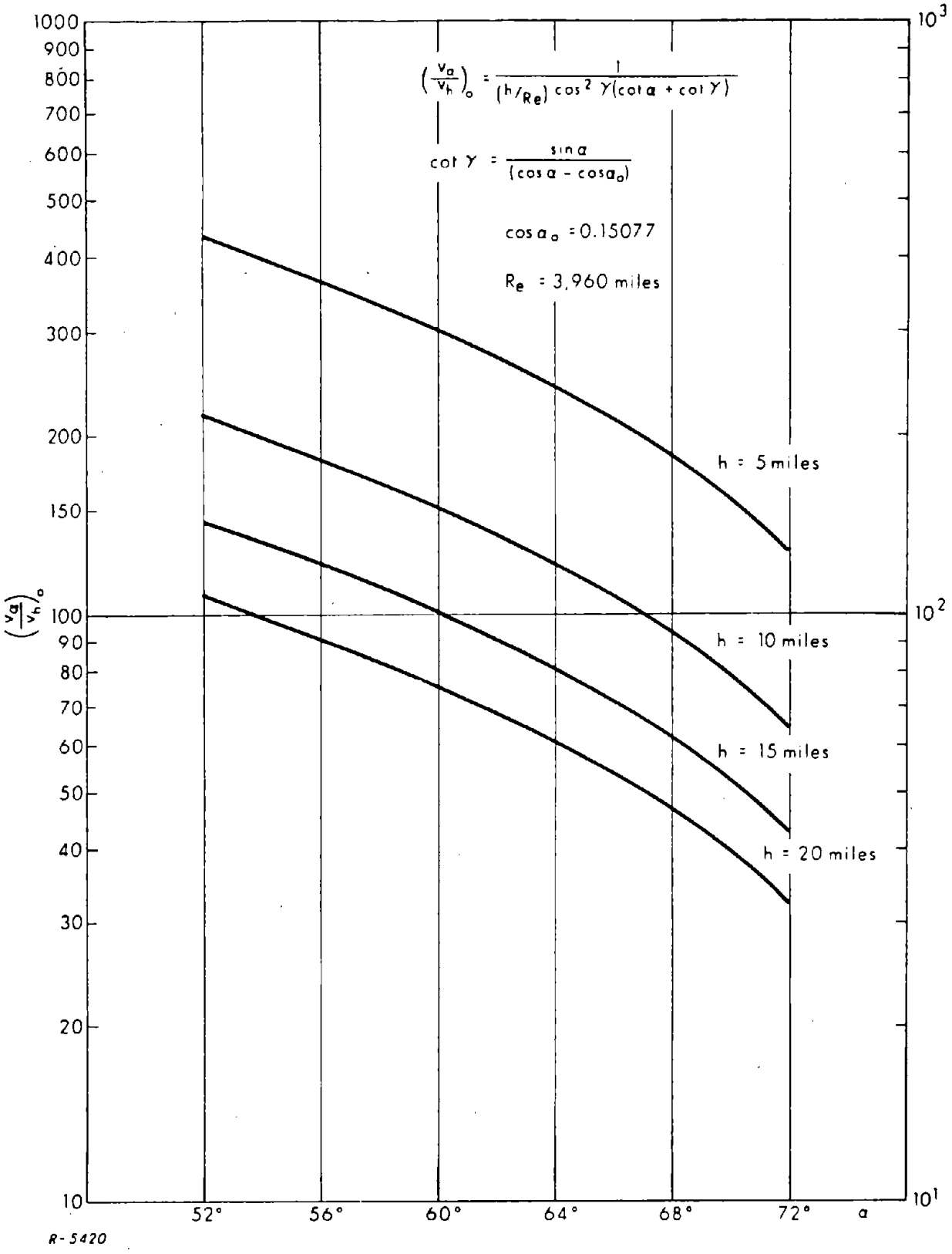

Fig. 5 Curves of $(\nu_a/\nu_h)_o$ as a Function of α for h = 5, 10, 15 and 20 Miles

or f_d is

$$f_d = -f_c \frac{1}{c} \frac{R_s}{R_d} (\cos \alpha - \cos \alpha_o) \left| -\nu_h + \cot \gamma \nu_a \right| \quad (16)$$

It is easily seen that for low grazing angles, γ, and for nominally level flight, the contribution of ν_a clearly dominates that of ν_h. This is so because, for aircraft flying at 600 mph or more, the aircraft will more than likely have a component ν_a on the order of 50 mph or more (compared to several mph for ν_h), and cot γ will be greater than 1. Consequently, except for cases where ν_a is very small, or where the synchronous satellite is almost directly overhead ($\alpha \approx 0$), f_d may be written as

$$f_d \approx -f_c \frac{1}{c} \frac{R_s}{R_d} \sin \alpha \ \nu_a \quad (17)$$

At the low grazing angles (10°-20°) where the multipath interference will be most severe, the direct-path doppler frequency, f_d, will be much larger than the relative multipath doppler frequency f_{ms}.

2.2.2 Scattering Physics of the NAV/SAT Link

The physics of the scattering, in conjunction with the geometry of the NAV/SAT link, yields information on

1) Whether, and under what conditions, the scattering is essentially specular or diffuse, and the characteristics of the scattered signal in each case.

2) The received average multipath power.

3) The fading bandwidth or spectral spreading of the scattered multipath signal as received by the moving aircraft.

4) The spread of time delays of the received multipath signal for the case of diffuse scattering.

5) The size of the first Fresnel zone for the case of specular scattering.

6) The size of the scattering region for the case of diffuse scattering.

2.2.2.1 Character of the Scattered Signal

The character of the received multipath interference depends on whether the surface of the earth at the scattering point M may be considered "rough" or "smooth" for the particular wavelength, λ, of the incident radiation, the grazing angle, γ, and the rms surface height variation, σ_w. The Rayleigh criterion is often used to differentiate between the two extremes of "rough" and "smooth". According to the Rayleigh criterion the surface is considered "smooth" if

$$\frac{\sigma_w \sin \gamma}{\lambda} < \frac{1}{8} \tag{18}$$

and "rough" otherwise.[1] Since most of the earth's surface is sea water, and since reflections off the sea surface represent a more serious problem than reflections off land, only reflections off the sea will be considered, and σ_w will be taken to represent the rms sea surface height fluctuation. The sea surface heights may be considered to be randomly distributed with an approximately Gaussian distribution.[2]

Applying the Rayleigh criterion to the 1.6 GHz frequency, it may be shown that the scattering is primarily diffuse for all sea states rougher than "slight" at grazing angles in excess of 10°, but that specular scattering becomes important for sea states calmer than "smooth" at grazing angles below 20°. In particular, the range of grazing angles, γ, at the transition point between "rough" and "smooth" scattering surface conditions, as determined by Eq. (12), for various sea states[3] are listed in Table 1 below.

Table 1

Grazing Angle, γ, for which $\sin \gamma = \frac{1}{8} \lambda/\sigma_w$ (λ = 18.75 cm)

Sea State	Approximate range of σ_ω	range of γ	Comment
smooth	5-10 cm	28°-13.5°	specular scattering becomes important below about 20°
slight	10-20 cm	13.5°-6.7°	specular scattering is only important near 10°
moderate	20-30 cm	Below 10°	specular scattering is entirely negligible
rough	30-50 cm	Below 10°	

For very "smooth" scattering surfaces only a specular multipath return is present. The amplitude and phase of the received multipath signal are determined essentially by the electromagnetic properties of the scattering surface (i.e. by the Fresnel reflection coefficients for the particular polarization of the incident radiation and angle of incidence) and the geometry of the link, and vary in a rather deterministic manner with the motion of the aircraft. As the surface becomes "rougher", either as a result of increasing grazing angle and/or rougher sea conditions, several things begin to happen. First, amplitude and phase fluctuations on the received multipath signal appear, as if cophasal and quadrature components having zero-mean Gaussian-distributed random amplitudes with unequal variances[4, 5] are simply added to the steady deterministic specular multipath component. Second, the power in the steady deterministic specular multipath component begins to diminish with increasing surface "roughness" as a result of a decrease in the mean-square scattering coefficient $\langle |\rho_s|^2 \rangle$, which is given by[6]

$$\langle |\rho_s|^2 \rangle = e^{-\left(\frac{4\pi \sigma_w \sin\gamma}{\lambda}\right)^2} \tag{19}$$

Further increases in surface "roughness" cause further diminishing of the power in the steady deterministic component of the received specular multipath component and cause the variances of the fluctuating cophasal and quadrature components, mentioned above, to increase and approach each other in value.

Finally, as the transition from "smooth" to "rough" is completed, the power in the steady specular component becomes negligibly small, and the scattering is essentially pure diffuse. For this case radiation is received from a much larger area of the scattering surface centered around the specular point, and multipath components having relative multipath delays in excess of τ_{ms} begin to appear.

2.2.2.2 Computation of the Relative Received Multipath Power

The relative received multipath power for the case of pure specular scattering is denoted by a_{ms}^2, and is given by

$$a_{ms}^2 = |R_o|^2 \, D^2 \, \langle |\rho_s|^2 \rangle \, F\left(R_d^2, R_1^2, R_2^2\right) \Gamma_s \Gamma_A \tag{20}$$

where $|R_o|$ is the magnitude of the reflection coefficient of a very smooth plane sea; D is the divergence factor to account for the sphericity of the earth's surface; $\langle |\rho_s|^2 \rangle$ is the mean square scattering coefficient which takes account of the slight random roughness of the scattering surface; $F\left(R_d^2, R_1^2, R_2^2\right)$ is a factor which takes the relative $1/r^2$ intensity losses into account if necessary; and Γ_s and Γ_A are the relative antenna gain factors of the synchronous satellite and the aircraft respectively, and includes the effects of polarization discrimination if any.

The magnitude of the reflection coefficient, $|R_o|$, for sea water may be obtained for horizontal and vertical polarization from Fig. 11.2 of Beckman and Spizzichino[7] which plots $|R_o|$ as a function of the grazing angle, Υ, for various wavelengths, λ. Special care must be taken in the case where circular or elliptical polarization is used in order to take cross-polarization and other effects into account.[8]

The divergence factor D is given by[9]

$$D = \left[1 + \frac{2 R_2 (R_1 + R_2)}{R_e (R_1 + 2 R_2) \sin \Upsilon}\right]^{-1/2} \left[1 + \frac{2 R_2 (R_1 + R_2)}{R_e (R_1 + 2 R_2)}\right]^{-1/2} \qquad (21)$$

where R_e is the earth radius, R_2 is the distance from the scattering point M to the airplane P, and $(R_1 + R_2)$ is the distance from the satellite S to the scattering point M. (See Fig. 1.) For the NAV/SAT link $D \approx 1$.

The mean square scattering coefficient $\langle |\rho_s|^2 \rangle$ was given as a function of wavelength λ, rms sea surface displacement σ_w, and the sine of the grazing angle Υ in Eq. (13). For the ratio $(\sigma_w \sin \Upsilon)/\lambda$ equal to 1/8, which is the Rayleigh criterion dividing line between "smooth" and "rough" scattering surfaces $\langle |\rho_s|^2 \rangle$ is equal to

$$\langle |\rho_s|^2 \rangle = e^{-(\pi/2)^2} \cong 0.085 \qquad (22)$$

which is fairly small.

The function $F\left(R_d^2, R_1^2, R_2^2\right)$ is simply given by

$$F\left(R_d^2, R_1^2, R_2^2\right) = \frac{R_d^2}{(R_1 + 2R_2)^2} \tag{23}$$

and reflects the fact that the $1/r^2$ intensity losses along the two paths are slightly different. Since $R_d \approx R_1 + 2R_2$ (i.e., $R_1 + 2R_2 - R_d \ll R_d$), this factor is essentially equal to 1 for the NAV/SAT link.

The relative satellite antenna gain factor, Γ_s, is essentially equal to 1 since the satellite must provide uniform coverage of the earth's surface and the angular separation between the direct-path and the multipath is very small at the satellite. The relative aircraft antenna gain factor, Γ_A, can be less than 1 as a result of the large angle between the directions of arrival of the direct-path and multipath which is in excess of 20°, and as a possible consequence of polarization discrimination.

In estimating a reasonable worst-case value of a_{ms}^2 the following assumptions are made:

1) $\left(|R_o|^2\right)_{\text{worst-case}} = 1$

2) $(D^2)_{\text{worst-case}} = 1$

3) $\left(\left\langle |\rho_s|^2 \right\rangle\right)_{\text{worst-case}} = e^{-(0.37\pi)^2} \cong 0.2583$

   Corresponding to $\gamma = 10°$ and $\sigma_w = 10$ cm.

4) $\left(F\left(R_d^2, R_1^2, R_2^2\right)\right)_{\text{worst-case}} = 1$

5) $\Gamma_s = 1$

6) $(\Gamma_A)_{\text{worst-case}} = 0.25$ (-6 db)

For these worst-case values $(a_{ms}^2)_{\text{worst-case}} = 0.06457$.

For the case of pure diffuse scattering, the average relative received multipath power is denoted by $2\sigma_m^2$, and may be computed approximately[10] under certain conditions. These conditions are:

1) The undulations of the scattering surface may be described by a two-dimensional Gaussian distribution for which the rms surface displacement is σ_w and the correlation length is L.

2) The ratio $2\sigma_w/L$ is small (less than 1/10)

3) The ratio $(\sigma_w \sin\gamma)/\lambda$ is greater than 1/8.

4) The autocorrelation function of the surface fluctuations is an analytic function.

The first condition is a fairly reasonable one in that measurements[2] indicate that it is approximately satisfied in practice, and it also simplifies the mathematics. The second condition is equivalent to requiring that the slopes of the waves be small. This requirement is essential for the Kirchhoff-Huygen approximation to be valid,[11] and for shadowing and multiple scattering effects to be unimportant. In addition, the rms slope must be sufficiently less than the grazing angle, γ, which would pertain for a perfectly smooth scattering surface in order that the reflection coefficient, R_o, used in the determination of the average received relative diffuse multipath power may be evaluated at the grazing angle γ. In this regard it is also important that $|R_o|^2$ not vary drastically with γ for those values of γ for which the approximate computation is made. In particular, the approximate computation will predict incorrect results for vartical polarization near the Brewster angle.[12] The third condition is the Rayleigh criterion condition for pure diffuse scattering.

If these conditions are well fulfilled, most of the received diffusely scattered multipath power will come from the region surrounding the specular point, and the method of steepest descent may be used in performing the integration required in summing the powers contributed from each elementary area of the scattering surface. The result for $2\sigma_m^2$ obtained by Durrani and Staras,[10] with appropriate modifications to take the characteristics of the NAV/SAT link into account*, is

* The computation by Durrani and Staras was for an orbiting satellite having an altitude in excess of 100 miles and for grazing angles which could extend down below 10°. We also include the aircraft relative antenna gain factor Γ_A.

$$2\sigma_m^2 \cong |R_o|^2 \; D^2 \; \Gamma_A \; Q(h, \gamma) \tag{24}$$

where $|R_o|^2$, D^2, and Γ_A are defined as before, and $Q(h, \gamma)$ is a function essentially of the aircraft altitude and the grazing angle (although Durrani and Staras define it in terms of the orbit height, the aspect angle, and the angle between the aircraft and specular point as measured from the earth's center). The function $Q(h, \gamma)$ is approximately equal to 1 except for large altitudes and small grazing angles. For the NAV/SAT application it may be approximated by 1. Again D^2 is approximately equal to 1. The worst-case value of $|R_o|^2$ for both horizontal and vertical polarization is approximately -2 db.[13] The aircraft antenna relative gain factor, Γ_A, is again taken as 0.25 (-6 db), so that $2\sigma_m^2$ is, in the worst-case,

$$\left(2\sigma_m^2\right)_{\text{worst-case}} \cong 0.16 \tag{25}$$

2.2.2.3 Computation of the Fading Bandwidth

A non zero fading bandwidth arises because of relative motions of the transmitter and receiver, and/or the scattering surface. If the transmitter and receiver were stationary with respect to each other and the scattering surface, and the only motion was that of the ocean waves, the fading bandwidth would be relatively small. However, the high aircraft velocities result in very much larger fading bandwidths.

The fading bandwidth may be determined by computing the autocorrelation function of the received diffusely scattered multipath signal for the case where carrier only is transmitted. Since the decorrelation time, τ_o, is much smaller than the periods of ocean waves, the sea may be considered as static in the computation. This autocorrelation function has been computed by Durrani and Staras[10] for aircraft motion which is coplanar and perpendicular to the plane of the aircraft, satellite, and earth center. †

† Small vertical aircraft velocities do not contribute significantly to the fading bandwidth (i.e. to further spectral spreading of the received diffuse multipath interference) if the aircraft velocity is on the order of 600 mph or more and is in level flight, and for grazing angles in excess of 10°.

In both of these cases the autocorrelation function is found to have a Gaussian shape $\exp\left(-(\tau/\tau_o)^2\right)$. For small aircraft altitudes (i.e. less than 20 miles) and for grazing angles in excess of 10°, the correlation times for these two cases are essentially equal, and given by

$$\tau_o = \left[\left(\frac{2\sigma_w}{L}\right)\ (2\pi f_c)\ \left(\frac{\nu}{c}\right)\ \sin\gamma\right]^{-1} \tag{26}$$

where ν/c is the ratio of the aircraft velocity to the velocity of light, and the other quantities have been defined previously.

The relative power density spectrum of the received multipath for the case where only a carrier is transmitted is

$$\Phi_{md}(\omega) = \frac{2\sigma_m^2}{\sqrt{\pi}\ B_m}\ e^{-(f/B_m)^2} \tag{27}$$

where B_m is equal to

$$B_m = \frac{1}{\pi\tau_o} = 2 f_c \left(\frac{\nu}{c}\right)\left(\frac{2\sigma_w}{L}\right)\ \sin\gamma \tag{28}$$

and ω is measured from the received multipath carrier frequency (including specular doppler offset). For ν = 600 mph and $(2\sigma_w/L) = 1/10$, B_m is

$$B_m \cong 286 \sin\gamma \text{ Hertz} \tag{29}$$

which for $\gamma = 10°$, yields $B_m \cong 50$ Hz.

2.2.2.4 Computations of the Sizes of the Scattering Region for Specular and Diffuse Scattering and the Multipath Time Delay Spread

For pure specular scattering, the primary contribution to the received multipath signal comes from the first Fresnel zone. This is an area of the scattering surface centered at the specular point such that the difference between the path distances of aircraft received radiation scattered off any point in this area and of aircraft received radiation scattered off the specular point is less than a half-wavelength of the radiation. A perfectly

smooth and flat area which is illuminated uniformly with radiation is assumed. For the NAV/SAT application, this area is approximately elliptical with semimajor and semiminor axes which are denoted by Δx_s and Δy_s respectively as shown in Fig. 6, and which may be determined from the equations

$$d_x - \left(\frac{h}{\sin\gamma} + \Delta x_s \cos\gamma\right) = \frac{\lambda}{2} \tag{30}$$

$$d_x = \left\{h^2 + \left(\frac{h}{\sin\gamma}\cos\gamma + \Delta x_s\right)^2\right\}^{1/2} \tag{31}$$

$$d_y - \frac{h}{\sin\gamma} = \frac{\lambda}{2} \tag{32}$$

$$d_y = \left\{\left(\frac{h}{\sin\gamma}\right)^2 + \Delta y_s^2\right\}^{1/2} \tag{33}$$

Expanding the square roots in Taylor series and retaining terms up to Δx_s^2 and Δy_s^2, Δx_s and Δy_s are approximately

$$\Delta x_s \cong \frac{1}{\sin\gamma}\sqrt{\frac{h\lambda}{\sin\gamma}} \tag{34}$$

$$\Delta y_s \cong \sqrt{\frac{h\lambda}{\sin\gamma}} \tag{35}$$

The maximum value of Δx_s and Δy_s occur for the maximum aircraft altitude (20 miles) and the minimum grazing angle ($\gamma = 10°$) and are approximately $\Delta y_s \approx 186$ meters and $\Delta x_s \approx 1070$ meters.

The size of the scattering region for pure diffuse scattering may be obtained as follows: The distances Δx_d and Δy_d (see Fig. 7) for which the diffuse multipath power reflected per unit area drops to 1/e of the diffuse multipath power reflected per unit area at the specular point M are computed and taken as representing size of the scattering region. The variation in diffuse multipath power reflected per unit area over the scattering region is a result primarily of the variation of the term[10]

$$e^{-\left[\frac{\tan^2\beta}{\left(\frac{2\sigma_w}{L}\right)^2}\right]} \tag{36}$$

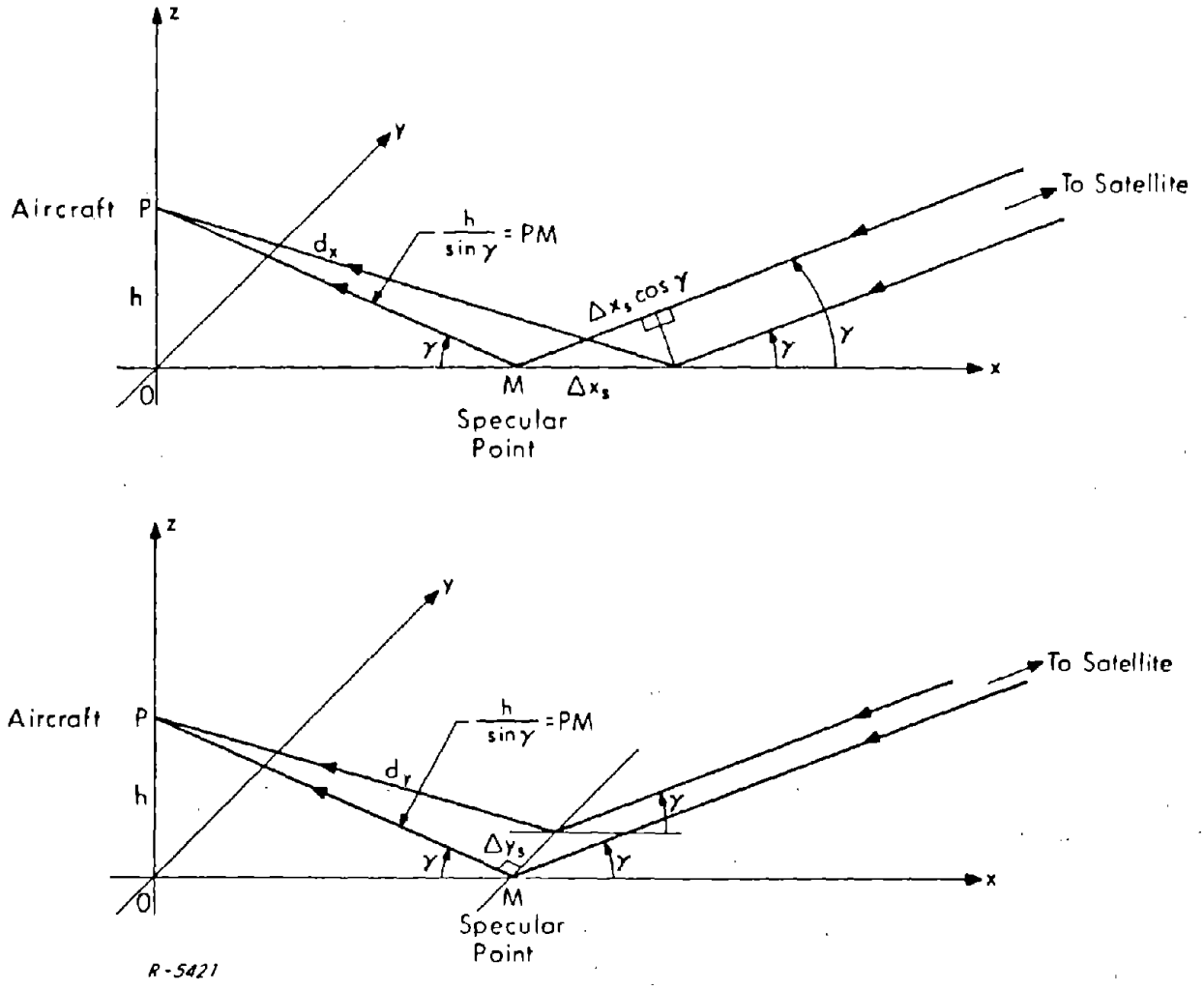

Fig. 6 Configuration for Computing the Semimajor and Semiminor Axes of the First Fresnel Zone Ellipse

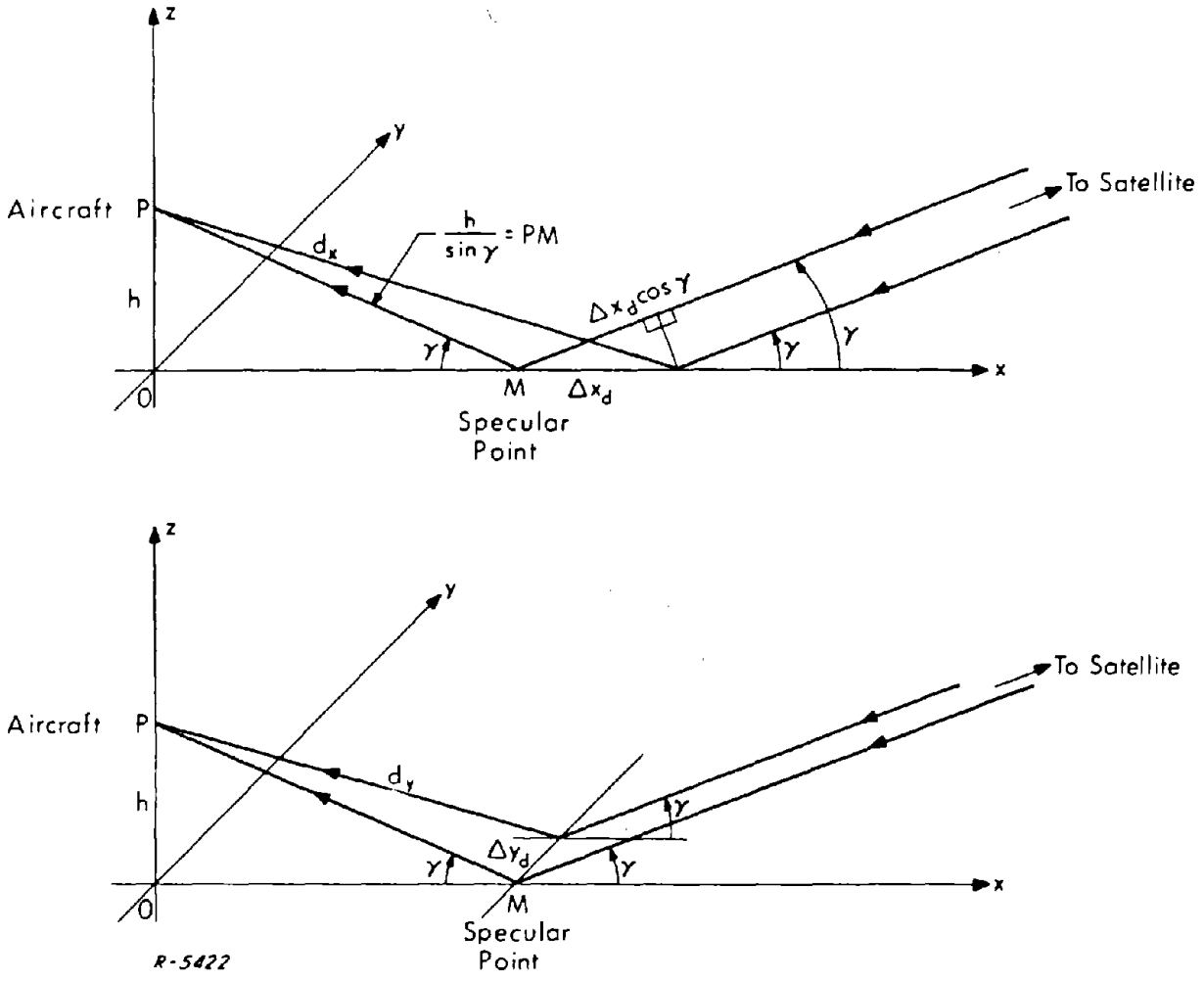

Fig. 7 Configuration for Computing the Time Delay Spread of the Diffuse Multipath Scattering

where here β is the angle made by the bisector of the incident and scattered rays with the z-axis. The quantity $\tan^2\beta$ is a function of the location of the unit scattering area with respect to the specular point; the grazing angle, γ, and the aircraft altitude, h. If Δx and Δy are the position coordinates with respect to the specular point of the unit scattering area under consideration, $\tan^2\beta$ is approximately given by

$$\tan^2\beta \approx \frac{1}{4h^2} \left\{ \sin^4\gamma \ \Delta x^2 + \Delta y^2 \right\} \tag{37}$$

to second order in Δx and Δy. Then Δx_d and Δy_d are

$$\Delta x_d = 2h \left(\frac{2\sigma_w}{L} \right) \frac{1}{\sin^2\gamma} \tag{38}$$

and

$$\Delta y_d = 2h \left(\frac{2\sigma_w}{L} \right) \tag{39}$$

This may be rewritten as

$$\Delta x_d = 2 \left(\frac{2\sigma_w}{L} \right) \sqrt{\frac{h}{\lambda \sin\gamma}} \ \Delta x_s \tag{40}$$

and

$$\Delta y_d = 2 \left(\frac{2\sigma_w}{L} \right) \sqrt{\frac{h}{\lambda \sin\gamma}} \ \Delta y_s \ (\sin\gamma) \tag{41}$$

where Δx_s and Δy_s are the semimajor and semiminor axes of the first Fresnel zone ellipse. Note that the factor $(\sin\gamma)$ in Eq. (41) means that the diffuse scattering region will be much more elongated in the x-direction than is the first Fresnel zone. Considering the locus of points Δx, Δy for which the diffuse multipath power reflected per unit area drops to 1/e of what it is at the specular point, it is noted that these points correspond to different relative multipath delays. Since the maximum spreading in relative multipath delay for this locus occurs for $\Delta y = 0$, $\Delta x = \Delta x_d$, the relative multipath

delay difference $(\tau_{md} - \tau_{ms})$ shall be taken to be a measure of the multipath delay spread. Here τ_{md} is, of course, the relative multipath delay for the scattering point at $\Delta y = 0$, $\Delta x = \Delta x_d$. The relative multipath time delay spread, $(\tau_{md} - \tau_{ms})$, is then

$$(\tau_{md} - \tau_{ms}) = \frac{1}{c}\left[d_x - \left(\frac{h}{\sin\gamma} + \Delta x_d \cos\gamma\right)\right] \tag{42}$$

where

$$d_x = \left\{h^2 + \left(\frac{h}{\sin\gamma}\cos\gamma + \Delta x_d\right)^2\right\}^{1/2} \tag{43}$$

If Δx_d is sufficiently smaller than $(h/\sin\gamma)$, d_x may be expanded to second order in Δx_d, and $(\tau_{md} - \tau_{ms})$ is found to be approximately given by

$$(\tau_{md} - \tau_{ms}) \approx \frac{2}{c}\,\frac{h}{\sin\gamma}\left(\frac{2\sigma_w}{L}\right)^2 = \left(\frac{2h}{c}\sin\gamma\right)\frac{1}{\sin^2\gamma}\left(\frac{2\sigma_w}{L}\right)^2$$

$$= \tau_{ms}\left[\frac{1}{\sin\gamma}\left(\frac{2\sigma_w}{L}\right)\right]^2 \tag{44}$$

To check the validity of this approximation consider the requirement that Δx_d be sufficiently less than $(h/\sin\gamma)$.

$$\Delta x_d = \left(\frac{h}{\sin\gamma}\right)\left[\frac{2}{\sin\gamma}\left(\frac{2\sigma_w}{L}\right)\right] \ll \left(\frac{h}{\sin\gamma}\right) \tag{45}$$

or

$$\left[\frac{2}{\sin\gamma}\left(\frac{2\sigma_w}{L}\right)\right] \ll 1 \tag{46}$$

For $\Upsilon \geqq 20°$ and $\left(\frac{2\sigma_w}{L}\right) \leq \frac{1}{15}$,

$$\left[\frac{2}{\sin\Upsilon} \quad \frac{2\sigma_w}{L}\right] \leq 0.390 \tag{47}$$

which is sufficiently less than 1 to conclude that the approximations will probably be valid to within about 10% error. However, for $\Upsilon \approx 10°$, and $(2\sigma_w/L) \approx 1/10$,

$$\left[\frac{2}{\sin\Upsilon} \quad \frac{2\sigma_w}{L}\right] \approx 1.15 \tag{48}$$

which is NOT less than 1. Consequently the approximations lose their validity as the grazing angle decreases and the seas become choppier. Not only does the expansion of Eq. (43) to second order in Δx_d become questionable, but so also does the expansion of $\tan^2\beta$ (Eq.(37)) to only second order in Δx and Δy, and the neglection of the dependence on Δx and Δy of the other factors which enter into the expression for the diffuse multipath power reflected per unit area. In addition, the validity of the conditions which must hold in order for the development of the diffuse multipath computations performed by Durrani and Staras[10] must be called into question at the low grazing angles. Unfortunately these authors apparently failed to realize this and extended their approximate results down to very low grazing angles for which all the assumptions and conditions used to derive their results break down. This leads them to the totally absurd conclusion that the scattered multipath power received by the aircraft (or orbiting satellite in their example) becomes negligible at very low grazing angles. What happens, of course, is that the diffuse multipath power drops and the specular multipath begins to dominate at the low grazing angles. In addition, shadowing and multiple scattering effects begin to play an important role at low grazing angles. These factors were apparently all ignored by Durrani and Staras.

In any event, it is reasonable to conclude that, for grazing angles between 10° and 20° for which the Rayleigh criterion for diffuse scattering is satisfied, the relative multipath time delay spread, $(\tau_{md} - \tau_{ms})$, is on the order of 10% to 50% of the relative specular multipath time delay, τ_{ms}. This delay spread must be compared to the period of the highest modulating frequency of the transmitted signal to determine whether a single modulation time delay, τ_{ms}, may be used in describing the received multipath signal, or if the received multipath signal must be described as the sum of various multipath signals each having a different relative time delay.

For the NAV/SAT application the period of the highest modulating frequency (320 kHz) is 3.125 μsec. The maximum relative specular multipath time delays, τ_{ms}, occur for the maximum aircraft altitude. For an aircraft altitude of 20 miles and a grazing angle of 20°, τ_{ms} is 73.5 μ sec, whereas at an aircraft altitude of 5 miles and a grazing angle of 10°, τ_{ms} is approximately 9.4 μ sec. Assuming minimum and maximum time delay spreads of 10% and 50% of τ_{ms}, the range of time delay spreads will be from approximately 1 to 35 μ sec. Since this is not a negligibly small fraction of the period of the highest modulating frequency a sum of multipath components having different modulation delays must be used in describing the received diffuse multipath signal. This is described further in the next section.

2.3 Characterization of the Received Multipath Signal

The received multipath signal is described in terms of the received direct-path as follows: The received direct-path signal may be written as

$$e_d(t) = \sqrt{2C} \sin \{\omega_c t + d(t) + \theta(t)\} \tag{49}$$

where C is the received direct-path signal power, ω_c is the transmitted carrier frequency in radians per second, d(t) is the direct-path carrier doppler phase

$$d(t) = \int_{-\infty}^{t} 2\pi f_d(t)dt + \phi_d \tag{50}$$

(where $f_d(t)$ is the instantaneous direct-path carrier doppler frequency and ϕ_d is the initial carrier phase), and $\theta(t)$ represents the received phase modulation, the doppler on which may be totally neglected. For the case of BINOR ranging, $\theta(t)$ is

$$\theta(t) = \beta\, b_{13}(t) \tag{51}$$

where β = 1.15 radians and $b_{13}(t)$ is a BINOR code waveform generated by hard limiting the sum of 13 coherently-generated square waves, the highest frequency square wave being at 320 kHz and the other square waves being at a frequency 2^{-k} times 320 kHz k = 1, 2, 3, ..., 12).

The received multipath signal is then written as the sum of a pure "steady" specular component, $e_{ms}(t)$, and a diffuse component, $e_{md}(t)$.

$$e_m(t) = \sqrt{2C}\, a_{ms} \sin\{\omega_c t + d(t) + d_{ms}(t) + \theta(t - \tau_{ms})\}$$
$$+ \sqrt{2C} \sum_{\tau_m} x_c(t, \tau_m) \sin\{\omega_c t + d(t) + d_{ms}(t) + \theta(t - \tau_m)\}$$
$$+ \sqrt{2C} \sum_{\tau_m} x_q(t, \tau_m) \cos\{\omega_c t + d(t) + d_{ms}(t) + \theta(t - \tau_m)\} \quad (52)$$

where a_{ms}^2 is the mean relative specular multipath power; $d_{ms}(t)$ is the relative specular multipath carrier doppler phase

$$d_{ms}(t) = \int_{-\infty}^{t} 2\pi f_{ms}(t)\, dt + \phi_{ms} \quad (53)$$

(where $f_{ms}(t)$ is the instantaneous relative specular multipath carrier doppler frequency, and ϕ_{ms} is the initial phase); τ_{ms} is the relative specular multipath time delay; $x_c(t, \tau_m)$ and $x_q(t, \tau_m)$ are independent zero mean Gaussian random variables having identical variances, $\sigma_m^2(\tau_m)$; and τ_m is the relative time delay associated with the diffuse multipath components. The sum over the various relative multipath delays means that delay intervals $\delta\tau_m$ are being considered such that $\delta\tau_m$ is at least as large as the period of the carrier, but is much smaller than the period of the highest modulating frequency component in $\theta(t)$. The relative received diffuse multipath power is

$$2\sigma_m^2 = 2 \sum_{\tau_m} \sigma_m^2(\tau_m) \quad (54)$$

Additional properties of $x_c(t, \tau_m)$ and $x_q(t, \tau_m)$ are:

1) $\langle x_c(t, \tau_m)\, x_q(t + \tau, \tau_m + \Delta\tau_m) \rangle = 0$ for all τ and $\Delta\tau_m$

2) $\langle x_c(t, \tau_m)\, x_c(t + \tau, \tau_m) \rangle = \langle x_q(t, \tau_m)\, x_q(t + \tau, \tau_m) \rangle = \phi(\tau, \tau_m)$

3) $\langle x_c(t, \tau_m)\, x_c(t + \tau, \tau_m + \Delta\tau_m) \rangle = \langle x_q(t, \tau_m)\, x_q(t + \tau, \tau_m + \Delta\tau_m) \rangle = 0$

for all τ and $|\Delta\tau_m| > \delta\tau_m$.

The first property expresses the statistical independence of $x_c(t, \tau_m)$ and $x_q(t + \tau, \tau_m + \Delta\tau_m)$ for all τ and $\Delta\tau_m$. The second property indicates that the autocorrelation functions of $x_c(t, \tau_m)$ and $x_q(t, \tau_m)$ are equal, and finally, the third property states that $x_c(t, \tau_m)$ and $x_c(t + \tau, \tau_m + \Delta\tau_m)$, and $x_q(t, \tau_m)$ and $x_q(t + \tau, \tau_m + \Delta\tau_m)$ are also statistically independent for all τ and for all $\Delta\tau_m$ greater than $\delta\tau_m$.

For purposes of analysis of the NAV/SAT receiver performance in the presence of multipath, the diffuse multipath signal may be written as

$$e_{md}(t) \approx \sqrt{2C}\, x_c(t) \sin\left\{\omega_c t + d(t) + d_{ms}(t) + \theta(t-\tau_{ms})\right\} + \sqrt{2C}\, x_q(t) \cos\left\{\omega_c t + d(t) + d_{ms}(t) + \theta(t-\tau_{ms})\right\} \quad (55)$$

where $x_c(t)$ and $x_q(t)$ are statistically independent zero-mean Gaussian random variables having identical variances given by σ_m^2. The power density spectra of $x_c(t)$ and $x_q(t)$ are identical and equal to

$$\Phi_m(\omega) = \frac{1}{2} \frac{(2\sigma_m^2)}{\sqrt{\pi}\, B_m} e^{-(f/B_m)^2} \quad (56)$$

where $2\sigma_m^2$ and B_m are given by Eqs. (24) and (28). Note that $\Phi_m(\omega)$ is 1/2 that of $\Phi_{md}(\omega)$ given in Eq. (28). This is because the total power in $x_c(t)$ or $x_q(t)$ is σ_m^2, while the <u>total</u> relative diffuse multipath power is $2\sigma_m^2$.

This representation of the diffuse multipath signal, $e_{md}(t)$, over estimates the undesired effects of the diffuse multipath component on the performance of the NAV/SAT receiver if worst-case values of τ_{ms} are used. Consequently, it will be used in the Task II analysis. This is so because the representation using a single relative multipath time delay is a more coherent interference than the representation which considers the entire spread of delay.

2.4 Aircraft Antennas for Communication Links Employing Navigation Satellites

2.4.1 Introduction

The selection of suitable aircraft antenna types for use with navigation satellites is discussed in this section. Both subsonic and supersonic aircraft applications are considered in choosing suitable types. The difference in speed between these two aircraft models, however, is not such as to allow the use of highly protruding antenna types at the lower speed. These types of antennas offer greater flexibility in pattern synthesis than do the flush mounted types most suitable for supersonic use. Thus the choice must ultimately be made from a group of antennas which are either flush mounted or else protrude from the aircraft surface without disturbing the aerodynamic integrity of the aircraft. This latter requirement implies that only low profile types can be used. The conical spiral antenna, for example, is ruled out by the low profile requirement even though it offers many advantages in flexibility of pattern synthesis.

There has of course been substantial previous work in this area,[15,16,17] and commercial types supposedly optimized for satellite use have already appeared.[18] This previous work has attempted to optimize a design tradeoff between multipath rejection, achieved by suppressing radiation on or below the horizon, and substantial hemispherical coverage directed at good reception from several satellites which, it is felt, improves system accuracy in some instances.

As far as can be determined at present, simultaneous reception of signals from multiple satellites is not contemplated as a standard operational regime. According to the best information available concerning planned systems, satellite transmissions will be processed in sequence even when more than one satellite is visible at any given time. Thus the former rationale for the choice of a nearly hemispherical radiation pattern no longer applies, and other considerations are used to determine a desirable radiation pattern and an antenna design capable of producing the desired pattern.

In view of the analytical work carried out under the present phase of the contract, and in view of supporting data which are now available, it appears that the most important determinant of the radiation pattern (and the antenna design suitable for the synthesis of this pattern) is the requirement for multipath suppression from angles near to and below the horizon.

Table 2

Aircraft Antenna Characteristics

Frequency Response	1540-1660 MHz; Bandwidth exceeds BINOR requirements but is chosen to be compatible with projected ATS communications experiments
Polarization	Circular
VSWR	1.50 maximum
Axial Ratio	≤ 1 dB on axis ≥ 2 dB at ±45° from axis
Radiation Pattern	Axial, circularly symmetric pattern. Beamwidth 3 dB 80 - 90° 10 dB 150 - 160°
Gain	≈ 5 dB on axis referred to a C. P. isotrope
Beam Squint	<5°
Sidelobes	<- 15 dB over ground plane. Not seriously modified in operational environment
Power Handling Capacity	Receive: no requirement Transmit: 200-500 watts average power

2.4.2 Aircraft Antenna Requirements

The requirements for the antenna element are listed in Table 2. The assumption is made here that the aircraft is in nominally level flight. The effects of aircraft motion will be considered later. The influence of the aircraft environment on the desired free space pattern will also be considered. Some of the tabulated antenna design parameters are discussed in more detail in this section. The radiation pattern is discussed in the following section.

The operating frequency has been chosen in accordance with present plans for L-band NAV/SAT operation. The bandwidth exceeds that required for the BINOR waveform which occupies less than ±5 MHz bandwidth but has instead been chosen equal to the bandwidth of the projected L-band ATS-E and later ATS experiments. The required 100 MHz bandwidth is not a difficult design objective and is easily met by several types.

Circular polarization has been chosen as usual for this application. Partial depolarization, or reversal of handedness of polarization, occurs after reflection from the ocean surface and the reverse polarized signal is not accepted by the circularly polarized aircraft antenna. This may provide additional multipath rejection capability in addition to that given by the antenna radiation pattern itself.

Another element of the polarization requirement is the axial ratio, i.e. the ratio of major to minor axis of the (in general) elliptically polarized antenna. This is a measure of the deviation from exact circular polarization. For almost every antenna type which produces an axial pattern, circularity is best on the antenna axis and falls off monotonically with angle. The axial ratio is a measure of polarization loss and this loss will depend on the relative orientation of satellite and aircraft antenna axes. A careful power budget for such a link should take into account the polarization loss. A maximum axial ratio of 2 dB within a 90° cone has been specified.

The voltage standing wave ratio (VSWR) is specified as 1.50 maximum and this specification is easily realizable with several antenna types over the specified frequency band.

Beam squint has been specified to be less than 5°. This specification is included here because of the importance of maintaining pattern symmetry with respect to the antenna axis so that deviations from the planned antenna angular coverage near the horizon will not occur. Beam squint arises when balanced antennas (e.g. spirals, dipoles) are fed from unbalanced lines. In making the transition from an unbalanced line (e.g. coax) to a balanced antenna structure, there exists on the balanced structure an in-phase component of current as well as the normal anti-phase or transmission line mode currents, unless an extremely careful transformation from feed to radiator is made. This in-phase drive excites higher order modes of radiation from the antenna which add vectorially with the normal radiation to produce a squinted main beam. The allowable beam tilt is specified to be 5° maximum.

2.4.3 Radiation Pattern Characteristics

As has been mentioned the main emphasis in this work has been the control and suppression of multipath effects at the aircraft terminal due to reflections from ocean surfaces. The aircraft antenna radiation pattern is the main instrument used in effecting multipath suppression and will be specified here as carefully as possible. Again, the aircraft is considered to be in nominally level flight and the influence of the aircraft structure will not be considered in detail. It will be assumed that the radii of curvature of portions of the aircraft near the antenna are large compared with the carrier wavelength. This specification is not sufficient to eliminate any influence by the aircraft on the radiation patterns and, infact, in a detailed antenna design these effects cannot be disregarded. In carrying out a detailed design it is necessary to simulate the presence of the aircraft using either a mock-up of neighbouring metallic surfaces, or aircraft and antenna scale models in conjunction with frequency scaling.

Table 2 gives the specification of the radiation pattern. The desired pattern is a beam pattern with circular symmetry about the beam axis. The 3 dB beamwidth is set at 80-90° and the 10 dB beamwidth at 150-160°. The sidelobe level is specified as no greater than -15 dB when patterns are taken over a ground plane and this specification should not be seriously modified by the aircraft environment. The pattern is illustrated in Fig. 8 for an antenna mounted on the dorsal surface of a modern jet aircraft.

The radiation pattern shown is not an ideal pattern for the satellite aircraft link since signals from 10-45° above the horizon are suppressed from 3 to 10 dB. It is however well-suited for multipath suppression since signals from +10° are suppressed by at least 10 dB, and for signals from satellites at higher elevation angles multipath rejection will be greater than 15 dB due to antenna directivity alone. Suppression due to polarization reversal of the multipath signal will add to this 15 dB figure. In addition, this radiation pattern can be implemented in a flush mounted configuration.

The gain has been specified as a nominal 5 dB referred to a circularly polarized isotropic antenna. This specification is not critical and must be consistent with the specified pattern shape. The precise antenna gain can be determined from the full radiation pattern taken either on a scale model or with a mock-up of nearby aircraft surfaces as described earlier.

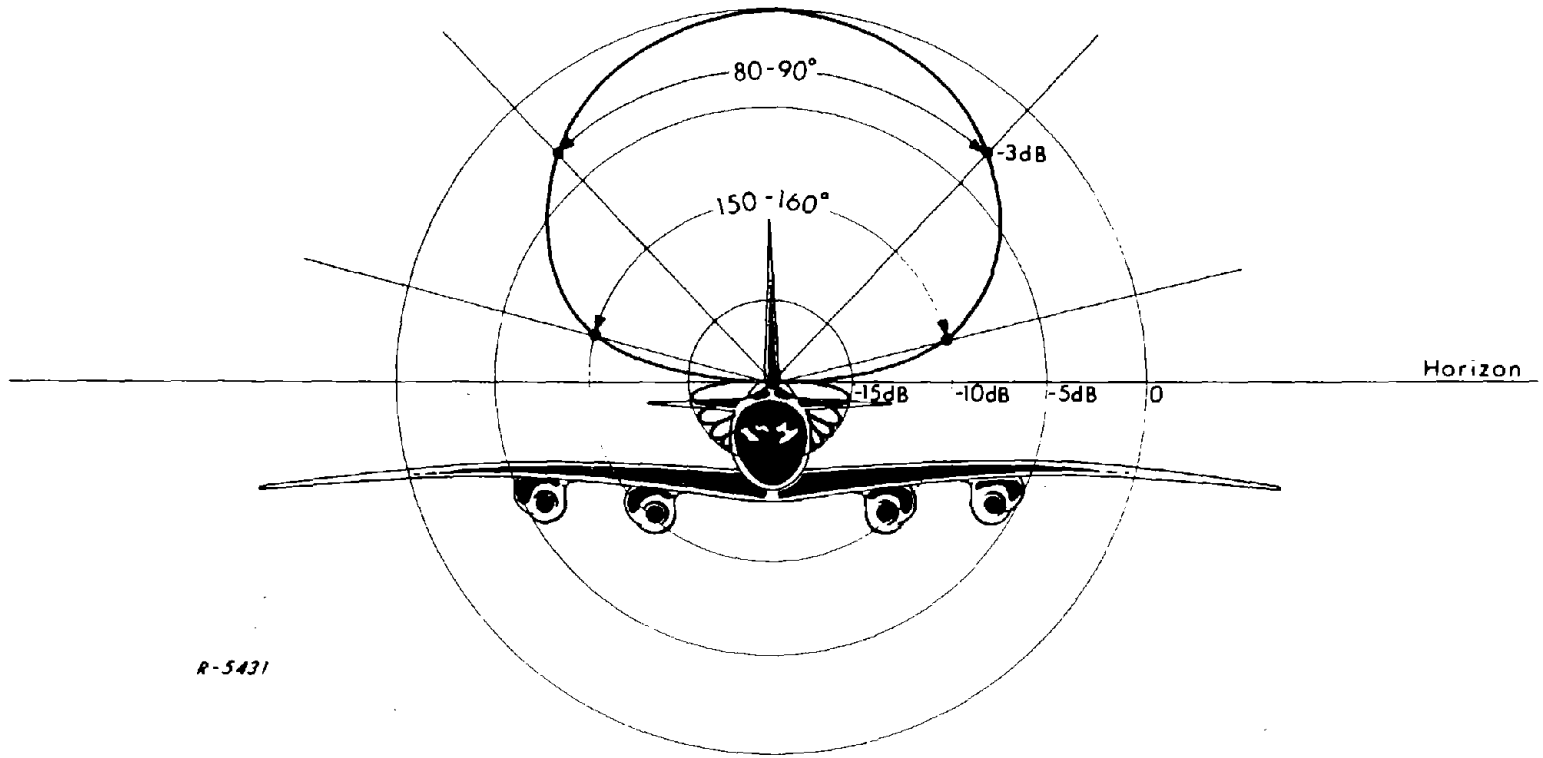

Fig. 8 Radiation Pattern for Multipath Rejection

2.4.4 Selection of Antenna Configuration

The performance characteristics of Table 2 constitute a difficult specification for the user aircraft antenna. Several antenna types do have the potential for meeting this specification if no constraint is placed on protrusion of the structure above the aircraft surface. However supersonic aircraft users cannot tolerate appreciable protrusions above the surface because of frictional heating effects and aerodynamic disturbances. This factor eliminates most candidate antenna designs which are not flush mounted. In particular, spiral antennas mapped onto conical structures are eliminated unless they can form part of a vertical tail member and maintain an unobstructed field of view. The advantages of the conical spiral are the number of design parameters available, including cone angle and spiral pitch, and the freedom from the requirement for a ground plane which lessens the dependence of the pattern on the aircraft structure. However, if this and other medium and high profile types are eliminated, the choice of a suitable element featuring good multipath rejection in accordance with the specification of Table 2 is made from a list of flush mounted or low profile types similar to that considered in the Interim Report of the present contract. These include cavity backed planar spirals (Archimedean or logarithmic i. e.), slotted flush mounted dipoles, curved dipole turnstiles and curved dipole crossed-slots. None of these types can be ruled out categorically when only L-band operation is considered since maximum protrusion above the aircraft surface is 2-2 1/2 inches for operation at 1600 MHz. The choice is dictated instead by considerations of radiation patterns. With the exception of the planar spirals, all of the types mentioned above produce hemispherical or near-hemispherical patterns (at least 0 dB over a 160° cone, referred to a C. P. isotrope). Such a pattern puts too much power on or near the horizon and all types producing such near-hemispherical patterns must be discarded.

Thus the cavity-backed planar spiral antenna emerges as the recommended choice for the SST-satellite link with good inherent multipath rejection capability. The choice between logarithmic and Archimedean is made on the basis of design and production costs. The Archimedean spiral is marginally simpler to design and fabricate and is recommended. A cost advantage might be obtained, however, from manufacturers with more experience in the design of logarithmic spirals and this latter approach is clearly acceptable.

Performance capabilities of the Archimedean two wire spiral antenna are compatible with the specification of Table 2. Most applications of the Archimedean spiral, in particular ECM use, have capitalized

on the wide bandwidths inherently available with this type. Manufacturers' catalogues show spirals with specifications maintained from 2-11 GHz. No commercial type appears to meet the present requirements completely but manufacturers see no deterrent to meeting the present specification completely. The theory of operation of this antenna is given in Section 3.4 of the Interim Report. The theory and applications are discussed in detail by Kaiser.[19]

2.4.5 Use of Switched Antennas

The formulation of the desired antenna pattern assumed that the aircraft was in level flight and that the satellite being utilized was essentially overhead. The effects on the multipath rejection capability of the aircraft antenna system of satellites at elevation angles well below the local zenith were not considered. Similarly when aircraft banking takes place during turns, the antenna being used in level flight operates in a less than optimum way. Thus the appearance of the satellite at low elevation angles increases the power arriving from a sector close to the horizon and thus potentially increases the multipath power received by the antenna; depending on the antenna pattern and aircraft orientation.

The addition of two antennas identical to the one specified in Table 2 can overcome most of the deleterious effects caused by the satellite appearing at low elevation angles relative to the aircraft. These additional antennas would be arranged circumferentially around the aircraft at the same longitudinal station as the primary antenna. This location would be chosen on the basis of adequacy of ground plane, absence of shadowing obstructions, etc. The situation is illustrated in Fig. 9. This system would be used as follows. When the satellite is at high and intermediate elevation angles antenna 2 is used in order to suppress multipath pick-up as much as possible. It should be noted that the angles of arrival at intermediate elevation angles are such that the direct signal will also be attenuated somewhat due to the pattern shape, and this should be taken into account in a detailed power budget. At satellite elevation angles below about 45°, antenna 1 or 3 (depending on aircraft heading) is used in order to maximize gain in the satellite direction. The appropriate antenna is selected by a simple switching arrangement.

In view of the low cost of the recommended basic antenna this approach appears to be an inexpensive and practical solution to the problems presented by the appearance of the synchronous satellites at various elevations with respect to the aircraft. And, in fact, even more elaborate arrangements of antennas and switching equipment can be envisaged in order to optimize multipath rejection by a simple, inexpensive antenna element.

Another possible configuration would use non-identical antennas. Primary coverage of a large overhead sector would be obtained using a spiral of the type discussed previously. Coverage of satellites at lower elevation angles would be obtained by the use of simple horn radiators (incorporating suitable arrangements for circular polarization) a few wavelengths in aperture width, producing a pattern with a 20-30 degree half-power beamwidth. This approach is practical at 1.6 GHz because of the aperture width. Switching arrangements would be similar to those mentioned above.

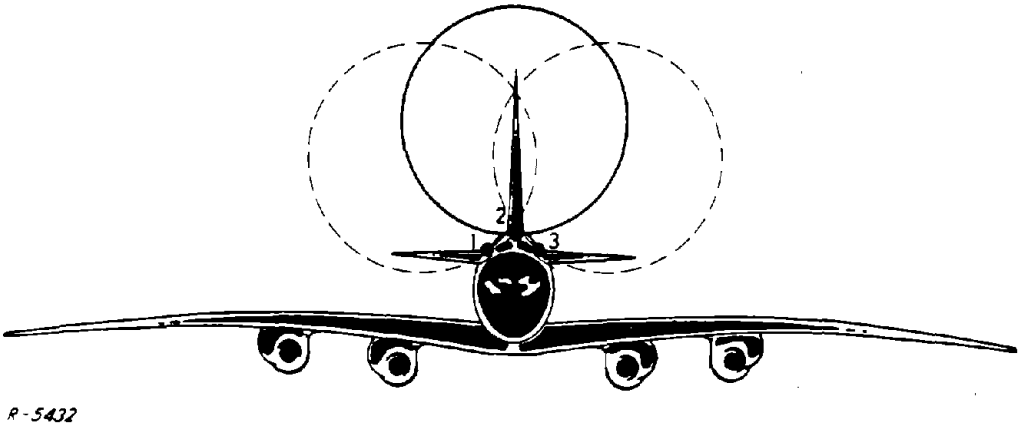

Fig. 9 Switchable Antenna Patterns to Compensate for In-Flight Maneuvers

3. BINOR ACQUISITION ANALYSIS

3.1 Summary

Calculations for the probability of correct acquisition of the BINOR code are made for three cases. In each subsequent case additional factors are included in the calculation. The three cases are:

a) Case where effects of multipath, carrier and clock loop phase jitter, and video filtering of the BINOR code in the receiver are neglected,

b) Case where effects of multipath are neglected but effects of carrier and clock loop phase jitter, and video filtering of the BINOR code in the receiver are included,

c) Case where multipath effects as well as the other effects are included.

The third case is, of course, the most complex, and is best understood in terms of the modifications required in the results of the first two cases.

Ranging accuracy is shown to be a function of the rms phase jitter in the clock loop. This phase jitter is shown to result from the presence of Gaussian noise and multipath components in the loop noise bandwidth.

3.2 System Model

A model of the NAV/SAT receiver is shown in functional block diagram form in Fig. 10. The functions of the various blocks are described in terms of their signal processing functions. These are most easily discussed in terms of case (a), in which multipath, and effects on acquisition of the BINOR code of phase jitter on the extracted carrier and clock loop reference signals are ignored. In this case the input RF signal may be written as

$$e_{RF}(t) = (2C)^{1/2} \sin [\omega_c t + d(t) + \beta b_{13}(t)] + n_{RF}(t) \quad (57)$$

where

C is the total received signal power;

ω_c is the carrier frequency and is $2\pi(1.6 \times 10^9)$ rad/sec.;

$d(t)$ is a slowly varying Doppler phase;

$b_{13}(t)$ is the BINOR code. It is generated by hard limiting 13 coherent equal amplitude square waves, each of which has a frequency 1/2 that of the next higher frequency square wave. The highest frequency square wave serves as the "clock" and has a frequency, $\omega_{c\ell}$, equal to $2\pi(320 \times 10^3)$ rad/sec. The frequency of the lowest frequency square wave is $2\pi(78.125)$ rad/sec.;

β is the phase deviation of the BINOR code on the RF carrier and is given as 1.15 radians; and,

$n_{RF}(t)$ is "white" Gaussian noise having double-sided noise power density denoted by $\Phi/2$.

The worst-case ratio C/Φ, including a 6 dB margin, is given as 35.7 dB-Hz.

The function of the carrier tracking loop is to acquire and track the carrier component of $e_{RF}(t)$, and use the extracted carrier as a reference signal to phase demodulate $e_{RF}(t)$, thereby producing the video signal $e_v(t)$ given by

$$e_v(t) = (C)^{1/2}(\sin\beta)\, b_{13}(t) + n_v(t) \qquad (58)$$

where $n_v(t)$ is "white" Gaussian noise of double-sided noise power density equal to $\Phi/2$.

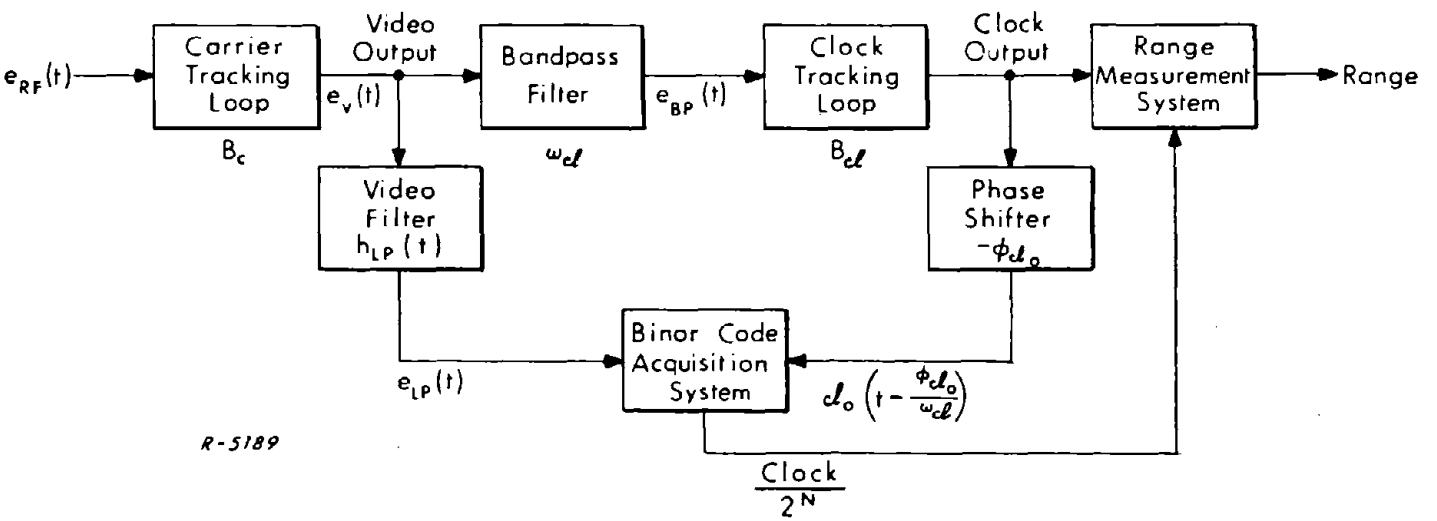

Fig. 10 Block Diagram of NAV/SAT Receiver Showing Basic Signal Processing Operations

This signal is bandpass filtered to extract the clock fundamental frequency, $\omega_{c\ell}$. This differs from an alternate configuration in which the clock loop is driven directly from the output of the lowpass filter. A careful analysis has shown that the phase variance for the alternate configuration is double that given by Eq.(61) below. Thus, by including the bandpass filter, performance is improved by 3 dB and approaches within 1 dB of the performance previously, but incorrectly assumed for the alternate configuration.

The output of the bandpass filter may be written as

$$e_{BP}(t) = (C)^{1/2} \sin\beta\, \rho_{13}\left(\frac{4}{\pi}\right) \sin \omega_{c\ell} t + n_{BP}(t) \tag{59}$$

where ρ_{13} is the correlation coefficient between $b_{13}(t)$ and $c\ell_o(t)$, the highest frequency square wave. (The correlation coefficients between $b_{13}(t)$ and each of its component square waves $c\ell_k(t)$ ($k = 0, 1, \cdots, 12$) are equal to ρ_{13}.) The factor $4/\pi$ is the relative amplitude of the first harmonic of $c\ell_o(t)$.* $n_{BP}(t)$ is Gaussian noise which has a flat noise power density (double-sided) of $\Phi/2$ over a bandwidth at least as wide as the clock loop noise bandwidth $B_{c\ell}$ centered around $\omega_{c\ell}$ (and $-\omega_{c\ell}$).

The function of the clock tracking loop is to acquire and track the clock frequency $\omega_{c\ell}$. The presence of $n_{BP}(t)$ results in a phase jitter on the extracted clock reference signal, $\phi_{c\ell_n}$, which is approximately Gaussian distributed and has a variance given by

$$\left\langle \phi^2_{c\ell_n} \right\rangle = \left(\frac{\Phi}{C}\right) \frac{B_{c\ell}}{\rho^2_{13} \sin^2\beta\left(\frac{8}{\pi^2}\right)} \tag{60}$$

where $2B_{c\ell}$ is the double-sided noise bandwidth of the clock loop and is determined by the requirement that the loop SNR is 10 dB at the worst-case value of (C/Φ):

$$(SNR)_L = \frac{\left(\frac{8}{\pi^2}\right) \rho^2_{13} \sin^2\beta}{(2B_{c\ell})} \left(\frac{C}{\Phi}\right)_o = 10 \tag{61}$$

*That $\rho_{13}(4/\pi)$ is the correlation coefficient between $b_{13}(t)$ and $\sin \omega_{c\ell} t$ may be seen by computing $\langle b_{13}(t) c\ell_o(t+\tau)\rangle$ which is found to equal $\rho_{13} \langle c\ell_o(t) c\ell_o(t+\tau)\rangle$ for all τ. $\langle b_{13}(t) \sin \omega_{c\ell_k} t\rangle = 4/\pi\, \rho_{13}$ is also true for $c\ell_1(t)$, but not for the other $c\ell_k(t)$ ($k \geq 2$).

With $(C/\Phi)_o = 35.7$ dB-Hz, and $\rho_{13} \tilde{=} 0.225586\ldots$, the required value of $(2B_{c\ell})$ is approximately 12.8 Hz. With this noise bandwidth the mean time to acquisition of the clock loop is approximately 0.4 sec.

Combining Eqs.(60) and(61)the phase variance may be written as

$$\left\langle \phi^2_{c\ell_n} \right\rangle = \frac{1}{20} \frac{(C/\Phi)_o}{(C/\Phi)} = \left\langle \phi^2_{c\ell_n} \right\rangle_a \tag{62}$$

during acquisition of the BINOR. During the range measurement the BINOR is turned off and only the clock square wave is transmitted (with phase deviation β). If an AGC system is used to decrease the signal gain in front of the clock loop in order to maintain the same loop noise bandwidth and damping coefficient, the loop SNR is modified by replacing ρ^2_{13} by 1 in Eq.(61) above. The result is that $(SNR)_L$ becomes equal to approximately 23 dB, and $\left\langle \phi^2_{c\ell_n} \right\rangle$

$$\left\langle \phi^2_{c\ell_n} \right\rangle = \rho^2_{13} \left\langle \phi^2_{c\ell_n} \right\rangle_a = \left\langle \phi^2_{c\ell_n} \right\rangle_r$$

$$= 0.0509 \left\langle \phi^2_{c\ell_n} \right\rangle_a \tag{63}$$

The variance of the clock loop phase jitter will be related to the rms range error in a later section. For purposes of acquisition analysis in case (a), the phase jitter on the extracted clock reference signal is ignored.

The phase shifter serves to compensate for phase shifts introduced in the video filter in a manner which will be explained in the discussion of case (b). Since the video filter is ignored in case (a), the effect of the phase shifter is also ignored, and the signal denoted by $e_{LP}(t)$ in Fig.10 is simply $e_v(t)$.

The BINOR code acquisition system serves to generate a square wave whose period is the same as that of the BINOR code and which is in phase with the lowest frequency square wave of the BINOR code. This is accomplished by successively frequency dividing down the extracted clock reference and comparing the phase of the resulting square waves with the phase of the corresponding square wave component of the received BINOR. The first divided down square wave is either in phase or 180^o out of phase with the corresponding square wave component in the received BINOR.

The phase is determined by multiplying the received BINOR by this divided down square wave, integrating the resulting product for a time ℓT (where T is the period of the BINOR code and ℓ is an integer), and sampling the output of the integrator. If the sampled output is positive, the square wave is assumed to have been in phase with the corresponding square wave of the BINOR code, whereas a 180^{o} phase relationship is assumed if the sampled output is negative. If the square wave was found to be in phase, it is frequency divided by two and the above process continued. If the square wave was found to be out of phase, it is first complemented and then frequency divided by two and the above process continued. If all decisions are made correctly the final frequency divided down square wave will be in phase with the BINOR code. This square wave is used in the range measurement system.

3.3 BINOR Code Acquisition Analysis - Case (a)

The purpose of an acquisition analysis is to determine the probability of correct acquisition in terms of the various parameters involved and to find out which value of ℓ must be used in the integrate and dump operation to insure at least a 99.9% probability of correct decision for the worst-case C/Φ.

On the assumption that the first (k - 1) decisions were made correctly, the output of the integrate and dump circuit at the end of the kth square wave acquisition is for case (a):

$$e_k = \pm(s_k + n_k) = \left(\int_0^{\ell T} (C)^{1/2} \sin\beta \; b_{13}(t) c\ell_k(t) dt + \int_0^{\ell T} n_v(t) \; c\ell_k(t) \; dt \right) \tag{64}$$

The "+" indicates the in phase case, and the "-" the out of phase case. $c\ell_k(t)$ is the kth frequency divided down square wave and is assumed in phase with the corresponding BINOR square wave component. The noise component of e_k is denoted by n_k and is Gaussian distributed with variance σ_k^2. The signal component of e_k is denoted by s_k and is

$$s_k = \ell T (C)^{1/2} \sin\beta \left\{ \frac{1}{\ell T} \int_0^{\ell T} b_{13}(t) c\ell_k(t) dt \right\} \tag{65}$$

The integral in brackets is the correlation coefficient between $b_{13}(t)$ and $c\ell_k(t)$ and is equal to ρ_{13} for all k, so that

$$s_k = \ell T(C)^{1/2} \sin\beta\ \rho_{13} \equiv \mu \tag{66}$$

for all k. The variance σ_k^2 is

$$\sigma_k^2 = \left\langle n_k^2 \right\rangle = \int_0^{\ell T} dt_1 \int_0^{\ell T} dt_2\ c\ell_k(t_1) c\ell_k(t_2) \left\langle n_v(t_1) n_v(t_2) \right\rangle \tag{67}$$

Since $n_v(t)$ is assumed "white",

$$\left\langle n_v(t_1)\ n_v(t_2) \right\rangle = \frac{\Phi}{2}\ \delta\ (t_1 - t_2) \tag{68}$$

where $\delta(t)$ is the unit impulse function. In this case σ_k^2 is easily seen to be given by

$$\sigma_k^2 = \frac{\Phi}{2}\ \ell T \equiv \sigma^2 \tag{69}$$

for all k.

The probability of correct acquisition of the kth divided down square wave, given that all preceeding (k - 1) divided down square waves were correctly acquired is

$$(P_c)_k = \int_{-s_k}^{\infty} P(\eta_k)\ d\eta_k \tag{70}$$

where $P(\eta_k)\ d\eta_k$ is the probability that the noise n_k lie between η_k and $\eta_k + d\eta_k$. The above is simply the probability that the sum $s_k + n_k$ be greater than zero, since only then will the sign of e_k be the same as the sign in front of the brackets in Eq. (64). For a Gaussian distributed n_k, $P(\eta_k)$ is

$$P(\eta_k) = \frac{1}{\sqrt{2\pi}\,\sigma_k}\ e^{-\eta_k^2 / 2\sigma_k^2} \tag{71}$$

so that

$$(P_c)_k = \int_{-s_k}^{\infty} P(\eta_k)\, d\eta_k = \int_{-\infty}^{s_k} P(\eta_k)\, d\eta_k = \int_{-\infty}^{o} P(\eta_k)\, d\eta_k + \int_{o}^{s_k} P(\eta_k)\, d\eta_k$$

$$= \frac{1}{2} + \frac{1}{2}\,\frac{2}{\sqrt{\pi}} \int_{o}^{\zeta_k} e^{-\zeta^2}\, d\zeta = \frac{1}{2}\,[1 + \mathrm{erf}(\zeta_k)] \qquad (72)$$

where $\zeta = \eta_k/\sqrt{2}\ \sigma_k$ and $\zeta_k = s_k/\sqrt{2}\ \sigma_k = \mu/\sqrt{2}\,\sigma$. The total probability of correct acquisition, $(P_c)_T$, is

$$(P_c)_T = \prod_{k=1}^{12} (P_c)_k = \left\{\frac{1}{2}[1 + \mathrm{erf}(\mu/\sqrt{2}\,\sigma)]\right\}^{12} \qquad (73)$$

for case (a).

The ratio $\mu/\sqrt{2}\,\sigma$ is

$$\mu/\sqrt{2}\ \sigma = \rho_{13} \sin\beta \sqrt{\ell T} \sqrt{\frac{C}{\Phi}} \qquad (74)$$

At the worst case C/Φ, this is

$$(\mu/\sqrt{2}\ \sigma)_o = \rho_{13} \sin\beta \sqrt{\ell T} \sqrt{(\frac{C}{\Phi})_o} \qquad (75)$$

with the correlation coefficient given by*

$$\rho_{13} = (\tfrac{1}{2})(\tfrac{3}{4})(\tfrac{5}{6})(\tfrac{7}{8})(\tfrac{9}{10})(\tfrac{11}{12}) = 0.225586\ldots$$

$$\sin\beta = \sin(1.15) = 0.912764$$

$$\sqrt{T} = (78.125)^{-1/2} = 0.113137$$

$$(C/\Phi)_o = 35.7\ \text{dB-Hz} = 3715.35$$

$$\sqrt{(\frac{C}{\Phi})_o} = 60.9537$$

$$(\mu/\sqrt{2}\ \sigma)_o = 1.41996\sqrt{\ell} \approx 1.420\sqrt{\ell} \qquad (76)$$

*Stiffler.

For $(P_c)_T = 99.9\% = 0.9990$, $(P_\epsilon)_T = 1 - (P_c)_T = 0.0010$. This is approximately equal to

$$(P_\epsilon)_T \approx 12 \; \frac{1}{2}\left[1 - \mathrm{erf}(\mu/\sqrt{2}\,\sigma)_o\right] = 0.0010$$

or

$$\left[1 - \mathrm{erf}\,(\mu/\sqrt{2}\,\sigma)_o\right] \approx 0.00016667 = \mathrm{erfc}(\mu/\sqrt{2}\,\sigma)_o \quad (77)$$

By using tables for erfc x (c.f. Abramowitz and Stegun, Handbook of Mathematical Functions, Dover Publications, 1965, p. 316), and using linear extrapolation, the required value of $(\mu/\sqrt{2}\,\sigma)_o$ is found to be

$$\left[\left(\frac{\mu}{\sqrt{2}\,\sigma}\right)\right]_{o_{\min}} \cong 2.663 \quad (78)$$

which agrees with results obtained for this case by others.

For $\ell = 3$ and $\ell = 4$, $(\mu/\sqrt{2}\,\sigma)_o$ equals

$$\left(\frac{\mu}{\sqrt{2}\,\sigma}\right)_o = \begin{cases} 2.459 & \ell = 3 \\ 2.840 & \ell = 4 \end{cases} \quad (79)$$

Consequently the required value of ℓ in this case is $\ell = 4$.

3.4 BINOR Code Acquisition Analysis - Case (b):

In this case the additional effects of carrier and clock loop phase jitter and video filtering are included. Under the assumption that both carrier and clock loops may still be treated as linear systems in the tracking mode (corresponding to the assumption of small phase jitter and/or tracking error), the carrier loop phase error consists of the sum of a tracking error, denoted by ϕ_{ct}, and a Gaussian distributed phase jitter, denoted by ϕ_{cn}, which results from the presence of Gaussian noise at the input to the carrier-tracking loop. In a second-order loop, the tracking error is

$$\phi_{ct} = \frac{\ddot{d}(t)}{\omega_n^2} = \frac{2\pi f_c}{c}\,\frac{\ddot{r}(t)}{\omega_n^2} = \frac{2\pi f_c}{\omega_n^2}\,\frac{g}{c}\left(\frac{\ddot{r}}{g}\right) \quad (80)$$

where

$$\omega_n = \frac{2B_c}{\left(\zeta_c + \frac{1}{4\zeta_c}\right)} \tag{81}$$

and $2B_c$ is the double-sided loop noise bandwidth ($2B_c = 50$ Hz) and ζ_c is the damping factor ($\zeta_c = 1/\sqrt{2}$). The factor $\ddot{r}(t)$ is the acceleration along the aircraft-satellite line-of-sight vector in ft/sec^2, and "g" is the acceleration due to gravity ($g = 32.2$ ft/sec^2). With $f_c = 1.6 \times 10^9$ Hz, ϕ_{ct} is

$$\phi_{ct} = 0.146\left(\frac{\ddot{r}}{g}\right) \tag{82}$$

The variance of the phase jitter ϕ_{cn} is

$$\left\langle \phi_{cn}^2 \right\rangle = \left(\frac{\Phi}{C}\right) \frac{B_c}{\cos^2 \beta}$$

$$= \frac{B_c}{\cos^2 \beta \left(\frac{C}{\Phi}\right)_o} \frac{(C/\Phi)_o}{(C/\Phi)} \tag{83}$$

$$= [0.04033] \frac{(C/\Phi)_o}{(C/\Phi)}$$

The sum of $\phi_{ct} + \phi_{cn}$ is denoted by ϕ_c. The video output, $e_v(t)$, is now

$$e_v(t) = (C)^{1/2} \sin\beta \cos\phi_c(t) b_{13}(t) + n_v(t) \tag{84}$$

and the output of the bandpass filter at the input to the clock loop is

$$e_{BP}(t) = (C)^{1/2} \sin\beta \cos\phi_c(t) \frac{4}{\pi} \rho_{13} \sin \omega_{c\ell} t + n_{BP}(t) \tag{85}$$

If $\phi_c(t)$ is small, its effect on the clock phase jitter through the term $\cos\phi_c(t)$ in Eq. (85) may be neglected, so that $\left\langle \phi_{c\ell_r}^2 \right\rangle$ is to a first approximation unchanged from the results given in Eqs. (62) and (63).

The output of the lowpass filter, whose impulse response is $h_{LP}(t)$ is

$$e_{LP}(t) = (C)^{1/2} \sin\beta \cos\phi_c(t)\left(b_{13} \otimes h_{LP}\right)_t + \left(n_v \otimes h_{LP}\right)_t \qquad (86)$$

where $\otimes$ denotes the operation of convolution.

The output of the k^{th} integrate and dump circuit (Eq. (8)) is modified to

$$e_k = \pm(s_k + n_k) = \pm\left(\int_o^{\ell T} dt(C)^{1/2} \sin\beta \cos\phi_c(t)\left(b_{13} \otimes h_{LP}\right)_t c\ell_k\left(t - t_o + \frac{\phi_{c\ell_n}(t)}{\omega_{c\ell}}\right)\right.$$

$$\left. + \int_o^{\ell T} dt\left(n_v \otimes h_{LP}\right)_t c\ell_k\left(t - t_o + \frac{\phi_{c\ell_n}(t)}{\omega_{c\ell}}\right)\right) \qquad (87)$$

where the effects of carrier loop phase jitter, video filtering, clock loop phase jitter, and the phase shifter delay

$$t_o = \frac{\phi_{c\ell_o}}{\omega_{c\ell}}$$

have been introduced. Since these effects are small, they may be treated as perturbing influences in the calculation of $(P_c)_k$ and $(P_c)_T$, in that only their dominant or lowest order effects need be considered.

The noise n_k is still Gaussian, although its variance σ_k^2 is slightly modified as a result of the combined effects of video filtering and multiplication by the k^{th} frequency-divided-down clock. The effect of clock jitter on the computation of σ_k^2 is negligible and may therefore be neglected. This is shown in Appendix A where σ_k^2 is written as

$$\sigma_k^2 = \sigma^2 \gamma_k^2 \qquad (88)$$

and where γ_k^2 is seen to be slightly less than 1 for the case where $h_{LP}(t)$ is a single-pole lowpass filter whose 3 dB bandwidth is made equal to the fifth harmonic of the clock. That is

$$h_{LP}(t) = \alpha e^{-\alpha t} \underline{u}_1(t) \qquad (89)$$

where $\alpha = 5\omega_{c\ell}$. A reasonably good approximation to $(P_c)_k$ may be obtained by using the expected value of s_k in Eq.(72). This over estimates $(P_c)_k$ somewhat, but only slightly. A more exact treatment would involve computing the expectation value of $(P_c)_k$. One way of doing this is to expand $(P_c)_k$ in a Taylor series about $(P_c)_k$ evaluated at the expectation value of s_k. This would require knowledge of the higher order statistics of s_k, and begins to get quite involved, even for second order statistics. Consequently it was felt that since $\phi_c(t)$ and $\phi_{c\ell_n}(t)$ are small, a more exact treatment would not contribute anything of significance in relation to the effort which would be required.

The expectation value of s_k is shown in Appendix B to be given by

$$\langle s_k \rangle = \mu e^{-\frac{1}{2}\sigma_{cn}^2} \cos \phi_{ct} E_{\phi_{c\ell_n}} \left(\chi_k \left(t_o - \frac{\phi_{c\ell_n}}{\omega_{c\ell}} \right) \right) \tag{90}$$

where

$$\mu = \ell T (C)^{1/2} \rho_{13} \sin\beta \tag{91}$$

$$e^{-\frac{1}{2}\sigma_{cn}^2} = E_{\phi_{cn}} \left(\cos \phi_{cn} \right) \tag{92}$$

$$\sigma_{cn}^2 = \left\langle \phi_{cn}^2 \right\rangle \tag{93}$$

$$\chi_k(\tau) \equiv \frac{1}{\rho_{13}} \int_{-\infty}^{\infty} d\xi h_{LP}(\xi) \psi_{c\ell_k b_{13}}(\tau - \xi) \tag{94}$$

and

$$\psi_{c\ell_k b_{13}}(\tau) = \frac{1}{\ell T} \int_o^{\ell T} b_{13}(t) c\ell_k(t + \tau) dt \tag{95}$$

The phase shifter time delay, t_o, is chosen so as to maximize χ_k when $\phi_{c\ell_n} = 0$. This choice of t_o yields the maximum $\langle s_k \rangle$ possible and also minimizes the effects of $\phi_{c\ell_n}$ on acquisition.

Since t_o is small, and since $|\phi_{c\ell_n}|$ is less than 90^o with very high probability for values of (C/Φ) greater than $(C/\Phi)_o$, it is only necessary to compute $\chi_k(\tau)$ for $|\tau| < T_{c\ell}/4 = 2\pi/4\omega_{c\ell}$. For $h_{LP}(t)$ as given in

Eq. (89), transient behavior may be considered to have almost completely died out after a time $t = T_{c\ell}/4$. Consequently, it is only necessary to compute $\psi_{c\ell_k b_{13}}(\tau)$ for $|\tau| < T_{c\ell}/2$. In this range, it may be shown* that $\psi_{c\ell_k b_{13}}(\tau)$ is given by

$$\psi_{c\ell_k b_{13}}(\tau) = \rho_{13}\left(1 - (1 - a_k)\frac{|\tau|}{(T_{c\ell}/2)}\right), \text{ for } |\tau| < \frac{T_{c\ell}}{2} \tag{96}$$

where a_k is the ratio of $\psi_{c\ell_k b_{13}}(T_{c\ell}/2)$ to $\psi_{c\ell_k b_{13}}(0)$, and is given in Table 3 below.

Table 3

VALUES OF a_k AND $(1 - a_k)$ AS A FUNCTION OF k

k	a_k	$(1 - a_k)$
1	0	1.0
2	1008/1848 = 0.545454...	0.454545...
3	1512/1848 = 0.818181...	0.181818...
4	1736/1848 = 0.93939...	0.060606...
5	1820/1848 = 0.984848...	0.015151...
6	1844/1848 = 0.997835...	0.0021645...
7-12	1.0	0

For the single-pole lowpass filter whose impulse response is given in Eq. (89), $\chi_k(\tau)$ is approximately

$$\chi_k(\tau) \cong 1 + \frac{1}{\alpha T_{c\ell}/2}(1 - a_k)(\alpha\tau - 1) \qquad -\frac{T_{c\ell}}{4} \lesssim \tau < 0 \tag{97}$$

*This was done by computing the BINOR code b_{13} bit by bit and evaluating $\psi_{c\ell_k b_{13}}(\tau)$ at $\tau = 0$ and $\tau = \pm T_{c\ell}/2$. This calculation of the BINOR code b_{13} and $\psi_{c\ell_k b_{13}}(\tau)$ was facilitated by making extensive use of readily derived properties of BINOR codes and the functions $\psi_{c\ell_k b_{13}}(\tau)$. A discussion of these calculations is somewhat lengthy and is therefore not presented.

$$\chi_k(\tau) = 1 + \frac{1}{\alpha T_{c\ell}/2}(1 - a_k)(\alpha\tau - 1)$$

$$- \frac{1}{\alpha T_{c\ell}/4}(1 - a_k)[(\alpha\tau - 1) + e^{-\alpha\tau}] \qquad (98)$$

$$0 < \tau < \frac{T_{c\ell}}{2}$$

where

$$\alpha = 5\omega_{c\ell} = \frac{10\pi}{T_{c\ell}} = \frac{5\pi}{T_{c\ell}/2} \qquad (99)$$

and

$$\tau = t_o - \phi_{c\ell_n}/\omega_{c\ell} = \left(\phi_{c\ell_o} - \phi_{c\ell_n}\right)\Big/\omega_{c\ell} \qquad (100)$$

Introducing Eqs. (99) and (100) into the above expressions for $\chi_k(\tau)$, Eqs. (97) becomes

$$\chi_k\left(\frac{\phi_{c\ell_n}}{\omega_{c\ell}} - t_o\right) = 1 + \frac{1}{5\pi}(1 - a_k)\left(5\phi_{c\ell_o} - 1\right) - \frac{1}{\pi}(1 - a_k)\phi_{c\ell_n} \qquad (101)$$

$$\phi_{c\ell_n} > \phi_{c\ell_o}$$

and

$$\chi_k\left(\frac{\phi_{c\ell_n}}{\omega_{c\ell}} - t_o\right) = 1 + \frac{1}{5\pi}(1 - a_k)\left(5\phi_{c\ell_o} - 1\right) - \frac{1}{\pi}(1 - a_k)\phi_{c\ell_n}$$

$$- \frac{2}{5\pi}(1 - a_k)\left(5\phi_{c\ell_o} - 1 + e^{-5\phi_{c\ell_o}} e^{5\phi_{c\ell_n}}\right) + \frac{2}{\pi}(1 - a_k)\phi_{c\ell_n} \qquad (102)$$

$$\phi_{c\ell_n} < \phi_{c\ell_o}$$

With $\phi_{c\ell_n} = 0$, $\phi_{c\ell_o}$ is chosen so that $\chi_k(-t_o) = (\chi_k)_{max}$. Differentiating Eq. (102) with respect to $\phi_{c\ell_o}$ and setting the derivative equal to zero, and putting $\phi_{c\ell_n} = 0$, $\phi_{c\ell_o}$ is found to be

$$\phi_{c\ell_o} = \frac{1}{5}\ell n\, 2 \qquad (103)$$

and $(\chi_k)_{max}$ is

$$(\chi_k)_{max} = 1 - \frac{1}{5\pi}(1 - a_k)\ell n\, 2 \tag{104}$$

With $\epsilon_k = \frac{1}{5\pi}(1 - a_k)$, and $\sigma^2_{c\ell_n} = \left\langle \phi^2_{c\ell_n} \right\rangle$, $E_{\phi_{c\ell_n}}\left(\chi_k\left[\left(\phi_{c\ell_n} - \phi_{c\ell_o}\right)/\omega_{c\ell}\right]\right)$

of Eq.(90) is shown (in Appendix C) to be given by

$$E_{\phi_{c\ell_n}}\left(\chi_k\left[\left(\phi_{c\ell_n} - \phi_{c\ell_o}\right)/\omega_{c\ell}\right]\right) = 1 - \epsilon_k\left\{-(1 - \ell n2)\,\mathrm{erf}\left(\frac{\ell n2}{\sqrt{2}\,5\sigma_{c\ell_n}}\right)\right.$$

$$+\left(\frac{5\sigma_{c\ell_n}}{\sqrt{2}}\right)\frac{2}{\sqrt{\pi}}\, e^{-\left(\frac{\ell n2}{\sqrt{2}\,5\sigma_{c\ell_n}}\right)^2}$$

$$\left. + e^{\left(\frac{5\sigma_{c\ell_n}}{\sqrt{2}}\right)^2}\,\frac{1}{2}\left[1 - \mathrm{erf}\left(\frac{5\sigma_{c\ell_n}}{\sqrt{2}} - \frac{\ell n2}{\sqrt{2}\,5\sigma_{c\ell_n}}\right)\right]\right\} \tag{105}$$

Alternatively, $E_{\phi_{c\ell_n}}\left(\chi_k\left[\left(\phi_{c\ell_n} - \phi_{c\ell_o}\right)/\omega_{c\ell}\right]\right)$ may be written as

$$E_{\phi_{c\ell_n}}\left(\chi_k\left[\left(\phi_{c\ell_n} - \phi_{c\ell_o}\right)/\omega_{c\ell}\right]\right) = (\chi_k)_{max} - \epsilon_k\left\{\left(\frac{5\sigma_{c\ell_n}}{\sqrt{2}}\right)\frac{2}{\sqrt{\pi}}\, e^{-\left(\frac{\ell n2}{\sqrt{2}\,5\sigma_{c\ell_n}}\right)^2}\right.$$

$$+ e^{\left(\frac{5\sigma_{c\ell_n}}{\sqrt{2}}\right)^2}\,\frac{1}{2}\left[1 + \mathrm{erf}\left(\frac{\ell n2}{\sqrt{2}\,5\sigma_{c\ell_n}} - \frac{5\sigma_{c\ell_n}}{\sqrt{2}}\right)\right]$$

$$\left. - \mathrm{erf}\left(\frac{\ell n2}{\sqrt{2}\,5\sigma_{c\ell_n}}\right) - \ell n2\left[1 - \mathrm{erf}\left(\frac{\ell n2}{\sqrt{2}\,5\sigma_{c\ell_n}}\right)\right]\right\} \tag{106}$$

or

$$E_{\phi_{c\ell_n}}\left(\chi_k\left[\left(\phi_{c\ell_n}-\phi_{c\ell_o}\right)/\omega_{c\ell}\right]\right)=(\chi_k)_{max}-\epsilon_k\Gamma\left(\sigma_{c\ell_n}\right)$$

Curves of $E_{\phi_{c\ell_n}}\left(\chi_k\left[\left(\phi_{c\ell_n}-\phi_{c\ell_o}\right)/\omega_{c\ell}\right]\right)$ as a function of $\sigma_{c\ell_n}$ are shown in Fig. 11

The probability of correct acquisition of the k^{th} frequency-divided-down square wave component, given that all previous (k - 1) components were correctly acquired, is now given by

$$(P_c)_k=\frac{1}{2}\left\{1+\operatorname{erf}\left[\frac{\mu}{\sqrt{2}\,\sigma}\left(e^{-\frac{1}{2}\sigma_{cn}^2}\cos\phi_{ct}\left[\frac{(\chi_k)_{max}}{\gamma_k}-\frac{\epsilon_k}{\gamma_k}\Gamma\left(\sigma_{c\ell_n}\right)\right]\right)\right]\right\} \qquad (107)$$

and, again, the total probability of correct decision, $(P_c)_T$, is,

$$(P_c)_T=\prod_{k=1}^{12}(P_c)_k \qquad (108)$$

It is interesting to compute the ratio of $(\chi_k)_{max}$ to γ_k, since the deviation of this ratio from 1 is a result of the lowpass filter $h_{LP}(t)$. The effect of the filter was seen to (1) round the peak of the function $\chi_k(\tau)$ and reduce its maximum from 1 to $(\chi_k)_{max}$, and (2) reduce the variance of the noise component at the output of the integrate and dump circuit by a factor γ_k^2. The rounding of the peak of $\chi_k(\tau)$ reduces the effects of clock jitter on acquisition, since, if the phase shifter phase $\phi_{c\ell_o}$ is chosen properly, the first order effect of $\phi_{c\ell_n}$ on acquisition probability is zero (corresponding to $\Gamma(\sigma_{c\ell n})$ having zero derivative at $\sigma_{c\ell_n}=0$). Consequently, if the ratio of $(\chi_k)_{max}$ to γ_k is not too much less than 1, the effect of the lowpass video filter $h_{LP}(t)$ is to improve the probability of correct acquisition by reducing its sensitivity to small clock jitter. The values of this ratio are given in Table 4, where it is seen that this ratio is indeed very close to 1, and even exceeds 1 slightly for $k > 4$.

Curves of $(P_c)_T$ computed from Eq. (73) and Eqs.(108) and(107) with $\phi_{ct}=0$ are presented in Fig. 12 as a function of $(C/\Phi)/(C/\Phi)_o$. In these curves it is seen that a value of $\ell = 4$ is required if a 99.9% probability of correct acquisition is to be achieved with a 6 dB margin allowance

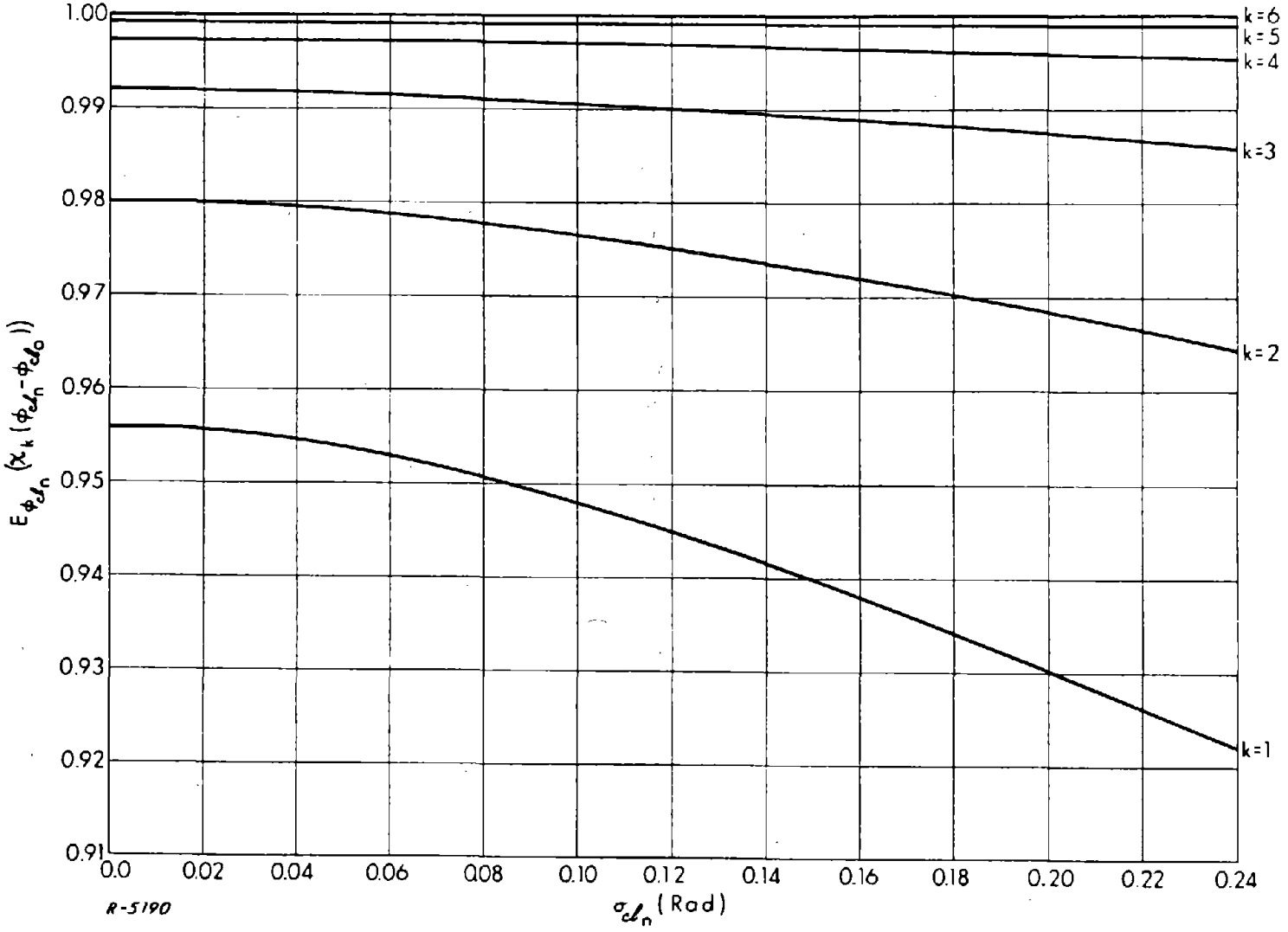

Fig. 11 $E_{\phi_{c\ell_n}}\left(\chi_k\left[\left(\phi_{c\ell_n}-\phi_{c\ell_o}\right)/\omega_{c\ell}\right]\right)$ vs. $\sigma_{c\ell_n}$ for k = 1, 2, ..., 6

(i.e., for $(C/\Phi)_o$ = 35.7 dB-Hz). If the margin allowance is reduced to 5 dB, the required acquisition probability may be achieved with ℓ = 3. A 3 dB margin allowance will permit the required acquisition probability to be achieved with ℓ = 2. If no circuit margin is required, ℓ = 1 is sufficient to achieve 99.9% acquisition probability.

Table 4

VALUES OF $(\chi_k)_{max}/\gamma_k$ FOR k = 1, 2, ···, 12

k	$(\chi_k)_{max}$	γ_k	$(\chi_k)_{max}/\gamma_k$
1	0.955873	0.967646	0.987834
2	0.979942	0.983956	0.995921
3	0.991977	0.992011	0.999966
4	0.997326	0.996013	1.001318
5	0.999331	0.998009	1.001327
6	0.999904	0.999005	1.000900
7	1.00	0.999502	1.000498
8	1.00	0.999751	1.000249
9	1.00	0.999875	1.000125
10	1.00	0.999938	1.000062
11	1.00	0.999969	1.000031
12	1.00	0.999984	1.000016

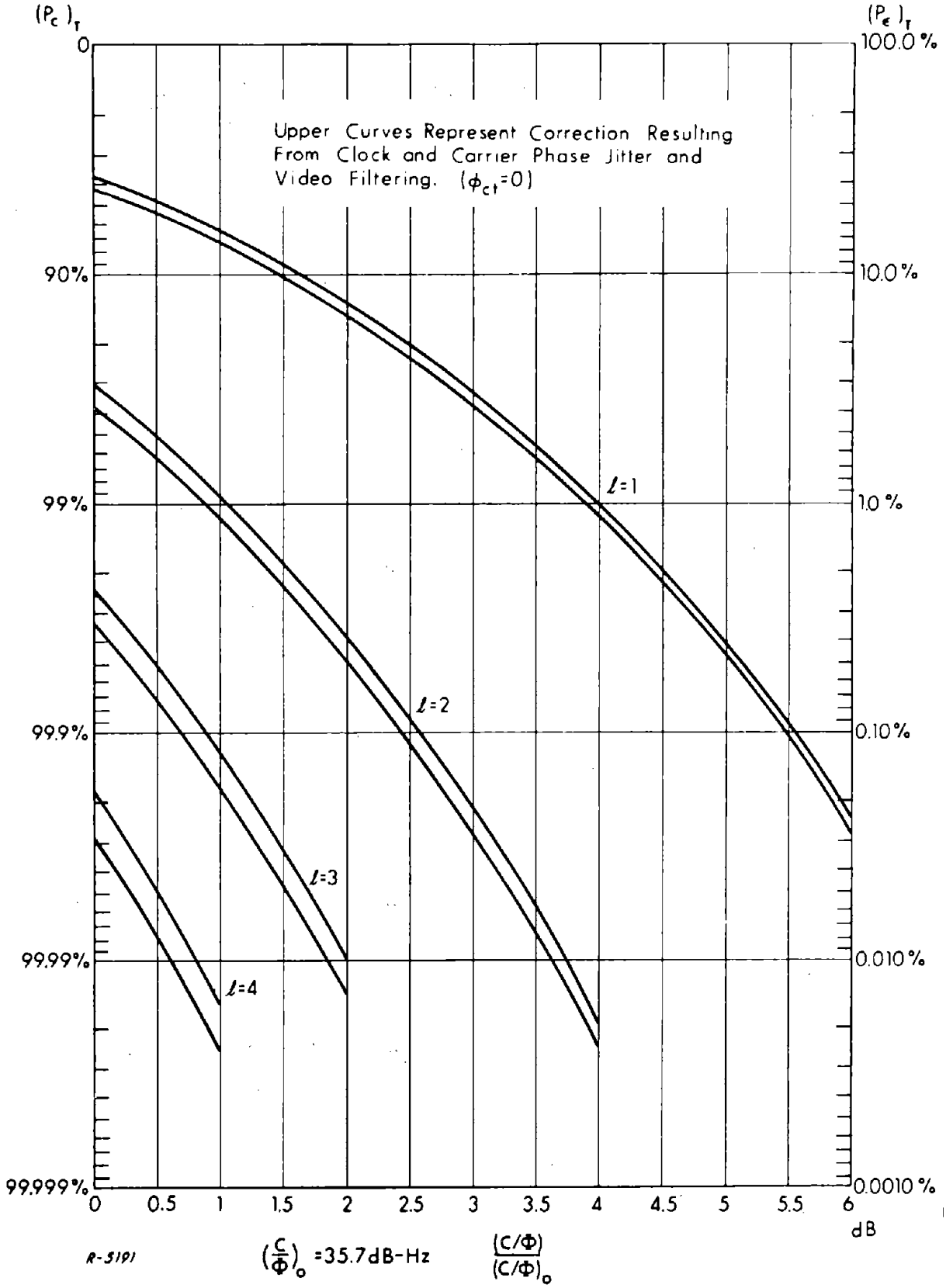

Fig. 12 Correction to Acquisition Probability Resulting from Clock and Carrier Jitter and Video Filtering (ϕ_{ct} = 0)

3.5 BINOR Code Acquisition Analysis - Case (c)

3.5.1 Characterization of the RF Multipath Signal

In this section a specular and a diffusely scattered multipath return is added to $e_{RF}(t)$ and their effects traced through the NAV/SAT receiver.

The specular multipath component of $e_{RF}(t)$ arises from coherent specular scattering of the transmitted signal from a very small region of the sea surface consisting essentially of the first Fresnel zone. This component of $e_{RF}(t)$ may be written as

$$e_{RF}(t)_{ms} = \sqrt{2C}\, a_{ms} \sin[\omega_c t + d(t) + d_{ms}(t) + \beta b_{13}(t - \tau_{ms})] \qquad (109)$$

where a_{ms} is the relative amplitude of the specular multipath component, τ_{ms} is the relative delay of the specular multipath component, and $d_{ms}(t)$ is the relative specular multipath Doppler phase given by

$$d_{ms}(t) = \int_{-\infty}^{t} \omega_{ms}(t)dt + \phi_{ms} \qquad (110)$$

Here ω_{ms} is the relative specular multipath Doppler frequency, and ϕ_{ms} is the initial phase of $d_{ms}(t)$.

The diffuse multipath component of $e_{RF}(t)$ arises from incoherent scattering of the transmitted signal from a much larger region of the sea surface centered on the specular region. If the modulation delays are taken to be essentially the same as for the specular scattering, this component of $e_{RF}(t)$ may be written as

$$e_{RF}(t)_{md} = \sqrt{2C}\, x_c(t)\sin[\omega_c t + d(t) + d_{ms}(t) + \beta b_{13}(t - \tau_{ms})] + \sqrt{2C}\, x_q(t)\cos[\omega_c t + d(t) + d_{ms}(t) + \beta b_{13}(t - \tau_{ms})] \qquad (111)$$

where $x_c(t)$ and $x_q(t)$ are independent Gaussian random variables having identical variances denoted by σ_m^2, and τ_{ms} is the delay associated with the specular multipath component.

Additional properties of the random functions $x_c(t)$ and $x_q(t)$ are

1) The cross correlation function $\langle x_c(t)x_q(t + \tau)\rangle$ is zero for all τ, and

2) The autocorrelation functions $\langle x_c(t)x_c(t + \tau)\rangle$ and $\langle x_q(t)x_q(t + \tau)\rangle$ are equal and may be denoted by $\phi_m(\tau)$.

The autocorrelation function $\phi_m(\tau)$ and its Fourier transforms, $\Phi_m(\omega)$ depend on such factors as the aircraft velocity, the sea state, the grazing angle, the wavelength of the incident radiation, and the aircraft altitude.

The presence of the multipath causes increased carrier and clock loop phase jitters and introduces extraneous components at the outputs of the integrate and dump filters. These can all affect the probability of correct acquisition of the BINOR. The multipath interference contains both deterministic and random elements. This is so because it consists of the reflection of a deterministic signal off a random rough surface. It should be expected that both of these features of the multipath interference will play a role in determining its effects on system performance. This is indeed the case.

3.5.2 Treatment of the Probability of Correct Acquisition

In estimating the effects of multipath on system performance it is necessary to compromise between the desire for a complete statistical description of these effects and the effort required to attain such a description. In discussing the probability of correct acquisition of the BINOR code, consideration is limited to a computation of the expected or average probability of correct acquisition obtained by averaging over appropriate random variables of the multipath interference. While this is not a complete statistical description of the probability of correct acquisition, it is still the most useful single statistical parameter in the case where the effects of multipath are small. It is also the simplest parameter to obtain, involving as it does no higher than second order statistics of the random multipath signal parameters. Confining the analysis to a computation of the average probability of correct acquisition is useful if the computation predicts that the effects of the multipath are small even when worst-case bounds are placed on the statistical parameters of the multipath interference, and if the objective is to determine whether or not the presence of a small multipath interference presents a serious problem.

In addition to the average probability of correct acquisition, additional worst-case possibilities are considered and estimates made of the frequency of occurrence of these worst-case conditions. The probability of correct acquisition under these additional worst-case conditions are computed.

3.5.3 Effects of Multipath on Carrier Loop Phase Jitter

The contribution of the multipath to the phase jitter on the carrier-tracking loop is now computed. The carrier component of $e_{RF}(t)$ is

$$\begin{aligned} e_c(t) &= \sqrt{2C}\,\cos\beta\,\sin[\omega_c t + d(t)] + n_c(t) \\ &+ \sqrt{2C}\,\cos\beta\,a_{ms}\,\sin[\omega_c t + d(t) + d_{ms}(t)] \\ &+ \sqrt{2C}\,\cos\beta\,x_c(t)\sin[\omega_c t + d(t) + d_{ms}(t)] \\ &+ \sqrt{2C}\,\cos\beta\,x_q(t)\cos[\omega_c t + d(t) + d_{ms}(t)] \end{aligned} \tag{112}$$

and where $n_c(t)$ is Gaussian noise of power density $\Phi/2$ (double-sided) over a bandwidth much larger than the carrier loop noise bandwidth.

The phase jitter of the carrier reference signal extracted by the carrier loop is now

$$\phi_c(t) = \phi_{ct} + \phi_{cn}(t) + \phi_{cs}(t) + \phi_{cd}(t) \tag{113}$$

where it is assumed that the loop is a linear system so that ϕ_{ct} and $\phi_{cn}(t)$ are essentially the same as for case (b). The phase jitter resulting from the specular multipath component is $\phi_{cs}(t)$, while that resulting from the diffuse multipath component is $\phi_{cd}(t)$. Using the phase model of the loop, the input phase, from $e_c(t)$, neglecting $n_c(t)$, is

$$\phi_i(t) = \tan^{-1}\left\{\frac{a_{ms}\sin[d_{ms}(t)] + x_c(t)\sin[d_{ms}(t)] + x_q(t)\cos[d_{ms}(t)]}{1 + a_{ms}\cos[d_{ms}(t)] + x_c(t)\cos[d_{ms}(t)] - x_q(t)\sin[d_{ms}(t)]}\right\} \tag{114}$$

which to first approximation is

$$\phi_i(t) \approx a_{ms}\sin[d_{ms}(t)] + x_c(t)\sin[d_{ms}(t)] + x_q(t)\cos[d_{ms}(t)] \tag{115}$$

Higher order terms are assumed negligible as are the effects of the amplitude fluctuations of $e_c(t)$. Assuming that the relative specular multipath Doppler frequency, ω_{ms}, changes only slowly with time, $\phi_{cs}(t)$ may be written as

$$\phi_{cs}(t) = |H_c(\omega_{ms}(t))|\,a_{ms}\sin\left[d_{ms}(t) - \phi_c(\omega_{ms}(t))\right] \tag{116}$$

where $|H_c(\omega)|$ is the amplitude of the loop transfer function and $\phi_c(\omega)$ is the phase of the loop transfer function $H_c(\omega)$. That is, $H_c(\omega)$ is given by

$$H_c(\omega) = |H_c(\omega)| e^{-j\phi_c(\omega)} \tag{117}$$

The phase jitter $\phi_{cd}(t)$ is a random variable which is approximately Gaussian distributed (if the loop is treated as a linear system) and whose variance is denoted by σ^2_{cd}. If the spectral broadening of $x_c(t)$ and $x_q(t)$ is much greater than the carrier loop noise bandwidth B_c, and if the power spectral density of $x_c(t)\sin[d_{ms}(t)] + x_q(t)\cos[d_{ms}(t)]$ is approximately constant over B_c, the variance σ^2_{cd} may be written as

$$\sigma^2_{cd} = \Phi_m(\omega_{ms})2B_c \tag{118}$$

where $\Phi_m(\omega_{ms})$ is the power spectral density of $x_c(t)\sin[d_{ms}(t)] + x_q(t)\cos[d_{ms}(t)]$ at $\omega = 0$.

Although only limited experimental data is available, there is some theoretical support to indicate[10] that for aircraft velocities on the order of 600 mph the spectral broadening of the diffuse multipath component can be significant at L band, and that the power density spectrum of $x_c(t)$ and $x_q(t)$ is Gaussian in shape. That is

$$\Phi_m(\omega) = \frac{\sigma^2_m}{\sqrt{\pi}\, B_m} e^{-(f/B_m)^2} \tag{119}$$

where the bandwidth B_m depends on aircraft velocity; the sea state; the grazing angle; the wavelength of the incident radiation; and to a lesser extent, the aircraft altitude. The total power in $x_c(t)$ and $x_q(t)$ is σ^2_m. Introducing Eq.(119) into Eq.(118), the variance σ^2_{cd} is written as

$$\sigma^2_{cd} = \frac{2\sigma^2_m}{\sqrt{\pi}} \left(\frac{B_c}{B_m}\right) e^{-(f_{ms}/B_m)^2} \tag{120}$$

To determine the relative importance of diffuse multipath in the carrier loop, σ^2_{cd} is compared to σ^2_{cn}.

$$\sigma_{cn}^2 = \frac{B_c}{\cos^2 \beta \left(\frac{C}{\Phi}\right)} \tag{121}$$

The ratio of σ_{cd}^2 to σ_{cn}^2 is less than or equal to

$$\frac{\sigma_{cd}^2}{\sigma_{cn}^2} \leqq \frac{2}{\sqrt{\pi}} \frac{\sigma_m^2}{B_m} \cos^2 \beta \left(\frac{C}{\Phi}\right)_o \tag{122}$$

at the minimum(C/Φ). Note that $2\sigma_m^2$ is the ratio of the received diffuse multipath power to the direct path power. An approximate calculation by Staras[10] indicates that for angles not too close to grazing, the scattering process itself discriminates against the multipath by approximately 2 dB. Allowing for an additional suppression of the multipath by the aircraft antenna of 6 dB, $2\sigma_m^2$ is -8 dB or 0.16. In order that the variance of the diffuse multipath phase jitter component be less than that of the Gaussian noise, B_m must be greater than

$$B_m > \frac{(2\sigma_m^2)}{\sqrt{\pi}} \cos^2 \beta \left(\frac{C}{\Phi}\right)_o \cong 56 \text{ Hz} \tag{123}$$

B_m has been estimated to be at least as large as this for grazing angles in excess of 10^o and for aircraft speeds in excess of 600 mph. Consequently, the diffuse multipath contribution to the carrier loop phase jitter is on the same order as that of the noise at minimum(C/Φ). Therefore, it doubles the effective noise power. At(C/Φ) ratios much higher than minimum, it may form the system noise floor.

If the relative multipath Doppler frequency ω_{ms} lies within the carrier loop noise bandwidth, an upper bound on $|\phi_{cs}(t)|$ is a_{ms}, and an upper bound on the rms carrier phase jitter from specular multipath is $1/\sqrt{2}\ a_{ms}$.

There is theoretical and experimental evidence to indicate[6] that for a Gaussian distributed sea surface with an rms deviation of 10 cm, and for λ = 18.75 cm, and $\gamma \geq 10^o$, the average relative specular multipath power, a_{ms}^2, is approximately 0.065 if a 6 dB multipath suppression factor resulting from aircraft antenna directivity is included.

3.5.4 Effects of Multipath on Clock Phase Jitter

The effects of multipath on clock phase jitter is now investigated. The video output, $e_v(t)$,

$$e_v(t) = (C)^{1/2} \sin\beta \cos \phi_c(t) b_{13}(t) + n_v(t)$$

$$+(C)^{1/2} \sin\beta\, a_{ms} \cos[d_{ms}(t) - \phi_c(t)]\, b_{13}(t - \tau_{ms})$$

$$+(C)^{1/2} \sin\beta \cos[d_{ms}(t) - \phi_c(t)]\, x_c(t) b_{13}(t - \tau_{ms})$$

$$-(C)^{1/2} \sin\beta \sin[d_{ms}(t) - \phi_c(t)]\, x_q(t) b_{13}(t - \tau_{ms}) \qquad (124)$$

and the output of the clock loop bandpass filter becomes

$$e_{BP}(t) = (C)^{1/2} \sin\beta\, \rho_{13}(\tfrac{4}{\pi}) \cos \phi_c(t) \sin[\omega_{c\ell} t] + n_{BP}(t)$$

$$+(C)^{1/2} \sin\beta\, \rho_{13}(\tfrac{4}{\pi}) a_{ms} \cos[d_{ms}(t) - \phi_c(t)] \sin[\omega_{c\ell} t - \omega_{c\ell} \tau_{ms}]$$

$$+(C)^{1/2} \sin\beta\, \rho_{13}(\tfrac{4}{\pi}) \cos[d_{ms}(t) - \phi_c(t)]\, x_c(t) \sin[\omega_{c\ell} t - \omega_{c\ell} \tau_{ms}]$$

$$-(C)^{1/2} \sin\beta\, \rho_{13}(\tfrac{4}{\pi}) \sin\left[d_{ms}(t) - \phi_c(t)\right] x_q(t) \sin\left[\omega_d t - \omega_{c\ell} \tau_{ms}\right] \qquad (125)$$

The phase jitter of the clock reference signal extracted by the clock-tracking loop is now

$$\phi_{c\ell}(t) = \phi_{c\ell_n}(t) + \phi_{c\ell_s}(t) + \phi_{c\ell_d}(t) \qquad (126)$$

where $\phi_{c\ell_n}(t)$ is assumed to be essentially unchanged from the situation of case (b). This means that the clock loop behaves in a linear fashion and that effects of carrier lock error, $\phi_c(t)$, on the noise phase jitter of the detected clock signal $\phi_{c\ell_n}(t)$, are still assumed negligible.

The phase jitter component $\phi_{c\ell_s}(t)$ results from the presence of the specular multipath clock component, and is approximately equal to

$$\phi_{c\ell_s}(t) \approx -|H_{c\ell}(\omega_{ms})|\, a_{ms} \cos[d_{ms}(t) - \phi_c(t) - \phi_{c\ell}(\omega_{ms})] \sin[\omega_{c\ell} \tau_{ms}] \qquad (127)$$

where $|H_{c\ell}(\omega_{ms})|$ and $-\phi_{c\ell}(\omega_{ms})$ are the amplitude and phase of the closed loop response of clock loop at the relative Doppler frequency of the specular multipath carrier component, ω_{ms}. Again, only the lowest order contribution to $\phi_{c\ell_s}(t)$ is considered.

The diffuse multipath phase jitter component, $\phi_{c\ell_d}(t)$, is determined by noting that the diffuse multipath component of the "phase input" of the loop is approximately

$$\phi_{id}(t) \approx -\cos[d_{ms}(t) - \phi_c(t)]\, x_c(t) \sin[\omega_{c\ell}\tau_{ms}] + \sin[d_{ms}(t) - \phi_c(t)]\, x_q(t) \sin[\omega_{c\ell}\tau_{ms}] \tag{128}$$

where the same type of approximation has been made here as was made for the carrier loop. The autocorrelation function of $\phi_{id}(t)$, neglecting carrier lock error, $\phi_c(t)$, is approximately

$$\left\langle \phi_{id}(t)\phi_{id}(t+\tau) \right\rangle = \sin^2[\omega_{c\ell}\tau_{ms}] \cos[\omega_{ms}\tau]\, \phi_m(\tau) \tag{129}$$

and its power spectrum is

$$\Phi_{id}(\omega) = \sin^2[\omega_{c\ell}\tau_{ms}] \frac{1}{2}[\Phi_m(\omega - \omega_{ms}) + \Phi_m(\omega + \omega_{ms})] \tag{130}$$

Again it is assumed that the power spectrum $\Phi_m(\omega)$ is spread out in frequency by an extent exceeding the clock loop noise bandwidth, $B_{c\ell}$, and $\Phi_{id}(\omega)$ is assumed to be essentially constant over the clock loop noise bandwidth. The spectrum $\Phi_m(\omega)$ is considered to be approximately Gaussian with bandwidth B_m such that

$$\Phi_m(\omega) = \frac{\sigma_m^2}{\sqrt{\pi}\, B_m} e^{-(f/B_m)^2} \tag{131}$$

The phase jitter $\phi_{c\ell_d}(t)$ is approximately Gaussian distributed with a variance, $\sigma^2_{c\ell_d}$, approximated by $\Phi_{id}(0)\, 2\, B_{c\ell}$. So, from Eq. (130),

$$\sigma^2_{c\ell_d} = \sin^2[\omega_{c\ell}\tau_{ms}] \frac{\sigma_m^2}{\sqrt{\pi}\, B_m} e^{-(f_{ms}/B_m)^2}\, 2B_{c\ell} \tag{132}$$

where $\sigma_m^2 = \left\langle x_c^2(t) \right\rangle = \left\langle x_q^2(t) \right\rangle$.

An upper bound on $\sigma^2_{c\ell_d}$ may be obtained by setting $f_{ms} = 0$, and replacing $\sin^2[\omega_{c\ell}\tau_{ms}]$ by 1.

$$\sigma^2_{c\ell_d} < \frac{2\sigma^2_m}{\sqrt{\pi}\, B_m} B_{c\ell} = \left(\sigma^2_{c\ell_d}\right)_{max} \tag{133}$$

This is to be compared with $\sigma^2_{c\ell_n}$ at minimum(C/Φ) which is given by

$$\sigma^2_{c\ell_n} = \frac{B_{c\ell}}{\rho^2_{13} \sin^2 \beta\left(\frac{8}{\pi^2}\right)\left(\frac{C}{\Phi}\right)_o} \tag{134}$$

With $B_{c\ell}$ selected, as before in Eq. (6) so as to make $\sigma^2_{c\ell_n} = 0.05$ at the minimum(C/Φ), $B_{c\ell}$ is 6.4 Hz, and the ratio of $(\sigma^2_{c\ell_d})_{max}$ to $\sigma^2_{c\ell_n}$ is

$$\frac{\left(\sigma^2_{c\ell_d}\right)_{max}}{\sigma^2_{c\ell_n}} = \frac{2\sigma^2_m}{\sqrt{\pi}\, B_m} \frac{B_{c\ell}}{\sigma^2_{c\ell_n}} \tag{135}$$

For the upper bound on the mean square clock phase error introduced by diffuse multipath, $\sigma^2_{c\ell_d}$, to be less than that introduced by the noise, $\sigma^2_{c\ell_n}$, at minimum(C/Φ), B_m must be greater than approximately 12 Hz.

The effects of the specular multipath on the clock loop are not likely to be as serious as with the carrier loop for two reasons. First, the factor $\sin[\omega_{c\ell}\tau_{ms}]$ in $\phi_{c\ell_s}(t)$ reduces its effect somewhat, particularly for $\omega_{c\ell}\tau_{ms}$ near multiples of π, and second, as a result of the smaller noise bandwidth of the clock loop, the relative multipath Doppler frequency ω_{ms}, is more likely to lie outside the clock loop noise bandwidth. Again, specular multipath should be almost entirely negligible except possibly for calm seas at low grazing angles.

During the ranging measurement the BINOR is replaced by just the square wave clock. This has the effect of setting ρ^2_{13} equal to 1 in Eq.(134). Equivalently, the result in Eq.(135) is modified by dividing the ratio of $(\sigma^2_{c\ell_d})_{max}/\sigma^2_{c\ell_n}$ by ρ^2_{13} to obtain the ratio which is valid during ranging. It is seen therefore, that the diffuse multipath could very well be the dominant source of noise during ranging. This will be true unless B_m is greater than about 450 Hz, which appears to be unlikely. The rms ranging error in the presence of multipath could be significantly larger

than the error computed on the basis of Gaussian noise alone. More will be said about this in a separate section.

3.5.5 Effects of Multipath on BINOR Acquisition

Proceeding to the question of BINOR acquisition probability, the output of the kth integrate and dump filter, assuming correct acquisition of all previous k - 1 square waves, is

$$e_k = \pm(s_k + n_k) \tag{136}$$

where s_k and n_k are now

$$s_k = \int_o^{\ell T} dt(C)^{1/2} \sin\beta \cos\phi_c(t) \left(b_{13} \otimes h_{LP}\right)_t c\ell_k\left(t - t_o + \frac{\phi_{c\ell}(t)}{\omega_{c\ell}}\right)$$

$$+ a_{ms} \int_o^{\ell T} dt(C)^{1/2} \sin\beta \cos[d_{ms}(t) - \phi_c(t)]$$

$$\times \left(b_{13} \otimes h_{LP}\right)_{t-\tau_{ms}} c\ell_k\left(t - t_o + \frac{\phi_{c\ell}(t)}{\omega_{c\ell}}\right) \tag{137}$$

and

$$n_k = \int_o^{\ell T} dt\left(n_v \otimes h_{LP}\right)_t c\ell_k\left(t - t_o + \frac{\phi_{c\ell}(t)}{\omega_{c\ell}}\right)$$

$$+ \int_o^{\ell T} dt(C)^{1/2} \sin\beta \cos[d_{ms}(t) - \phi_c(t)] x_c(t)$$

$$\times \left(b_{13} \otimes h_{LP}\right)_{t-\tau_{ms}} c\ell_k\left(t - t_o + \frac{\phi_{c\ell}(t)}{\omega_{c\ell}}\right)$$

$$- \int_o^{\ell T} dt(C)^{1/2} \sin\beta \sin[d_{ms}(t) - \phi_c(t)] x_q(t)$$

$$\times \left(b_{13} \otimes h_{LP}\right)_{t-\tau_{ms}} c\ell_k\left(t - t_o + \frac{\phi_{c\ell}(t)}{\omega_{c\ell}}\right) \tag{138}$$

Examination of n_k reveals that n_k consists of a term arising from the presence of Gaussian noise and two terms arising from the presence of diffuse multipath. All of these terms are Gaussian distributed, and consequently may be treated as a single Gaussian random noise component whose variance is simply the sum of the variances of the separate components.

Examination of s_k reveals that it consists of two components. The first is the desired signal component modified by the presence of carrier and clock phase jitter. If it were not for these phase jitters, this component of s_k would be a deterministic constant. Instead, it is now a random variable. (Although not a Gaussian random variable.) The second component of s_k arises from the presence of the specular multipath component, and is also a random variable. It is random not only as a result of $\phi_c(t)$ and $\phi_{c\ell}(t)$, but also because $d_{ms}(t)$ is random (ϕ_{ms} is uniformly distributed from 0 to 2π), as is a_{ms}.

For a given s_k, the probability of correct acquisition is simply

$$\left(P_c\{s_k\}\right)_k = \frac{1}{2}\left[1 + \operatorname{erf}\left(\frac{s_k}{\sqrt{2\langle n_k^2\rangle}}\right)\right] \tag{139}$$

If the probability of obtaining each given s_k were known, it would theoretically be possible to obtain the probability distribution of $\left(P_c\{s_k\}\right)_k$. This would be a useful thing to know, since it contains complete statistical information. The statistics of s_k are extremely difficult to obtain, however, because of the way the random variables $\phi_c(t)$, $\phi_{c\ell}(t)$ and $d_{ms}(t)$ enter into s_k. That is, statistics of their behavior over a period of time equal to ℓT are needed. In addition, these variables enter into s_k through the carrier jitter term $\cos\phi_c(t)$, the clock jitter term $c\ell\ (t - t_o + \phi_c\ (t)/\omega_{c\ell})$, and the relative carrier Doppler term $\cos[d_{ms}(t) - \phi_c(t)]$, which further complicates matters. These functions multiply the filtered BINOR as well as each other (as indicated in Eq.(138)) and are then integrated over a time ℓT in order to form s_k. Consequently, the effort involved in obtaining a generalized distribution of $\left(P_c\{s_k\}\right)_k$ would be considerable at the very least. Fortunately, however, much useful information can be obtained with much less effort by recognizing that on the average, and for the majority of the time, the effects of the perturbations (i.e., the phase jitters, $\phi_c(t)$ and $\phi_{c\ell}(t)$, and of the specular multipath) are small. In fact they must be small if the system is to work properly. What is of interest primarily is the possibility of these perturbations causing the total probability of correct acquisition to drop from the required 99.9% to, say, 98%, rather than from 99.9% to say 80%. In other words, the following approach is justified: 1) assume that the effects of these perturbations are small, 2) develop an analysis

and determine answers on this basis, and 3) see if the results are consistent with this assumption when reasonable values for phase jitter variances, and multipath parameters are introduced. If the results are consistent with the assumptions then the results are valid. If not, then the system must be modified to reduce the perturbations and their effects so that they will indeed be small. With this in mind, $\langle s_k \rangle$ is written as the sum of the average value of s_k plus the deviation from the average.

$$s_k = \langle s_k \rangle + \left(s_k - \langle s_k \rangle \right) \tag{140}$$

The deviation from the average is assumed to be much less than the average, and is the random component of s_k. Introducing Eq.(140) into Eq.(139) and expanding $\left(P_c\{s_k\} \right)_k$ in a Taylor series about $\langle s_k \rangle$, the following approximation is obtained

$$\left(P_c\{s_k\} \right)_k \approx \frac{1}{2}\left[1 + \operatorname{erf}\left(\frac{\langle s_k \rangle}{\sqrt{2\langle n_k^2 \rangle}} \right) \right]$$

$$+ \frac{1}{2}\left(\frac{2}{\sqrt{\pi}} e^{-\langle s_k \rangle^2 / 2\langle n_k^2 \rangle} \right) \frac{\left(s_k - \langle s_k \rangle \right)}{\sqrt{2\langle n_k^2 \rangle}}$$

$$- \frac{1}{2!}\,\frac{1}{2}\left(\frac{2}{\sqrt{\pi}} e^{-\langle s_k \rangle^2 / 2\langle n_k^2 \rangle} \right)\left(\frac{2\, s_k}{\sqrt{2\langle n_k^2 \rangle}} \right) \frac{\left(s_k - \langle s_k \rangle \right)^2}{2\langle n_k^2 \rangle} \tag{141}$$

to second order.

The average of s_k is

$$\langle s_k \rangle = \mu E_{\phi_c}(\cos \phi_c) E_{\phi_{c\ell}}\left(\chi_k\left(t_o - \frac{\phi_{c\ell}}{\omega_{c\ell}} \right) \right) \tag{142}$$

Here orders of statistical averaging and time integration have been interchanged, and ϕ_c and $\phi_{c\ell}$ have been assumed to be statistically independent. The specular multipath component of s_k averages to zero as a result of the uniform distribution of d_{ms}. The lowest-order contribution of the specular multipath component of s_k is discussed further below.

To a good approximation, $E_{\phi_c}(\cos\phi_c)$ is

$$E_{\phi_c}(\cos\phi_c) \approx \cos\phi_{ct}\, J_o\left(|H_c(\omega_{ms})|\, a_{ms}\right) e^{-\frac{1}{2}\left(\sigma_{cn}^2+\sigma_{cd}^2\right)} \tag{143}$$

The expectation value

$$E_{\phi_{c\ell}}\left(\chi_k\left(t_o - \frac{\phi_{c\ell}}{\omega_{c\ell}}\right)\right)$$

is computed by realizing that the results of Appendix C need only be modified by replacing $\phi_{c\ell_o}$ by $\phi_{c\ell_o} - \phi_{c\ell_s}$ and $\sigma_{c\ell_n}$ by $\sigma_{c\ell} = (\sigma_{c\ell_n}^2 + \sigma_{c\ell_d}^2)^{1/2}$, and then averaging over $\phi_{c\ell_s}$. That is,

$$E_{\phi_{c\ell}}\left(\chi_k\left(t_o - \frac{\phi_{c\ell}}{\omega_{c\ell}}\right)\right) = E_{\phi_{c\ell_s}}\left(1 - \epsilon_k\left[-\left(1 - \ell n2 + 5\phi_{c\ell_s}\right)\operatorname{erf}\left(\frac{\ell n2}{\sqrt{2}\,5\sigma_{c\ell}} - \frac{\phi_{c\ell_s}}{\sqrt{2}\,\sigma_{c\ell}}\right)\right.\right.$$

$$+\left(\frac{5\sigma_{c\ell}}{\sqrt{2}}\right)\frac{2}{\sqrt{\pi}}\, e^{-\left(\frac{\ell n2}{\sqrt{2}\,5\sigma_{c\ell}} - \frac{\phi_{c\ell_s}}{\sqrt{2}\sigma_{c\ell}}\right)^2}$$

$$\left.\left. + e^{5\phi_{c\ell_s}}\, e^{\left(\frac{5\sigma_{c\ell}}{\sqrt{2}}\right)^2}\, \frac{1}{2}\left[1 + \operatorname{erf}\left(\frac{\ell n2}{\sqrt{2}\,5\sigma_{c\ell}} - \frac{5\sigma_{c\ell}}{\sqrt{2}} - \frac{\phi_{c\ell_s}}{\sqrt{2}\sigma_{c\ell}}\right)\right]\right]\right) \tag{144}$$

For the noise and multipath levels which pertain to the NAV/SAT application, $\phi_{c\ell_s}/\sqrt{2}\,\sigma_{c\ell}$ is less than 1, so that Eq.(144) may be expanded in a Taylor series about $\phi_{c\ell_s} = 0$ prior to averaging. This is derived in

Appendix D to second order in $\phi_{c\ell_s}$, and is

$$E_{\phi_{c\ell}}\left(\chi_k\left(t_o - \frac{\phi_{c\ell}}{\omega_{c\ell}}\right)\right) \approx (\chi_k)_{max} - \epsilon_k \Gamma(\sigma_{c\ell})$$

$$- \epsilon_k |H_{c\ell}(\omega_{ms})|^2 \frac{1}{2} a_{ms}^2 \sin^2[\omega_{c\ell}\tau_{ms}] \frac{1}{2}(5)^2 e^{\left(\frac{5\sigma_{c\ell}}{\sqrt{2}}\right)^2}$$

$$\times \frac{1}{2}\left[1 + \text{erf}\left(\frac{\ell n 2}{\sqrt{2}\, 5\sigma_{c\ell}} - \frac{5\sigma_{c\ell}}{\sqrt{2}}\right)\right] \qquad (145)$$

where $\Gamma(\sigma_{c\ell})$ is defined by Eq.(106), and

$$|H_{c\ell}(\omega_{ms})|^2 \frac{1}{2} a_{ms}^2 \sin^2[\omega_{c\ell}\tau_{ms}] = E_{\phi_{c\ell_s}}\left(\phi_{c\ell_s}^2\right) \qquad (146)$$

Of special interest is the leading term in $\left(P_c\{s_k\}\right)_k$. This provides an estimate of the effects of the perturbations on the probability of correct acquisition. It is also the leading term in a computation of the expectation or average value of $\left(P_c\{s_k\}\right)_k$, and represents the lowest order effects of ϕ_c, $\phi_{c\ell}$, and the diffuse multipath. The lowest order effect of the specular multipath component of s_k is contained in the second order term of Eq.(141), and is

$$-\frac{1}{2}\frac{\langle s_k\rangle}{\sqrt{2\langle n_k^2\rangle}}\left(\frac{2}{\sqrt{\pi}} e^{-\langle s_k\rangle^2/2\langle n_k^2\rangle}\right)\left(\frac{\langle s_k^2\rangle_{ms}}{2\langle n_k^2\rangle}\right) \qquad (147)$$

where $\langle s_k^2\rangle_{ms}$ is the variance of the specular multipath component of s_k. This variance is worst-case estimated in Appendix E, where it is shown to be given approximately by

$$\langle s_k^2\rangle_{ms} \approx \frac{1}{2} a_{ms}^2 \mu^2 \chi_k^2(t_o - \tau_{ms}) \qquad (148)$$

The variance $\langle n_k^2\rangle$, as mentioned previously, is equal to the sum of the variances of the component of n_k involving $n_v(t)$ and the diffuse multipath component. The former is essentially the same as for case (b) since the only difference is in the phase jitter on $c\ell_k(t - t_o + \phi_{c\ell}(t)/\omega_{c\ell})$, and this phase jitter was shown to have negligible effect in the computation

of the variance in Appendix A. Consequently, $\langle n_k^2 \rangle$ for case (c) is equal to

$$\langle n_k^2 \rangle \approx \sigma^2 \gamma_k^2 + \langle n_k^2 \rangle_d \tag{149}$$

where $\langle n_k^2 \rangle_d$ is the variance of the diffuse multipath component of n_k. This is computed in Appendix F to be approximately

$$\langle n_k^2 \rangle_d \approx \mu^2 \frac{(2\sigma_m^2)}{\sqrt{\pi}\, 2B_m \ell T} \left(\chi_k^o(\tau_{ms})\right)^2 \tag{150}$$

where σ_m^2 and B_m were defined by Eq. (131) and the superscript "o" in $\chi_k^o(\tau_{ms})$ indicates that the lowpass video filter was neglected in the computation.

To proceed further, note that the multipath delays are small compared to the periods of the $\chi_k^o(\tau)$ functions for the larger values of k. Also the functions $\chi_k^o(\tau)$ are constant and equal to 1 for small τ for $k \geq 7$. A worst-case estimate of $\langle n_k^2 \rangle_d$ may be made by assuming $(\chi_k^o(\tau_{ms}))^2 = 1$ for all k and for all τ_{ms} (likely to be encountered in the NAV/SAT application). Then

$$\langle n_k^2 \rangle_d < \frac{\mu^2 \sigma_m^2}{\sqrt{\pi}\, \ell T B_m} \tag{151}$$

The total variance $\langle n_k^2 \rangle$ is then less than

$$\langle n_k^2 \rangle \lesssim \sigma^2 \gamma_k^2 \left[1 + \left(\frac{\mu}{\sqrt{2}\,\sigma}\right)^2 \frac{2\sigma_m^2}{\sqrt{\pi}\, \gamma_k^2 \ell T B_m}\right] \tag{152}$$

With $\ell = 4$, $(\mu/\sqrt{2}\,\sigma)$ at minimum (C/Φ) was shown in Sec. 3.3 (case (a)) to be equal to 2.840. With $2\sigma_m^2$ equal to 0.16, and with $\gamma_k^2 \approx 1$, the variance of the diffuse multipath component will be less than the variance of the noise if

$$B_m > \frac{2\sigma_m^2}{\sqrt{\pi}\, \ell T} \left(\frac{\mu}{\sqrt{2}\,\sigma}\right)^2 \cong 14.3 \text{ Hz} \tag{153}$$

As mentioned, it is expected that B_m will be at least several times as large as this.

3.5.6 Computation of $(P_c)_T$, the Total Expected Probability of Correct BINOR Acquisition

The total expected probability of correct BINOR acquisition $(P_c)_T$ is simply given by the product of the 12 conditional probabilities $(P_c)_k$. The conditional probability, $(P_c)_k$, is the average value of $(P_c\{s_k\})_k$, and from Eq. (141) through (152) is approximately given by

$$(P_c)_k \approx \frac{1}{2}\left[1 + \operatorname{erf}\left\{\left(\frac{\mu}{\sqrt{2}\,\sigma}\right) f_k\right\}\right] - \frac{1}{2}\left(\frac{\mu f_k}{\sqrt{2}\,\sigma}\right)^3 \left(\frac{2}{\sqrt{\pi}}\, e^{-\left(\frac{\mu}{\sqrt{2}\sigma} f_k\right)^2}\right)\left(\frac{1}{2} a_{ms}^2\right) \frac{\chi_k^2 (t_o - \tau_{ms})}{g_k^2} \qquad (154)$$

where

$$f_k = \frac{(\cos\phi_{ct})\left(J_o\left(|H_c(\omega_{ms})|\, a_{ms}\right)\right)\left(e^{-\frac{1}{2}\sigma_{cn}^2\left(1+\left(\frac{\sigma_{cd}^2}{\sigma_{cn}^2}\right)\right)}\right)\left(E_{\phi_{c\ell}}\left(\chi_k\left(t_o - \phi_{c\ell}/\omega_{c\ell}\right)\right)\right)}{\left(\gamma_k^2 + \frac{\langle n_k^2\rangle_d}{\sigma^2}\right)^{1/2}} \qquad (155)$$

and g_k is

$$g_k = \left(\gamma_k^2 + \frac{\langle n_k^2\rangle_d}{\sigma^2}\right)^{1/2} f_k \qquad (156)$$

Worst-case approximations may be made as follows. In f_k and g_k,

$$\gamma_k^2 \to 1 \qquad (157)$$

$$J_o\left(|H_c(\omega_{ms})|\, a_{ms}\right) \to J_o(a_{ms}) \qquad (158)$$

$$e^{-\frac{1}{2}\sigma_{cn}^2\left(1+\left(\frac{\sigma_{cd}^2}{\sigma_{cn}^2}\right)\right)} \to e^{-\frac{1}{2}\sigma_{cn}^2\left(1+\left(\frac{\sigma_{cd}^2}{\sigma_{cn}^2}\right)_{max}\right)} \qquad (159)$$

and $E_{\phi_{c\ell}}\left(\chi_k\left(t_o - \phi_{c\ell}/\omega_{c\ell}\right)\right)$, which is given approximately by

$$E_{\phi_{c\ell}}\left(\chi_k\left(t_o-\phi_{c\ell}/\omega_{c\ell}\right)\right) \approx (\chi_k)_{max} - \epsilon_k \Gamma(\sigma_{c\ell})$$

$$-\left(\epsilon_k \left|H_{c\ell}(\omega_{ms})\right|^2 \frac{1}{2} a_{ms}^2 \sin^2[\omega_{c\ell}\tau_{ms}]\left(\frac{5}{\sqrt{2}}\right)^2 e^{\left(\frac{5\sigma_{c\ell}}{\sqrt{2}}\right)^2}\right.$$

$$\left. \times \frac{1}{2}\left[1 - \operatorname{erf}\left(\frac{5\sigma_{c\ell}}{\sqrt{2}} - \frac{\ell n 2}{\sqrt{2}\, 5\sigma_{c\ell}}\right)\right]\right) \qquad (160)$$

where

$$\sigma_{c\ell} = \sigma_{c\ell_n}\left(1 + \left(\frac{\sigma_{c\ell_d}^2}{\sigma_{c\ell_n}^2}\right)\right)^{1/2} \qquad (161)$$

becomes, with

$$\sigma_{c\ell} \to \sigma_{c\ell_n}\left(1 + \left(\frac{\sigma_{c\ell_d}^2}{\sigma_{c\ell_n}^2}\right)_{max}\right)^{1/2}$$

$$E_{\phi_{c\ell}}\left(\chi_k\left(t_o - \phi_{c\ell}/\omega_{c\ell}\right)\right) \to (\chi_k)_{max} - \epsilon_k \Gamma(\sigma_{c\ell})$$

$$-\left(\epsilon_k \frac{1}{2} a_{ms}^2 \left(\frac{5}{\sqrt{2}}\right)^2 e^{\left(\frac{5\sigma_{c\ell}}{\sqrt{2}}\right)^2} \times \frac{1}{2}\left[1 - \operatorname{erf}\left(\frac{5\sigma_{c\ell}}{\sqrt{2}} - \frac{\ell n 2}{\sqrt{2}\, 5\sigma_{c\ell}}\right)\right]\right) \qquad (162)$$

and finally

$$\frac{\langle n_k^2\rangle_d}{\sigma^2} \to \left(\frac{\langle n_k^2\rangle_d}{\sigma^2}\right)_{max} \qquad (163)$$

In the last term in Eq. (98), $\chi_k^2(t_o - \tau_{ms}) \to 1$. The ratios $\left(\sigma_{cd}^2/\sigma_{cn}^2\right)_{max}$, $\left(\sigma_{c\ell d}^2/\sigma_{c\ell_n}^2\right)_{max}$, $\left(\sigma_{c\ell_d}^2/\sigma_{c\ell_n}^2\right)_{max}$, and $\left(\langle n_k^2\rangle_d/\sigma^2\right)_{max}$ are obtained from from Eqs. (122), (135), and (151).

Four situations are investigated below in which different B_m are considered as well as the presence or absence of a small specular component. In each case, a 6 dB aircraft antenna suppression of the multipath is assumed. In estimating the relative power in the specular multipath component, a_{ms}^2, an rms water surface displacement, σ_w, of 10 cm and a minimum grazing angle, γ, of 10^o was introduced into the equation (given in Beckman and Spizzichino, p. 246) which relates the average relative power of the specularly scattered component to σ_w, $\sin\gamma$, and the wavelength λ.

$$a_{ms}^2 = \left(\frac{1}{4}\right) e^{-\left(\frac{4\pi\sigma_w \sin\gamma}{\lambda}\right)^2} = 0.06457 \qquad (164)$$

The factor $\left(\frac{1}{4}\right)$ multiplying the exponential arises from the assumed 6 dB antenna suppression factor.

Again, as above in Sec. 3.5.3, a 2 dB suppression of the diffuse multipath component by the scattering process itself is assumed, so that with the antenna suppression factor of 6 dB, the relative power in the diffuse $2\sigma_m^2$ multipath component, is -8 dB, or 0.16.

The four situations are, specifically:

1) Aircraft flying at approximately 600 mph at low grazing angles. Assumed values for B_m and a_{ms} are $B_m \approx 50$ Hz and $a_{ms}^2 \approx 0.06457$.

2) Aircraft flying at about 2000 mph at low grazing angles. Then, B_m is sufficiently large so that the diffuse multipath interference has almost negligible effects. B_m is considered infinite, and a_{ms}^2 is still 0.06457.

3) Aircraft is flying at speeds exceeding 600 mph and for grazing angles in excess of 20^o. B_m is assumed to be approximately 200 Hz and a_{ms}^2 is assumed zero.

4) Same as 1) but with $\ell = 5$ instead of $\ell = 4$.

The probability of correct BINOR acquisition is evaluated at the worst-case (C/Φ) = 35.7 dB-Hz. Tables of the values of the various factors in Eqs. (154) to (163) are presented in Appendix H. For convenience, Table H-5 showing the total probability of correct BINOR acquisition is repeated below.

Table H-5

TOTAL PROBABILITY OF CORRECT BINOR ACQUISITION $(P_c)_T$

Situation	$(P_c)_T = \prod_{k=1}^{12} (P_c)_k$
1	0.980 or 98.0%
2	0.996 or 99.6%
3	0.998 or 99.8%
4	0.993 or 99.3%

The results of Table H-5, which give the total average probability of correct BINOR acquisition for the four situations considered indicate that

a) even for the worst-case conditions considered, the average probability of correct BINOR acquisition for the most difficult situation (i.e., situation number 1) is still fairly good, there being only a 2% chance of not acquiring the BINOR correctly for $\ell = 4$.

b) for the same situation as in 1, but with a 25% increase in integration time (i.e., situation number 4) the probability of not acquiring the BINOR correctly drops to less than 1%.

c) for the situation in which the grazing angle exceeds 20° and specular multipath may be ignored (situation 3), the average probability of correct BINOR acquisition is 99.8%. This is the largest of the four situations considered, and barely falls short of the desired 99.9%, and

d) for the case where only the specular multipath was considered (situation number 2), the value of $(P_c)_T$ became 99.6%. As aircraft speed is increased the effects of the diffuse multipath become less important as a result of the additional frequency spreading. This situation then represents an upper limit on how good the average probability of correct BINOR acquisition can get as higher aircraft speeds are considered.

Examination of the table of conditional probabilities $(P_c)_k$, (Table H-4 in Appendix H) reveals that the values of $(P_c)_k$ for the k = 1 case is the lowest of all the k's. This is primarily a result of the effects of clock jitter as may be seen from the portion of Table H-2 showing the clock jitter signal suppression fact $E_{\phi_{c\ell}}(\chi_k(t_o - \phi_{c\ell}/\omega_{c\ell}))$. This situation is compensated for somewhat by the factor γ_k^2 in Eq. (99) which was set equal to 1 for all k (and is approximately equal to 1 for $k \geq 3$), but which is equal to 0.9363 for k = 1. In addition, the factor $\chi_k^{o2}(\tau_{ms})$ which was set equal to 1 in estimating $(\langle n_k^2 \rangle_d)_{max}$ is more likely to be less than 1 for the k = 1 case than for the larger k, since τ_{ms} is likely to be at least as large as several periods of the first divided-down square wave component of the BINOR. Consequently, $\chi_k^{o2}(\tau_{ms})$ (for k = 1) can be anywhere between 0 and 1, depending on τ_{ms}. This means that $(P_c)_k$ for k = 1 will more than likely be somewhat larger than that indicated in Table H-4.

An additional worst-case possibility must be considered in which, for one or more of the acquisitions of the square-wave components of the BINOR, the specular multipath part of the signal component at the output of the k^{th} integrate and dump filter, s_k, is at, or very close to, its maximum possible value for a given a_{ms}, and is of opposite sign from the desired signal part of s_k.

The conditions which must be satisfied simultaneously in order for this to occur for the k^{th} acquisition may be seen, from Eq. (137), to be

1) τ_{ms} must be either small compared to the period of the k^{th} divided-down square wave component (most easily satisfied for the larger values of k), or a multiple of one-half this period (most easily satisfied for the smaller values of k).

2) The relative carrier Doppler frequency, $f_{ms} = \omega_{ms}/2\pi$, must be small compared to the inverse of the integrate and dump filter integration time, ℓT. And finally,

3) The initial value of the relative multipath Doppler phase, ϕ_{ms}, (see Eq.(110) must be very close to 0^o or 180^o, whichever value causes the sign of the specular multipath part of s_k to be opposite that of the desired signal part of s_k.

It is much more probable that this worst-case possibility occurs for the large values of k since at the low grazing angles for which a specular multipath component is likely to be present, τ_{ms} is indeed small compared to the periods of these square-wave components, thereby satisfying the first alternative of condition 1). For the low values of k, this alternative is no longer satisfied, and the special values of τ_{ms} required to satisfy the second alternative of condition 1) occur only occasionally. Consequently, attention will be focussed only on the large values of k.

To assure that conditions 2) and 3) are satisfied, it is sufficient to require that during the integration time, ℓT, the relative carrier Doppler phase, $d_{ms}(t)$, remain within $\pm 30^o$ of the required 180^o. In order to estimate the probability of satisfying this requirement, the $\pm 30^o$ range may be considered to be divided equally between requirements on the initial phase ϕ_{ms} and on the relative Doppler frequency f_{ms}. In particular, the requirements chosen are $\phi_{ms} = 180^o \pm 15^o$, and $|f_{ms}\, \ell T| \leq 15^o/360^o$. The probability that ϕ_{ms} lie within this range (assuming a uniformly distributed probability distribution for ϕ_{ms}) is equal to the ratio of 30^o to 360^o, or 0.0825. The relative Doppler frequency $|f_{ms}|$ must be less than about 0.8 Hz for $\ell = 4$ and $T = (78.125)^{-1}$ sec. For aircraft speeds in excees of 600 mph and for a carrier frequency of 1.6 GHz, it is fairly improbable that the relative Doppler frequency will be as low as this. This is seen to be particularly true when the effects of unavoidable vertical aircraft motions on the relative Doppler frequency are considered. This was developed further in Section 2.

If the required conditions are fulfilled for the k^{th} square-wave component, the probability of its correct acquisition, $(P_c)_k$, becomes, to a good approximation,

$$(P_c)_k \approx \frac{1}{2}\left[1 + \mathrm{erf}\left(\frac{\mu}{\sqrt{2}\,\sigma}\, f_k \left(1 - a_{ms}\right)\right)\right] \tag{165}$$

where f_k is as given in Eq.(155).

It is of interest to see how the results for the total probability of correct BINOR acquisition $(P_c)_T$, are modified for situation(1) when one or more of the values of $(P_c)_k$ for k = 7 through 12 of Table H-4 are replaced by the values obtained from Eq.(165). The value of $(P_c)_k$

obtained from Eq. (109) with $a_{ms}^2 = 0.06457$ and $(\mu/\sqrt{2}\,\sigma)f_k = 2.363$ is

$$(P_c)_k = \frac{1}{2}\left[1 + \mathrm{erf}\left(\frac{\mu}{\sqrt{2}\,\sigma} f_k(1 - a_{ms})\right)\right] = 0.993660 \qquad (166)$$

When this value is used to replace n of the values of $(P_c)_k$ for k = 7 - 12 in Table H-4, the values of $(P_c)_T$ given below in Table 5 are obtained.

Table 5

$(P_c)_T$ FOR SITUATION (1) VS. n

n	(P_c)
0	98.00%
1	97.52%
2	97.03%
3	96.55%
4	96.08%
5	95.60%
6	95.13%

Consequently, even in the rather unlikely event of this additional worst-case possibility occurring for as many as 6 square-wave acquisitions, a condition requiring an even smaller relative Doppler carrier frequency than the 0.8 Hz considered above, the total probability of correct acquisition of the BINOR code is reduced only to roughly 95%. For the more likely case where 1 or, at most, 2 acquisitions have this additional worst-case condition, the total probability of correct BINOR acquisition is reduced only to approximately 97%. These values may be entirely acceptable in view of the fact that the conditions under which they occur happen relatively infrequently.

3.6 Ranging Errors Caused by Multipath

When the BINOR code is replaced by the clock square wave after acquisition, the signal power in the clock loop increases by a factor of $1/\rho_{13}^2 \cong 19.65$ or approximately 13 dB. In the absence of multipath, and

with the loop designed so as to maintain a constant noise bandwidth, the loop SNR increases by the same factor. However, if multipath is present, the variance of the multipath component of the clock phase jitter on the extracted clock signal increases by the factor $1/\rho_{13}^2$, (as shown in Eq. (63)) and may now exceed the variance of the noise component of the clock phase jitter as discussed in Sec. 3.5.5. In other words, with multitap present, the rms phase error on the clock during ranging may be determined primarily by the multipath rather than by the front end noise.

The total phase jitter on the extracted clock may be written, as in Eq. (126), as

$$\phi_{c\ell}(t) = \phi_{c\ell_n}(t) + \phi_{c\ell_s}(t) + \phi_{c\ell_d}(t) \tag{167}$$

The variance of this phase jitter, $\sigma_{c\ell}^2$, is

$$\sigma_{c\ell}^2 = \sigma_{c\ell_n}^2 + \sigma_{c\ell_s}^2 + \sigma_{c\ell_d}^2 \tag{168}$$

The variance of the specular multipath component may be seen, from Eq. (127), to be equal to

$$\sigma_{c\ell_s}^2 = |H_{c\ell}(\omega_{ms})|^2 a_{ms}^2 \frac{1}{2} \sin^2[\omega_{c\ell}\tau_{ms}] \tag{169}$$

The variance of the diffuse multipath component is the same as given in Eq. (132) and is

$$\sigma_{c\ell_d}^2 = \sin^2[\omega_{c\ell}\tau_{ms}] \frac{2\sigma_m^2}{\sqrt{\pi}\, B_m} e^{-(f_{ms}/B_m)^2} B_{c\ell} \tag{170}$$

The variance of the noise component is now ρ_{13}^2 times what it was during BINOR acquisition (when it was 0.05) or

$$\sigma_{c\ell_n}^2 = \rho_{13}^2(0.05) \tag{171}$$

As a consequence of the factor $\sin^2[\omega_{c\ell}\tau_{ms}]$, there will be certain ranges of multipath delays for which $\sin^2[\omega_{c\ell}\tau_{ms}]$ will be close to zero and the multipath will be unimportant, and certain ranges for which it will be close to one and the multipath will be an important factor in ranging performance. Since worst-case possibilities are of primary concern, $\sin^2[\omega_{c\ell}\tau_{ms}]$ is set equal to 1. In addition, $|H_{c\ell}(\omega_{ms})|^2$ and

$\exp(-f_m^2/B_m^2)$ are also set equal to 1. The first three aircraft flight situations discussed in the previous section are considered. The results are presented in Table 6.

Table 6

RMS CLOCK PHASE ERROR DURING RANGING

$$\sigma_{c\ell} = \left[\sigma^2_{c\ell_n} + \left(\sigma^2_{c\ell_s}\right)_{max} + \left(\sigma^2_{c\ell_d}\right)_{max}\right]^{1/2}$$

Situation	$\sigma^2_{c\ell_n}$	$\sigma^2_{c\ell_{s\ max}}$	$\sigma^2_{c\ell_{d\ max}}$	$\sigma_{c\ell}$
1	0.002545	0.032285	0.001555	0.21537
2	0.002545	0.032285	0.000000	0.18663
3	0.002545	0.000000	0.002889	0.07372

The values of total clock error $\sigma_{c\ell}$ given in Table 6 should be compared with the value of $\sigma_{c\ell_n}$, which is the value of $\sigma_{c\ell}$ in the absence of multipath and is equal to 0.05045. It is seen that $\sigma_{c\ell}$ for the third situation is about 40% higher than $\sigma_{c\ell_n}$. This is the situation which pertains to most aircraft most of the time. When specular multipath is present it may dominate over the noise and the diffuse multipath as indicated in situations 1 and 2. Fortunately the relative multipath carrier Doppler frequency for high speed aircraft is most likely to lie outside the clock loop noise bandwidth, and $|H_{c\ell}(\omega_{ms})|^2$ may be sufficiently less than 1 to suppress the specular multipath variance, $\sigma^2_{c\ell_s}$, to the point where its contribution to $\sigma_{c\ell}$ is on the same order as $\sigma^2_{c\ell_n}$. For a clock loop noise bandwidth, $B_{c\ell}$, of 6.4 Hz, and for a loop damping coefficient of 0.707, a relative carrier-doppler frequency of only 5 Hz will cause $|H_{c\ell}(\omega_{ms})|^2$ to drop to 0.1.

The rms range error is related to $\sigma_{c\ell}$ through the relationship

$$\sigma_R = c\left(\frac{\sigma_{c\ell}}{2\pi f_{c\ell}}\right) \tag{172}$$

where c is the velocity of light ($\sim 10^9$ ft/sec), and $f_{c\ell}$ is the clock frequency (320 kHz). In terms of rms range error, the results are as given in Table 7.

Table 7

RMS RANGE ERROR

Situation	σ_R (feet)
no multipath	25.1
1	107.1
2	92.8
3	36.7

Several possibilities exist for reducing σ_R. The simplest of these are 1) to increase the clock frequency, $f_{c\ell}$, and 2) to reduce the clock loop noise bandwidth during ranging. The latter possibility reduces $\sigma^2_{c\ell s}$ by reducing $|H_{c\ell}(\omega_{ms})|^2$ for relative carrier Doppler frequencies which lie outside the now reduced clock loop noise bandwidth.

3.7 Summary and Conclusions

From the analyses conducted in Secs. 3.5 and 3.6, the following conclusions may be drawn:

1) The presence of a small multipath interference will not cause a drastic reduction in the total probability of correct BINOR acquisition if

a) at least a 6 dB aircraft antenna discrimination against the multipath is maintained.

b) aircraft speeds are on the order of 600 mph or more so that the frequency spreading of the diffuse multipath component is on the order of 50 Hz or more.

c) the grazing angle exceeds 10^o and the rms displacement of the sea surface exceeds 10 cm, so that the average relative specular multipath power is no larger than approximately 0.065.

For the vast majority of the time the grazing angle exceeds 20^o and the aircraft antenna multipath discrimination exceeds 6 dB. The specular multipath component is then negligible, and the frequency spreading of the diffuse multipath component is more on the order of

100 to 200 Hz. The effects of the multipath in this case become almost entirely negligible during BINOR acquisition.

For grazing angles close to 10^{o}, specular multipath may become a problem for calm seas at 1.6 GHz. However, the probability of correct BINOR acquisition is still on the order of 98% on the average for $\ell = 4$, and may be improved to 99.3% by making $\ell = 5$. Analyses of additional worst-case possibilities that may occur in the presence of specular multipath indicate that it is very unlikely that the probability of correct BINOR acquisition (with $\ell = 4$) will fall below 95% at the worst-case SNR used in all of the calculations.

During the ranging measurement, in the present system, the multipath becomes an important consideration. This is so because the BINOR is removed and only square-wave clock is transmitted. This increases the signal and multipath powers in the clock loop to the point where the multipath, rather than the noise, becomes the limiting factor. This appears to be especially true when specular multipath is present. However, the differential doppler offset between the direct-path and multipath carrier frequencies may be sufficiently high compared to the clock loop noise bandwidth to cause considerable suppression of the specular multipath clock component. This would substantially reduce the limiting effects of the specular multipath component on ranging accuracy. The diffuse multipath component causes an increase in rms range error of approximately 50% over that caused by front-end noise alone. The effect of the diffuse component is reduced only when the fading bandwidth is much smaller than the differential doppler which is unlikely in the present application.

4. MODULATION DESIGN

4.1 Introduction

The discussion begins with an investigation of the possible modulation methods by which the ambiguity resolving square waves may be applied to the 320 kHz subcarrier. Low deviation PM is selected. Then the optimum method for encoding these square waves is considered. The BINOR technique (hard limited sum of square waves) is rejected in favor of a simple sum of square waves. Optimum deviations for the square waves on the subcarrier and the subcarrier on to the carrier are selected. Then, a description of the ambiguity resolving procedure is presented. The discussion concludes with a hardware design exercise. This effort results in a detailed Block Diagram of a range data demodulation and measurement system appropriate to the optimized ranging modulation.

4.2 Subcarrier Modulation Methods

Two forms of modulation are analyzed and evaluated. The first consists of a PM ranging subcarrier which is partially amplitude modulated by the ambiguity resolving signal. The second technique consists of a PM ranging subcarrier which is partially phase modulated by the ambiguity resolving signal. The resulting spectrum of each is derived and evaluated in terms of convenience and efficiency in the NAV/SAT system.

4.2.1 Partial AM

This specific form of modulation is described by

$$e_1(t) = \sqrt{2S} \sin \left[\omega_c t + \delta_1 \left(1 + \beta_1 b(t) \right) \sin \omega_{sc} t \right] \tag{173}$$

where

S = signal power

ω_c = carrier frequency = 2πx1.6 GHz

δ_1 = subcarrier phase deviation

ω_{sc} = subcarrier frequency = 2πx320 kHz

β_1 = ambiguity signal smplitude modulation deviation

$b(t)$ = ambiguity signal (sum of square waves or BINOR)

The various components of the spectrum of $e_1(t)$ can be found by a simple trigonometric expansion. Thus,

$$\frac{e_1(t)}{\sqrt{2S}} = \cos(\omega_c t)\cos\left(\delta_1\left(1+\beta_1 b(t)\right)\sin\omega_{sc}t\right) + \cos(\omega_c t)\sin\left(\delta_1\left(1+\beta_1 b(t)\right)\sin\omega_{sc}t\right) \quad (174)$$

Equation (174) can be further expanded as

$$\begin{aligned}\frac{e_1(t)}{\sqrt{2S}} = {} & \sin(\omega_c t)\left[\cos(\delta_1\sin\omega_{sc}t)\cos(\delta_1\beta_1 b(t)\sin\omega_{sc}t)\right. \\ & \left. - \sin(\delta_1\sin\omega_{sc}t)\sin(\delta_1\beta_1 b(t)\sin\omega_{sc}t)\right] \\ & + \cos(\omega_c t)\left[\sin(\delta_1\sin\omega_{sc}t)\cos(\delta_1\beta_1 b(t)\sin\omega_{sc}t)\right. \\ & \left. + \cos(\delta_1\sin\omega_{sc}t)\sin(\delta_1\beta_1 b(t)\sin\omega_{sc}t)\right]\end{aligned} \quad (175)$$

The characteristics of b(t), the ambiguity resolving signal component, can now be exploited to continue the expansion. As noted above (b(t) is either a BINOR code or a sum of square waves. For the BINOR case, b(t) = ±1. Then Eq. (175) is rewritten as

$$\frac{e_1(t)}{\sqrt{2S}} = \sin(\omega_c t)\left[\cos(\delta_1 \sin \omega_{sc} t)\cos(\delta_1 \beta_1 \sin \omega_{sc} t) - b(t)\sin(\delta_1 \sin \omega_{sc} t)\sin(\delta_1 \beta_1 \sin \omega_{sc} t)\right]$$
$$\cos(\omega_c t)\left[\sin(\delta_1 \sin \omega_{sc} t)\cos(\delta_1 \beta_1 \sin \omega_{sc} t) + b(t)\cos(\delta_1 \sin \omega_{sc} t)\sin(\delta_1 \beta_1 \sin \omega_{sct})\right] \quad (176)$$

Each of the four terms of Eq. (176) can be expanded and each will contribute a distinct component to the signal spectrum. The first coefficient of sin $\omega_c t$ in Eq. (176) is

$$K_1 = \cos(\delta_1 \sin \omega_{sc} t)\cos(\delta_1 \beta_1 \sin \omega_{sc} t)$$
$$= \frac{1}{2}\left[\cos(\delta_1 (1 + \beta_1) \sin \omega_{sc} t) + \cos(\delta_1 (1 - \beta_1) \sin \omega_{sc} t)\right] \quad (177)$$

Employing the Bessel expansion of $\cos(\Delta \sin \Phi) = J_o(\Delta) + 2 \sum_{2k} J_{2k}(\Delta) \cos(2k)\Phi$ and $\sin(\Delta \sin \Phi) = 2 \sum_{2k+1} J_{2k+1}(\Delta) \sin(2k+1)\Phi$, the coefficient K_1 may be approximated by

$$K_1 \approx \frac{1}{2} \left[J_o\left(\delta_1 (1 + \beta_1)\right) + J_o\left(\delta_1 (1 - \beta_1)\right) \right] \quad (178)$$

Similarly, the second coefficient of $\sin \omega_c t$, K_2, may be expanded and approximated by

$$K_2 \approx \frac{1}{2} \left[J_o\left(\delta_1 (1 + \beta_1)\right) - J_o\left(\delta_1 (1 - \beta_1)\right) \right] b(t) \quad (179)$$

In the same manner, the coefficients of $\cos \omega_c t$, K_3 and K_4 are, approximately,

$$K_3 \approx \left[J_1\left(\delta_1 (1 + \beta_1)\right) + J_1\left(\delta_1 (1 - \beta_1)\right) \right] \sin \omega_{sc} t \quad (180)$$

and

$$K_4 \approx \left[J_1\left(\delta_1 (1 + \beta_1)\right) - J_1\left(\delta_1 (1 - \beta_1)\right) \right] b(t) \sin \omega_{sc} t \quad (181)$$

This completes the expansion of $e_1(t)$ to first order. With the aid of Eqs. (178), (179), (180), and (181), the modulated signal is approximated by

$$\begin{aligned}\frac{e_1(t)}{\sqrt{2S}} \approx\ & \sin(\omega_c t)\left[\frac{1}{2}\left[J_o\left(\delta_1(1+\beta_1)\right)+J_o\left(\delta_1(1-\beta_1)\right]\right]\right. \\ & + \sin\omega_c t\left[\frac{b(t)}{2}\left[J_o\left(\delta_1(1+\beta_1)\right)-J_o\left(\delta_1(1-\beta_1)\right)\right]\right] \\ & + \cos\omega_c t\left[J_1\left(\delta_1(1+\beta_1)\right)+J_1\left(\delta_1(1-\beta_1)\right)\right]\sin\omega_{sc}t \\ & + \cos\omega_c t\left[J_1\left(\delta_1(1+\beta_1)\right)+J_1\left(\delta_1(1-\beta_1)\right)\right]b(t)\sin\omega_{sc}t\end{aligned} \tag{182}$$

The first term of Eq. (182) is the carrier component of the signal. The second term indicates an AM modulation of the carrier induced by the ambiguity resolving code, b(t). Thus, in the vicinity of the carrier, the spectrum of the signal is that of a random square wave amplitude modulated sinewave with maximum amplitude proportional to $J_o(\delta_1(1+\beta_1)$ and minimum amplitude proportional to $J_o(\delta_1(1-\beta_1))$*.

The third term of Eq. (182) is the subcarrier component and the last term is the AM induced on the subcarrier by the code. Again, the spectrum in

---

* It is noted that since $J_o(x)$ and $J_1(x)$ are not monotonic, the roles of maximum and minimum may be interchanged depending on the values of δ_1 and β_1.

the vicinity of the subcarriers is that of a random square wave amplitude modulated sinusoid with maximum amplitude proportional to $J_1(\delta_1(1+\beta_1))$ and minimum proportional to $(\delta_1(1-\beta_1))$. The approximate spectrum of $e_1(t)$ is shown in Fig. 13.

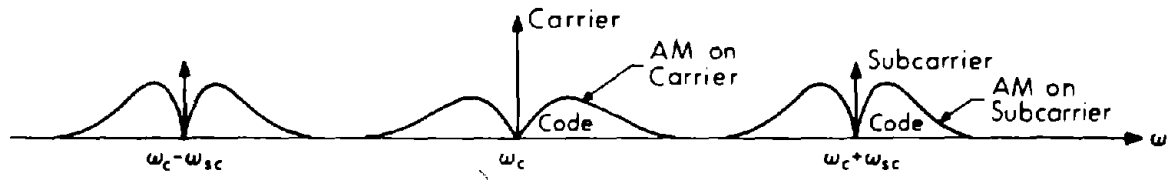

Fig. 13 Approximate Spectrum of a Carrier, Phase Modulated by a Subcarrier which is Amplitude Modulated by a BINOR Code

Derivation of a similar spectrum for the case in which b(t) is the sum of square waves is substantially more complicated. However, under the assumptions that $\delta_1 < 1, \beta_1 < 1$ and $|b(t)|_{max} = 1$, Eq. (175) may be approximated by

$$\frac{e_1(t)}{\sqrt{2S}} \approx \sin(\omega_c t)\left[1 - (\delta_1 \sin\omega_{sc}t)(\delta_1\beta_1 b(t)\sin\omega_{sc}t)\right] + \cos(\omega_c t)\left[\delta_1\sin\omega_{sc}t + \delta_1\beta_1 b(t)\sin\omega_{sc}t\right] \quad (183)$$

$$\approx \sin(\omega_c t)\left[1 - \frac{\delta_1^2\beta_1}{2}\right] + \cos(\omega_c t)[\delta_1\sin\omega_{sc}t + \delta_1\beta_1 b(t)\sin\omega_{sc}t] + \text{terms at twice subcarrier}$$

Eq. (183) is similar in form to Eq. (182). Again, the spectrum in the vicinity of the carrier is that of a sinusoid which is amplitude modulated by the sum of square waves, b(t), with deviation $\delta_1^2\beta_1/2$. Similarly, the spectrum in the vicinity of the subcarrier is, again, that of a sinwave, amplitude modulated by b(t) with deviation, β_1. Therefore, the spectrum shown in Fig. 13 for the BINOR case is also an adequate description of the signal spectrum when b(t) is the sum of square waves. The attributes of the partial AM spectrum will be discussed below relative to those of the partial PM spectrum which is derived next.

4.2.2 Partial PM

The partial PM signal is defined as follows:

$$e_2(t) = \sqrt{2S}\left[\sin\ \omega_c t + \delta_2 \sin\left(\omega_{sc} t + \beta_2\, b(t)\right)\right] \tag{184}$$

where δ_2 = sub carrier phase deviations

β_2 = ambiguity signal phase modulation deviation

Again, the carrier, subcarrier and ambiguity code components can be found by straightforward expansion of Eq. (184).

$$\frac{e_2(t)}{\sqrt{2S}} = \sin(\omega_c t)\ \cos\left(\delta_2 \sin\left(\omega_{sc} t + \beta_2\, b(t)\right)\right) \cos\ \omega_c t\ \sin\left(\delta_2 \sin\ \left(\omega_{sc} t + \beta_2\, b(t)\right)\right) \tag{185}$$

But, using the Bessel expansions,

$$\cos\ \left(\delta_2 \sin\ \left(\omega_{sc} t + \beta_2\, b(t)\right)\right) = J_o\ (\delta_2) + \ldots \tag{186}$$

and

$$\sin\left(\delta_2 \sin\left(\omega_{sc}t + \beta_2 b(t)\right)\right) = 2J_1(\delta_2)\sin\left(\omega_{sc}t + \beta_2 b(t)\right)+\ldots$$

$$= 2J_1(\delta_2)\cos\left(\beta_2 b(t)\right)\sin(\omega_{sc}t) \qquad (187)$$

$$+ 2J_1(\delta_2)\sin\left(\beta_2 b(t)\right)\cos(\omega_{sc}t) + \ldots$$

Eq. (187) can be further simplified when b(t) is a BINOR code. Then, $\cos(\beta_2 b(t)) = \cos\beta_2$ and $\sin(\beta_2 b(t)) = b(t)\sin\beta_2$. In this case $e_2(t)$ is approximated by

$$\frac{e_2(t)}{\sqrt{2S}} \approx J_o(\delta_2)\sin(\omega_c t)$$

$$+ 2J_1(\delta_2)\cos\beta_2 \sin(\omega_{sc}t)\cos(\omega_c t) \qquad (188)$$

$$+ 2J_1(\delta_2)\sin\beta_2\, b(t)\cos(\omega_{sc}t)\cos(\omega_c t)$$

The first term of Eq.(188) is the carrier component. The second term is the subcarrier component and the third term is the subcarrier's phase modulation due to the code. The approximate spectrum of the partial PM signal is shown in Fig. 14.

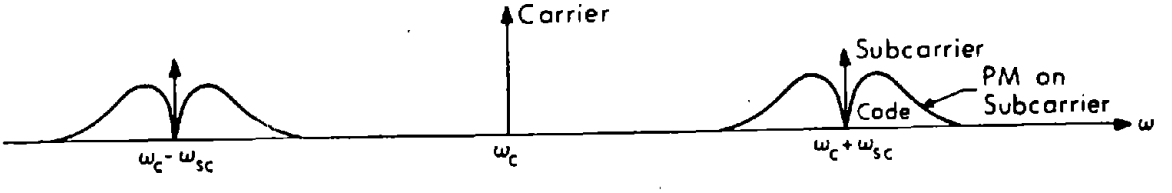

R-5404

Fig. 14 Approximate Spectrum of a Carrier, Phase Modulated by a Subcarrier which is Phase Modulated by a BINOR Code

A similar spectrum is derived for the case in which b(t) is the sum of square waves. Appendix I shows that when b(t) is the sum of four unity amplitude square wave each with deviation $\beta_2/4 < 1$, such that $|\beta_2 b(t)|_{max} = \beta_2$, then

$$\cos\left(\beta_2\, b(t)\right) \approx \cos^4 \frac{\beta_2}{4} \tag{189}$$

and

$$\sin\left(\beta_2\, b(t)\right) \approx b(t) \sin \frac{\beta_2}{4} \cos^3 \frac{\beta_2}{4} \tag{190}$$

Substituting the approximations of Eq. (189) and (190) into Eq. (187) results in an approximation for $e_2(t)$ given by

$$\begin{aligned} \frac{e_2(t)}{\sqrt{2S}} \approx\ & J_o(\delta_2) \sin(\omega_c t) \\ & + 2J_1(\delta_2) \cos^4 \frac{\beta_2}{4} \sin(\omega_{sc} t) \cos(\omega_c t) \\ & + 2J_1(\delta_2)\, b(t) \sin \frac{\beta_2}{4} \cos^3 \frac{\beta_2}{4} \cos(\omega_{sc} t) \cos(\omega_c t) \end{aligned} \tag{191}$$

Eq. (191) has the same form as Eq. (188), therefore, the approximate spectrum of Fig. 14 is also valid for the case in which b(t) is the sum of square waves.

4.2.3 Evaluation of Spectra

The most obvious difference between the spectra of Figs. 13 and 14 is the presence of AM sideband around the carrier in the partial AM case of Fig. 13. These sidebands are undesirable and form the basis for selecting partial PM over partial AM. First, the presence of the sidebands limits the flexibility of the waveform. In particular, if the ranging modulation provides a clear spectrum in the vicinity of the carrier, this region can be used for data communication purposes in which straightforward data modulation techniques applied to the carrier. Alternatively, if the region around the carrier is kept clear, the problem of carrier acquisition is that much simpler. More important, the presence of significant AM sidebands around the carrier indicates that the ambiguity resolving code power is distributed inefficiently in the signal spectrum. Consequently, both the AM sidebands about the subcarrier and about the carrier must be demodulated and combined in the partial AM case to provide overall performance which is competitive with that of the partial PM signal structure. It is concluded that more receiver hardware is required by the partial AM signal to provide equivalent performance.

4.3 Ambiguity Resolution Techniques

The BINOR coding scheme was evolved for cases where a binary (two-level) signal is required or when the system is peak deviation limited. The BINOR lends itself to a relatively simple demodulator implementation when each of the ambiguity resolving tones is measured in sequence. However, full utilization of the data energy in the BINOR signal requires a rather complex implementation because for full utilization of data energy these operations should be done in parallel. For example, consider a BINOR code consisting of thirteen tones, i.e., clock plus twelve ambiguity resolving tones. The correlation coefficient of each tone in this code is $\rho_{13} = 0.225$. Now $(\rho_{13})^2$ is a measure of the available power in each tone but it is the energy which determines the accuracy derivable from each. Thus, if each tone is measured in sequence for 1/13 of the total measurement time, then accuracy is

proportional to $(1/13)\ \rho_{13}^2$. One method suggested for reducing this effect without vastly increasing complexity is to transmit the entire code in 6 groups consisting of clock + 2 ambiguity resolving tones. The tone correlation coefficient during each group is $\rho = 1/2$, thus, while each tone is still measured for 1/13 of the total time, the energy per measurement is substantially increased. This idea can be carried to the limit by simply transmitting each of the tones separately in sequence. In this way the nonlinear interaction among components and the subsequent spectral spreading of component energy is avoided entirely. The major disadvantage of sequencing to this extent is the added complexity of the transmitter. In addition, this type of implementation does not provide for failure during the sequence. That is, failure during one step of the sequence constitutes a total failure which cannot be compensated until the sequence repeats itself. Parallel mechanizations fail more gracefully in that poor operation during part of the total measurement time does not necessarily imply total failure.

Parallel operation of the BINOR technique with twelve ambiguity resolving tones requires twelve phase locked loop and twelve phase measurements. Clearly, this involves a substantial increase in hardware complexity at the receiver over that required for sequential operation. The amount of hardware required can be reduced if some of the tones are deleted from the code. For example, every other tone can be sent while still providing the same performance if the phase of each of these tones is measured with twice the precision. Thus, the number of PLL's and phase measurements required for ambiguity resolution is reduced by a factor of 2. Similarly, every third tone can be sent while maintaining performance if each of these tones is measured with 4 times the precision. The number of PLL's and phase measurement devices may thus be reduced by a factor of 3.

On the basis of the above discussion it is decided that parallel operation with a reduced number of tones should be investigated further. The number of tones and the method by which the tones are combined, i.e., BINOR or straight sum, depends on

mission requirements. These latter requirements determine whether or not the system will be peak deviation limited, which in turn determines the utility of the BINOR code vs. the sum of square waves.

4.4 Deviation Requirements

At this point, a modulation optimization is carried out in order to determine, roughly, the various deviations which will meet mission requirements. If it is found that a b(t) in the form of a sum of square wave can provide the necessary performance while still in the linear phase modulation region, i.e., $\sin \phi \approx \phi$, then it will be concluded that the sum of square waves provides performance superior to that of the BINOR code because nonlinear interactions are avoided.

The ground rules assumed in the optimization process are:

1) The modulation is partial PM as defined above, with b(t) = sum of square waves

2) Total time to acquire including range measurement but excluding carrier acquisition is 1 sec.

3) Total signal power-to-noise density ratio is S/N_o = 36 dB = 4000.

4.4.1 Signal-to-Noise Ratio Expressions

Assuming a modulated signal of the form of Eq. (184), the signal-to-noise density available for carrier tracking is

$$(S/N_o)_c = \frac{2S}{N_o} J_o^2(\delta_2) \overline{\sin^2(\omega_c t)} = \frac{S J_o^2(\delta_2)}{N_o} \qquad (192)$$

Thus, the r. m. s. phase error in a carrier loop with double side noise bandwidth, B_{mc}, is

$$\Delta\phi_c = \frac{1}{\sqrt{\frac{2S}{N_o B_{mc}} J_o^2(\delta_2)}} \tag{193}$$

The demodulated tone power at the subcarrier frequency, ω_{sc}, is found from Eq. (191). After demodulation by the carrier reference, $\sqrt{2}\cos\omega_c t$, the subcarrier is

$$e_{sub}(t) = \sqrt{S}\left(2J_1(\delta_2)\cos^4\frac{\beta_2}{4}\right)\sin(\omega_{sc}t) \tag{194}$$

The noise density after demodulation is again N_o; thus, the $\sqrt{2}$ amplitude of the reference accounts for coherent addition of signal and incoherent addition of noise after demodulation so that the signal-to-noise density is given by

$$(S/N_o)_t = \frac{2S}{N_o} J_1^2(\delta_2)\cos^8\frac{\beta_2}{4} \tag{195}$$

Thus, the phase error of a subcarrier tracking loop with noise bandwidth B_{nt} is

$$\Delta\phi_t = \frac{1}{\sqrt{\frac{4S}{N_o B_{nt}}\left(J_1(\delta_2)\cos^4\frac{\beta_2}{4}\right)^2}} \tag{196}$$

Finally, the demodulated code power is found from Eq. (191) as follows: the code term of Eq. (191) is multiplied by the carrier reference, yielding

$$e_{\substack{\text{sub}\\\text{code}}}(t) = \sqrt{S}\left(2J_1(\delta_2)\, b(t) \sin\frac{\beta_2}{4} \cos^3\frac{\beta_2}{4}\right)\cos(\omega_{sc}t) \tag{197}$$

This, in turn, is multiplied by the subcarrier reference $\sqrt{2}$ $\cos(\omega_{sc}t)$ which yield the video code signal

$$e_{code}(t) = \frac{\sqrt{2S}}{2}\left(2J_1(\delta_2)\, b(t) \sin\frac{\beta_2}{4} \cos^3\frac{\beta_2}{4}\right) \tag{198}$$

Each of the square waves in the code is filtered to extract its fundamental sinusoidal components. Each of these is described by,

$$e_{amb}(t) = \frac{4}{\pi}\frac{\sqrt{2S}}{2}\left(2J_1(\delta_2) \sin\frac{\beta_2}{4} \cos^3\frac{\beta_2}{4}\right)\sin\omega_i t \tag{199}$$

where ω_1 is an ambiguity resolution tone frequency. Therefore, the available signal-to-noise density for these tones is given by

$$(S/N_o)_a = \frac{16}{\pi^2}\frac{S}{N_o}\left(J_1(\delta_2) \sin\frac{\beta_2}{4} \cos^3\frac{\beta_2}{4}\right)^2 \tag{200}$$

The phase error in each of the ambiguity resolving tone loops of noise bandwidth, B_{na}, is, thus, given by

$$\Delta\phi_a = \frac{1}{\sqrt{\frac{32}{\pi^2}\frac{S}{N_o B_{na}}\left(J_1(\delta_2)\sin\frac{\beta_2}{4}\cos^3\frac{\beta_2}{4}\right)^2}} \qquad (201)$$

Equations (192) through (201) provide the quantitative data required to determine the utility of the modulation scheme. But, before establishing deviation requirements, the optimum number of tones to be transmitted must be determined.

4.4.2 Number of Tones

This section analyzes the relative merits of transmitting 4 tones or 6 tones. The 4 tones would be 40 kHz, 5 kHz, 625 Hz and 78.125 Hz, i.e., the tone ratio is 8. For the 6 tone case the ratio is 4 between tone frequencies and the tones would be 80 kHz, 20 kHz, 5 kHz, 1250 Hz, 312.5 Hz and 78.125 Hz. The analysis determines the deviations required to provide 99.9 % probability of acquisition P_{acq} in 1 second given that $S/N_o = 4000$.

A detailed description of the acquisition process for the type of system considered here is given in Section 4.5. However, for the purpose of this analysis is need only be noted that ambiguity resolution will be completed successfully if each of the tones is measured to a specific accuracy.

Consider the 4 tone configuration. The maximum error permitted per tone is $\Delta\phi_{a\,max} = \pm 22.5^o$. Thus, the probability of exceeding an error of 22.5^o on each individual tone P_{ei} must be small enough so that the probability of acquisition exceeds 99.9%. That is,

$$P_{acq} = (1 - P_{ei})^4 \geq .999 \qquad (202)$$

but P_{acq} is approximately

$$P_{acq} \approx 1 - 4\,P_{ei} \tag{203}$$

Combining Eqs. (202) and (203) yields

$$P_{ei} \leq .00025 \tag{204}$$

Such a probability of error will be achieved if 22.5^{o} is 3.66 times the r.m.s. phase error per tone, i.e.,

$$\Delta\phi_a \leq \frac{22.5}{3.66} \text{ degrees} = \frac{\pi}{8 \times 3.66} \text{ radians} \tag{205}$$

Substituting this in Eq. (201) yields that

$$J_1(\delta_2) \sin\frac{\beta_2}{4} \cos^3\frac{\beta_2}{4} \geq \frac{1}{\frac{\pi}{(8 \times 3.66)}\,\frac{8}{\pi}\,\sqrt{2000}} \tag{206}$$

$$= \frac{3.66}{45} = .0813$$

where, it is assumed that $B_{na} = 1$ and $S/N_oB_{na} = 4000$. Eq. (206) may be approximated for small $\beta_2/4$ as

$$J_1(\delta_2)\,\beta_2 \geq .325 \tag{207}$$

An entirely similar computation may be carried out for the case of tones. Then the maximum permitted error is 45^{o}, but 6 tones must be measured with a total probability of success of 99.9%. That is

$$P_{acq} \approx 1 - 6\,P_{ei} \tag{208}$$

and

$$P_{ei} \leq .000166 \tag{209}$$

This probability will be achieved if 45° is 3.77 times the r.m.s. error, i.e.,

$$\Delta\phi_a \leq \frac{45^{\circ}}{3.77} \text{ degrees} = \frac{\pi}{(4)\ (3.77)} \text{ radians} \tag{210}$$

This result cannot be substituted in Eq. (201) because Eq. (201) is appropriate specifically to the 4 tone system. The corresponding error for a 6 tone system is derived along the lines of Appendix I to be

$$\Delta\phi_a = \frac{1}{\sqrt{\frac{32}{\pi^2}\ \frac{5}{N_o B_{na}}\left(J_1(\delta_2)\ \sin\frac{\beta_2}{6}\ \cos^5\frac{\beta_2}{6}\right)^2}} \tag{211}$$

Now, substituting Eq. (210) in (211) yields that

$$J_1(\delta_2)\ \sin\frac{\beta_2}{6}\ \cos^5\frac{\beta_2}{6} \geq \frac{1}{\frac{\pi}{(4)\ (3.77)}\ \frac{4}{\pi}\ \sqrt{8000}} \tag{212}$$

$$= \frac{3.77}{89.5} = .0422$$

Again, assuming that $\beta_2/6$ is small, then, Eq. (212) may be approximated by

$$J_1(\delta_2)\,\beta_2 \geq .253 \tag{213}$$

Comparison of Eq. (213) with Eq. (207) shows that to a first order approximation the 6 tone system requires less peak deviation on the subcarrier (with given deviation δ_2) than the 4 tone system. It is further concluded that a more exact calculation will not alter this result. The deviation criterion is not the only optimization criterion. In fact, equipment complexity could be a more important factor if the deviation requirements of both Eq. (213) and Eq. (207) can be met easily. The deviation requirements are met easily if values of δ_2 and β_2 can be found which simultaneously provide the required ranging accuracy (such as defined by Eq. (205) for the case of 4 tones) while satisfying Eq. (207) or (213).

Assuming that 1) the desired accuracy in ranging is 30 ft., i.e., $\Delta\phi_t$ must be less than 60.4 mr, 2) S/N_o is 4000, and 3) the noise bandwidth of the range tone is arbitrarily chosen to be 8 cps, then, Eq. (196) may be recast as

$$J_1(\delta_2)\cos^4\frac{\beta_2}{4} \geq \frac{1}{(6.04\times10^{-2})\sqrt{\frac{(4)\,(4000)}{(8)}}} = .368 \tag{214}$$

A similar equation can be generated for the case of 6 ambiguity resolving tones, namely,

$$J_1(\delta_2)\cos^6\frac{\beta_2}{6} \geq .368 \tag{215}$$

At this point, let us summarize the optimization conditions for the 4 and 6 tone system in TABLE 8.

TABLE 8. Optimization Conditions for Ambiguity Resolving Tones

Condition	4 Tones	6 Tones
Signal power-to-noise density	4000	4000
Amb. res. bandwidth, B_{ma}	1 cps	1 cps
Range tone bandwidth, B_{mt}	8 cps	8 cps
Total prob of acquisition	99.9%	99.9%
Prob of error per tone	.00025	.000166
Max permitted error per tone	22.5^{o}	45^{o}
Deviation product for ambiguity resolution	$J_1(\delta_2) \sin\frac{\beta_2}{4} \cos^3\frac{\beta_2}{4} \geq .0813$	$J_1(\delta_2) \sin\frac{\beta_2}{6} \cos^5\frac{\beta_2}{6} \geq .0422$
Deviation product for ranging accuracy	$J_1(\delta_2) \cos^4\frac{\beta_2}{4} \geq 0.368$	$J_1(\delta_2) \cos^5\frac{\beta_2}{6} \geq 0.368$

If the deviations selected just meet the conditions of TABLE 8, then for the 4 tone case

$$\frac{J_1(\delta_2) \sin\frac{\beta_2}{4} \cos^3\frac{\beta_2}{4}}{.0813} = \frac{J_1(\delta_2) \cos^4\frac{\beta_2}{4}}{0.368} = 1 \tag{216}$$

or

$$\tan\frac{\beta_2}{4} = \frac{.0813}{368} = .221 \tag{217}$$

and, thus,

$$\beta_2 = 50^\circ \tag{218}$$

the subcarrier deviation required is found from

$$J_1(\delta_2)\ \cos^4(12.5^\circ) = .368 \tag{219}$$

or

$$J_1(\delta_2)\ \frac{.368}{.908} = .405 \tag{220}$$

or, finally

$$\delta_2 = 0.9 \tag{221}$$

The deviations required to meet the conditions of TABLE 9 with 6 tones are found similarly, namely

$$\frac{J_1(\delta_2)\sin\frac{\beta_2}{6}\ \cos^5\frac{\beta_2}{6}}{.0422} = \frac{J_1(\delta_2)\cos^6\frac{\beta_2}{6}}{0.368} = 1 \tag{222}$$

or

$$\tan\frac{\beta_2}{6} = \frac{.0422}{0.368} = 0.115 \tag{223}$$

and, thus, for this case,

$$\beta_2 = 39^\circ \tag{224}$$

Again, the subcarrier deviation required is found from

$$J_1(\delta_2)\cos^6(6.5°) = .368 \qquad (225)$$

or

$$J_1(\delta_2) = \frac{.368}{.9616} = .383 \qquad (226)$$

or, finally,

$$\delta_2 = .84 \qquad (227)$$

The deviation requirements are summarized in TABLE 9. It is noted that the 6 tone system has slightly lower suppression effect on the carrier. All other performance factors are essentially the same. The slight improvement in performance with the 6 tone system is obtained at considerable expense in term of equipment complexity. In particular, two more phase locked trackers and phase measurements and two more ambiguity resolution computations are required by the 6 tone system relative to the 4 tone system. For this reason, the 4 tone ambiguity resolution technique is selected.

TABLE 9. Deviation Requirements

deviation, mod. parameter	4 tones	6 tones
carrier dev. δ_2	0.9	0.84
carrier amplitude, $J_o(\delta_2)$	0.8075	0.8312
peak subcarrier dev. β_2	50°	39°
individual square wave amp	12.5°	6.5°
ranging accuracy (1 second ave.)	10 ft	10 ft
prob. of acquisition	99.9%	99.9%

4.4.3 Comparison with BINOR

The discussion above shows that the requirements imposed by characteristics of the mission are such that rather low deviations may be employed in the modulation. It was suggested in Sect. 4.3 that under these conditions the BINOR modulation technique would not be as desirable as a straight linear combination of ambiguity resolving tones. This section will attempt a comparison of the performance obtainable with a BINOR code versus the square wave performance derived above.

First, the performance obtainable with subcarrier technique, in general, can be compared with a normal implementation of the BINOR technique in which a BINOR code is applied directly to the carrier. Basically, the subcarrier technique provides complete acquisition of range data in about 1 sec (excluding carrier acquisition) while avoiding sequencing of the transmitted signal. The carrier component amplitude is constant and is suppressed roughly 2 dB by the presence of the ranging and ambiguity resolving signals. The ranging signal provides the required accuracy in an 8 cps bandwidth. Therefore, if the ranging data (which is available during the entire acquisition internal) is averaged over 1 sec an r.m.s. error due to noise of roughly 10 ft. can be achieved. The probability of correct ambiguity resolution is the same, under the same conditions, for both techniques. The excess of ranging accuracy may be traded for a shorter acquisition time or increased carrier power, as desired. By avoiding sequencing, the subcarrier technique offers important advantages with respect to spacecraft reliability and total "mean time to acquire" as discussed in Sec. 4.3. However, an important advantage of the BINOR is the simplicity of receiver hardware with the normal implementation of the technique. The relative complexity of the receiver implementation required for the subcarrier technique will be discussed in Sec. 4.6 below.

The BINOR combining technique may be used in an alternate way to provide the ambiguity resolving tones using the modulation waveform of Eq. (184). For example, a BINOR may be constructed

by hard limiting the sum of 5 square waves at 80 kHz, 5 kHz, 1250 Hz, and 312.5 Hz. It is instructive to compare the performance achievable with this 5 tone BINOR vs. a 5 tone linear combination.

The number of linear tones is reduced to 5 to provide a fair comparison with the BINOR which is typically realized with an odd number of components when equal weighting of all components is employed. Thus, both techniques considered will provide ambiguity resolution down to 500 miles instead of the full 2000 miles.

Since only 5 tones instead of 6 are employed, the probability of correct acquisition is given by 1-5 (.000166) = 99.917%. This modification allows for much of the previous analysis of the 6 tone linear sum case to be used here.

The implementation for demodulation of the 5 tone BINOR consists of 5 PLL's which employ square wave reference signals at the appropriate frequencies. The demodulated video BINOR is distributed to the inputs of these PLL's without any filtering. It has been shown that such an arrangement leads to degraded performance because the harmonics of the square wave reference convert more noise than useful error signal down to video. Nonetheless, the PLL's are assumed to operate in the normal manner for the purposes of this analysis. It is thus assumed that the components of the BINOR code which are available for tracking by the PLL's are described

$$e_{bi}(t) = \frac{\sqrt{2S}}{2} \left(2 J_1 (\delta_2) \rho_5 \sin \beta_b\right) e_{sqi}(t) \qquad (228)$$

where $\rho_5 = .375$ is the BINOR correlation coefficient, β_b is the deviation of the subcarrier by the BINOR signal, and $e_{sqi}(t)$ is a square wave at frequency ω_i. Equation (228) corresponds to Eq. (199) for the sum of 4 squares.

Equation (199) is modified for the case of 5 square waves to be

$$e_{amb}(t) = \frac{4}{\pi} \frac{\sqrt{2S}}{2} \left(2 J_1 (\delta_2) \sin \frac{\beta_2}{5} \cos^4 \frac{\beta_2}{5} \right) \sin (\omega_i t) \tag{229}$$

To form a valid basis for comparison, the carrier deviation, δ_2, must be the same in both cases. Furthermore, the suppression of the subcarrier by the ambiguity resolution code must be the same in both cases. This latter requirement leads to a specification for β_b. That is, from Eq. (188) and (191) (modified for 5 tones)

$$\cos \beta_b = \cos^5 \frac{\beta_2}{5} \tag{230}$$

Since the probability of acquisition has been appropriately modified, Eq. (223) can be rewritten for 5 tones as

$$\tan \frac{\beta_2}{5} = 0.115 \tag{231}$$

or $\beta_2 = 32.5^\circ$. Thus, from Eq. (230)

$$\cos \beta_b = .968$$

$$\beta_b = 14.5^\circ \tag{232}$$

Under the assumed conditions for comparison, examination of Eq. (228) and (229) shows that the BINOR technique will provide superior performance if

$$\rho_5 \sin \beta_b \geq \frac{4}{\pi\sqrt{2}} \sin \frac{\beta_2}{5} \cos^4 \frac{\beta_2}{5} \qquad (233)$$

substituting from Eq. (230) yields

$$\rho_5 \tan \beta_b \geq \frac{4}{\pi\sqrt{2}} \tan \frac{\beta_2}{5} \qquad (234)$$

Inserting numerical values

$$\rho_5 \tan \beta_b = (.375)\ (.258) = .09675$$

and (235)

$$\frac{4}{\pi\sqrt{2}} \tan \frac{\beta_2}{5} = (.9)\ (.115) = .1035$$

The results of Eq. (235) show that the BINOR code is slightly inferior to the sum of square wave. Actually, the results are not as close as they appear to be due to the optimistic assumptions concerning the BINOR implementation. It may be argued that since it is shown in Sec. 4. 4. 2 that a 4 tone sum-of-squares system is inferior to a 6 tone system it is possible that a 3 tone BINOR would be competitive with a truncated version of the 4 tone waveform. This assumption is not quite true, as shown in Appendix J. The question, in any case, seems academic because a 3 tone system (BINOR or linear sum) with a ratio of 8 between tone frequencies will not provide the required maximum unambiguous range.

In summary, it is noted that this comparative analysis has shown that a BINOR code can be used as indicated in Eq. (188) to provide ambiguity resolution in a subcarrier modulation system. It is also found that the BINOR code will provide performance slightly inferior to that obtainable with a linear sum of square waves.

4.5 Ambiguity Resolution

It was assumed in Sec. 4.4.2 that if the phase measurement error on each tone of the 4 tone system was less than 22.5°, then ambiguity would be resolved correctly. In other words, when the ratio between tone frequencies is 8, then the measurement must provide accuracy better than $\pm \pi/8$. Similarly, for the 6 tone system in which the ratio between tones if 4, the maximum permitted error is $\pm \pi/4$. This section discusses the ambiguity resolution calculation. In particular, a ratio-of-8 system considered as shown in Fig.15.

For the purposes of illustration, the true phase in binary form is written above each waveform. Examination of these numbers shows that ambiguity resolution in the absence of noise is trivial. Denoting the higher frequency 7-bit phase measurement by $A = a_7a_6a_5a_4a_3a_2a_1$ and the lower frequency 7-bit phase measurement by $B = b_7b_6b_5b_4b_3b_2b_1$, the ambiguity resolved phase measurement is just $b_7b_6b_5a_7a_6a_5a_4a_3a_2a_1$. Thus, the precision of the answer is contributed by the higher of the two frequencies while the most significant bits come from the lower of the two frequencies. The next step in the ambiguity resolution process consists of similar operation in which the 10-bit number just derived is combined with the first 3 bits of the phase measurement of the next lower square wave, etc.

The noise induced errors complicate the process because then the lower frequency phase measurement may be off by 22.5°, i.e., $\phi_\ell = b_7b_6b_5b_4b_3b_2b_1 \pm 0001$. Clearly, an error of this magnitude can change the value of b_4 and, more importantly, b_5. Therefore, in the presence of noise ambiguity, resolution proceeds as follows: the most significant bit in the higher tone, a_7, is compared with b_4. If they agree they answer is given by

$$b_7b_6b_5a_7a_6a_5a_4a_3a_2a_1$$

In other words, if $a_7 = b_4$, then $b_7b_6b_5$ must be correct or the phase measurement error is in excess of 22.5°. (The modulation has been designed so that this does not happen frequently.)

When a_7 does not equal b_4, it is possible that an error of less than 22.5° has been induced in the measurement of the lower tone phase. Since a_7 is the most significant number of a 7-bit measurement it is assumed to be correct.

Lack of agreement between b_4 and a_7 does not necessarily mean that b_5 is incorrect. However, from Fig. 15 it is clear that errors of less than 22.5° denoted as "Type I" will increment b_5, while errors such as that denoted by "Type III" do not affect b_5. In order to determine which type of error has occurred, a difference is formed as follows:

$$\Delta = a_7a_6a_5a_4 - b_4b_3b_2b_1$$

then if $\Delta > 0$ and $a_6 = 0$, then a Type III error has occurred and then the correct phas is $b_7b_6b_5a_7a_6a_5a_4a_3a_2a_1$. If $\Delta > 0$, but $a_6 = 1$, then $b_7b_6b_5$ must be decremented, since a Type I error has occurred. That is, the correct phas is $b'_7b'_6b'_5a_7a_6a_5a_4a_3a_2a_1$, where $b'_7b'_6b'_5 = (b_7b_6b_5 - 001)$. Similarly, when $\Delta < 0$ and $a_6 = 0$, a Type II error has occurred and $b_7b_6b_5$ must be incremented to form $b^*_7b^*_6b^*_5 = (b_7b_6b_5 + 001)$ and the correct phase is $b^*_7b^*_6b^*_5a_7a_6a_5a_4a_3a_2a_1$. Finally, when $\Delta < 0$ and $a_6 = 1$, a Type III error has occurred and the correct phas is formed as $b_7b_6b_5a_7a_6a_5a_4a_3a_2a_1$ as before. The algorithm of resolving phase ambiguities is shown in Fig. 16. Fig. 16 shows that the ambiguity resolution process continues after the first cycle described above as follows: the next highest tone phase measurement, say $c = c_7c_6 \ldots c_1$ is read in and compared with $b_7b_6b_5a_7a_6 \ldots a_1$. In particular, c_4 is compared with the most significant bit of the previously derived partially resolved phase (this may be $b_7b'_7$ or b^*_7, as defined above). Then the algorithm is repeated, for example, if $c_4 = b_7$, the further resolved result is $c_7c_6c_5b_7b_6b_5a_7 \ldots a_1$, etc. Thus, the loop of Fig. 16 is

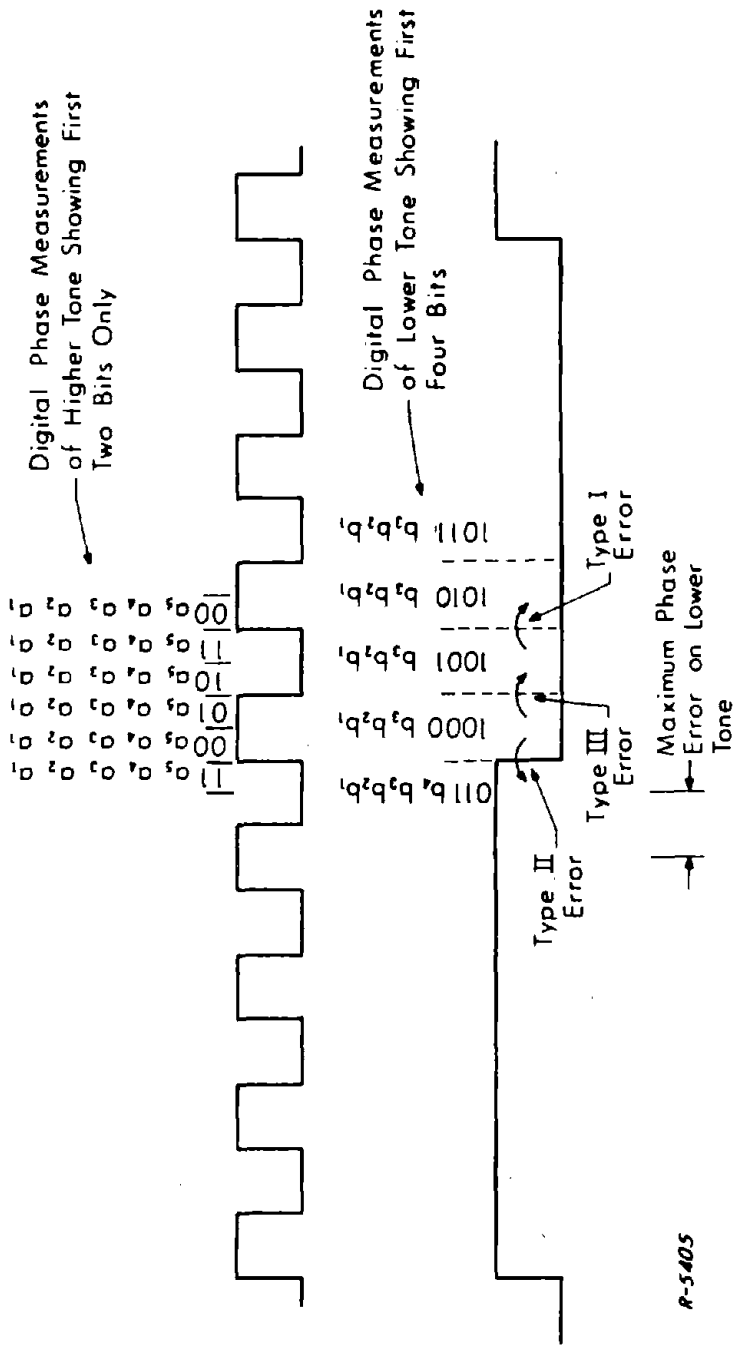

Fig. 15. Ambiguity Resolution

traversed four times for a 4 tone ambiguity resolution systems. A similar operation involving six ambiguity resolution computations is required for a 6 tone system. In that case the result after two loops of computation would be of the form $c_7c_6b_7b_6a_7a_6a_5 \ldots a_1$, etc.

Implementation of the ambiguity resolution algorithm of Fig. 16 is straightforward. Very few digital integrated circuits are required and the time required for the entire operation is negligible relative to the 1 sec acquisition time.

4.6 Phase Measurement Implementation

A complete block diagram of a possible implementation for the proposed modulation is shown in Fig. 17. Discussion of the carrier loop and in particular the carrier acquisition subsystem is deferred to Section 5. It need only be said that the constraints or the design parameters of the carrier loop are essentially the same as those previously considered. The exceptions are that the carrier component is slightly suppressed by the presence of the data which is always "ON" and that during range data acquisition the carrier component is substantially bigger than that previously considered.

Similar components are appropriate to the subcarrier tracking loop. But at this point, a technique is introduced to simplify the phase tracking measurement hardware required for the subcarrier component and the ambiguity resolution square waves. The implementation simplification is based on a device which combines the phase-locked loop operation and the phase measurement operation. The device is realized using digital modules as shown in Fig. 18. The operation is as follows: an input tone and a reference tone are supplied to the device. The reference tone is at a frequency which is 128 (2^7) times higher than the input tone to be measured. The reference tone is divided down in frequency in a 7-stage digital divider (counter). It is recognized that the contents of the divider is equal to the phase of the reference tone divided down to the input tone's frequency. Thus, when the input tone has a positive going zero crossing, the contents of the divider constitutes the phase difference between input and reference. For example, the

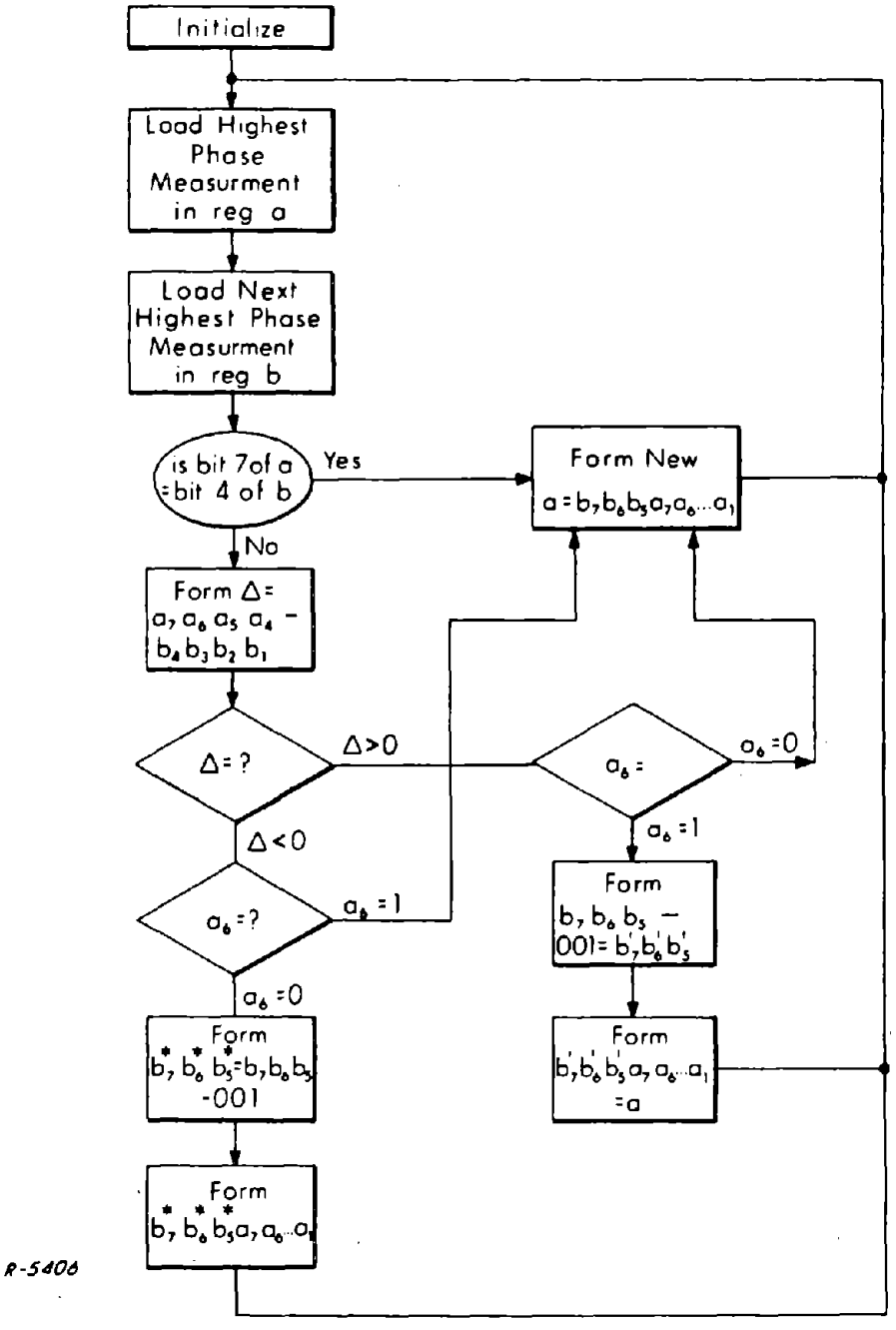

Fig. 16. Algorithm for Ambiguity Resolution

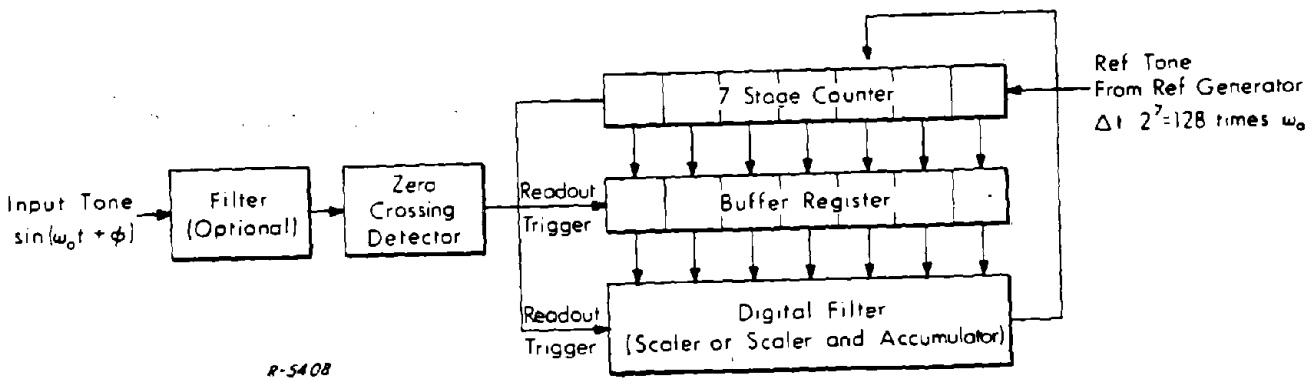

Fig. 17. Phase Tracking Digital Phase Meter

the contents of the divider would be 000000 at the positive going zero crossing of the input if the two signals were in phase. The phase difference between the two is read out of the divider by using the positive going zero crossing of input as a trigger for a buffer register. The contents of the buffer register drive a digital filter. This may consist of merely a scaler (i. e., gain), thus simulating a first order phase-locked loop. More likely, the digital filter will consist of a scaler and an accumulator to simulate the lead network compensation of the second order phase-locked loop.

The output of the digital filter is used to modify the count in the digital divider so that the input and reference are in phase, thus closing the loop. The count in the divider may be altered conveniently at the instant when the contents of the divider are zero. At that moment a trigger pulse is produced which causes the output number of the digital filter to be loaded into the counter. It is noted that the divider acts as a digital VCO, in this instance. For example, if the digital filter output is constant, then the contents of the divider are continually incremented. As a result, the unit recycles more rapidly and simulates a positive frequency offset. When this input is removed the phase accumulated by this process is retained and the unit continues to recycle at its nominal center frequency.

3

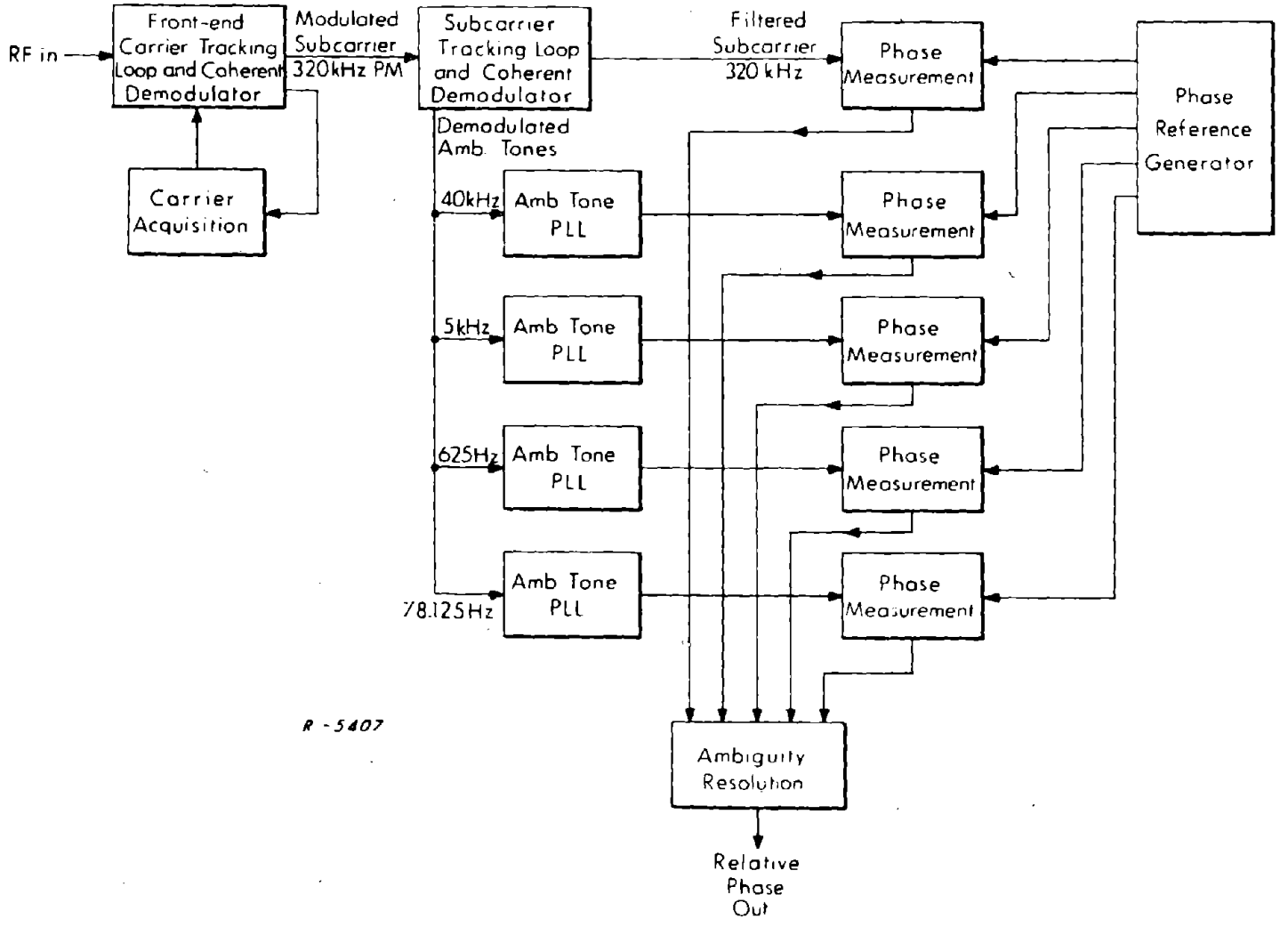

Fig. 18. Receiver Implementation

A second divide down counter is attached to the high frequency reference source. The contents of this counter are never modified and define the system reference phase. After a time sufficient for the digital phase locked loop just described to stabilize, the contents of the tracking loop divider are read out when the reference divider's contents are zero. This readout constitutes a filtered digital phase measurement of the input tone relative to the system reference phase.

A receiver demodulation system employing 7-bit digital phase tracking and measuring device is shown in Fig. 19. The carrier tracking and ambiguity resolution computation portions of the receiver are deleted.

The implementation shown in Fig. 19 starts with the output of the carrier loop coherent demodulator and provides as output the 5 digital phase measurements (relative to the system reference phase) required for unambiguous range measurement. The five 7-bit relative phase measurements may be obtained at a maximum rate 78.125 meas. per sec. Specifically, these are read when the contents of the reference oscillator divider (right-hand side of Fig. 19 are zero. The phase measurements may, in fact, be read out at this high rate provided each is averaged in an accumulator over the 1 sec acquisition interval. Then at the end of the interval the data is loaded into the ambiguity resolution computer and the resolved range is computed.

4.7 Summary

A ranging modulation has been designed for NAV/SAT applications which provides the following characteristics:

1) No sequencing is required at the satellite transmitter. All modulation functions are carried simultaneously.

2) Signal format provides for convenient generation at the satellite.

3) Ranging accuracy on the order of 10 ft.

4) 99.9% prob. of correct amb. resolution in 1 sec.

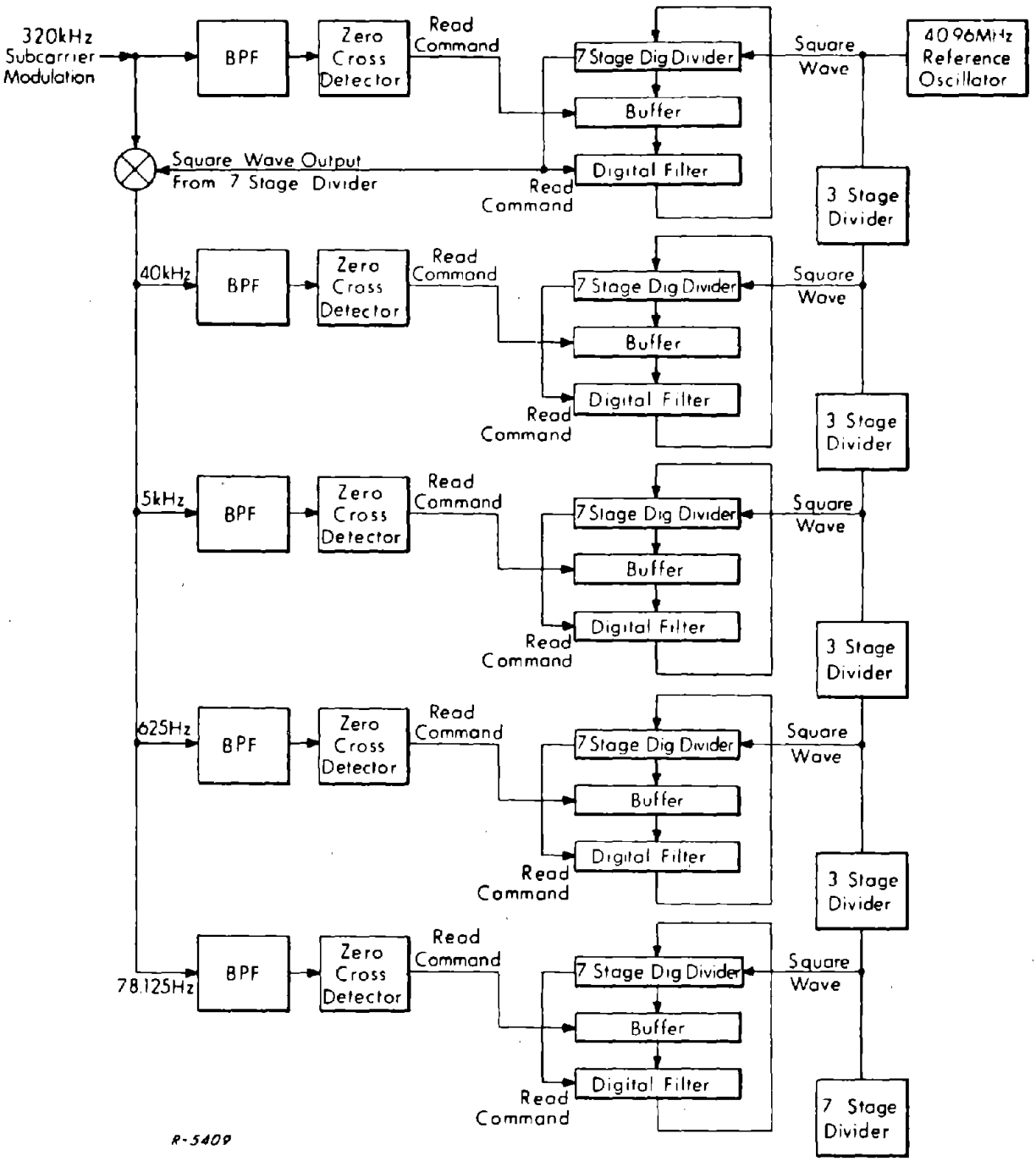

Fig. 19. Digital Data Demodulation and Measurement

5) Carrier suppression of 2 dB by modulation.

6) Carrier and clock jitter have negligible effect on ambiguity resolution process.

7) Improved performance in the presence of diffuse multipath because all data is averaged over the entire acquisition interval.

8) Receiver demodulator complexity comparable to that required for the BINOR (when range measurement phase meter and system reference generator are included in the comparison).

9) Receiver hardware lends itself readily to medium or large-scale integration.

10) The signal format can provide simultaneous data transmission capability employing straightforward communication transmission and reception concepts and implementations.

These characteristics are desirable for the NAV/SAT application. It is therefore recommended that the modulation technique be given further consideration. In particular, modulation deviations may be readjusted to reduce ranging accuracy (which is 3 times better than required) in trade for shorter acquisition time and/or higher probability of acquisition and/or higher carrier component power. It is noted, however, that these alterations are not necessary for successful implementation of the modulation technique. Further analysis of the demodulation and measurement technique will yield improvements in implementation beyond those of Fig. 19. Again, it is noted that the complexity of implementation as it now stands in Fig. 19 is on a par with other proposed systems. It is further recommended that the communication capabilities of the signal format be investigated in more detail to determine the optimum modulation method and maximum data rate capability.

5. DIVIDE DOWN PLL ACQUISITION

5.1 Introduction

Carrier acquisition is an important consideration in the design of every PLL. There are four basic ways to handle the acquisition problem: design the PLL pull-in range to cover the entire acquisition range, employ discriminator aiding, sweep the VCO until the frequency offset is within the PLL pull-in range, or employ a divide down acquisition aid. This section is devoted to a discussion of the divide down acquisition approach. Design parameters are derived and computer simulation results are presented.

5.2 Design Description

The block diagram for a PLL employing divide down acquisition is shown in Fig. 20. The diagram shows two loops. The outer loop comprises the main PLL and the inner loop implements the divide down acquisition aid. The input signal, r(t), is mixed with the output of the loop VCO to produce a convenient IF frequency. The result of the mixing operation is filtered by a bandpass filter whose width is sufficient to encompass the entire carrier uncertainty region. It is assumed that the SNR in this bandwidth may be less than unity. The output of the bandpass filter is applied to the divide down acquisition loop limiter input and to the input of a narrow bandpass filter in the main PLL. When the acquisition aid has reduced the carrier uncertainty to within the bandwidth of the narrow bandpass filter, a carrier component signal will be applied to the main PLL limiter and the main PLL will acquire, disconnecting the acquisition aid loop. The narrow bandpass filter bandwidth is selected so that the SNR at its output is high.

The discussion below is concerned with the performance of the acquisition aid loop before acquisition is completed. Fig. 21 shows a block diagram of just the relevant components of the system, i.e., the divide down acquisition loop. The rest of this section will be devoted to an analysis of this loop. The output of the wide bandpass filter is limited, frequency divided by N, and compared against a similarly divided reference in a linear phase detector. The output of the phase detector is filtered and applied to the input of the loop VCO.

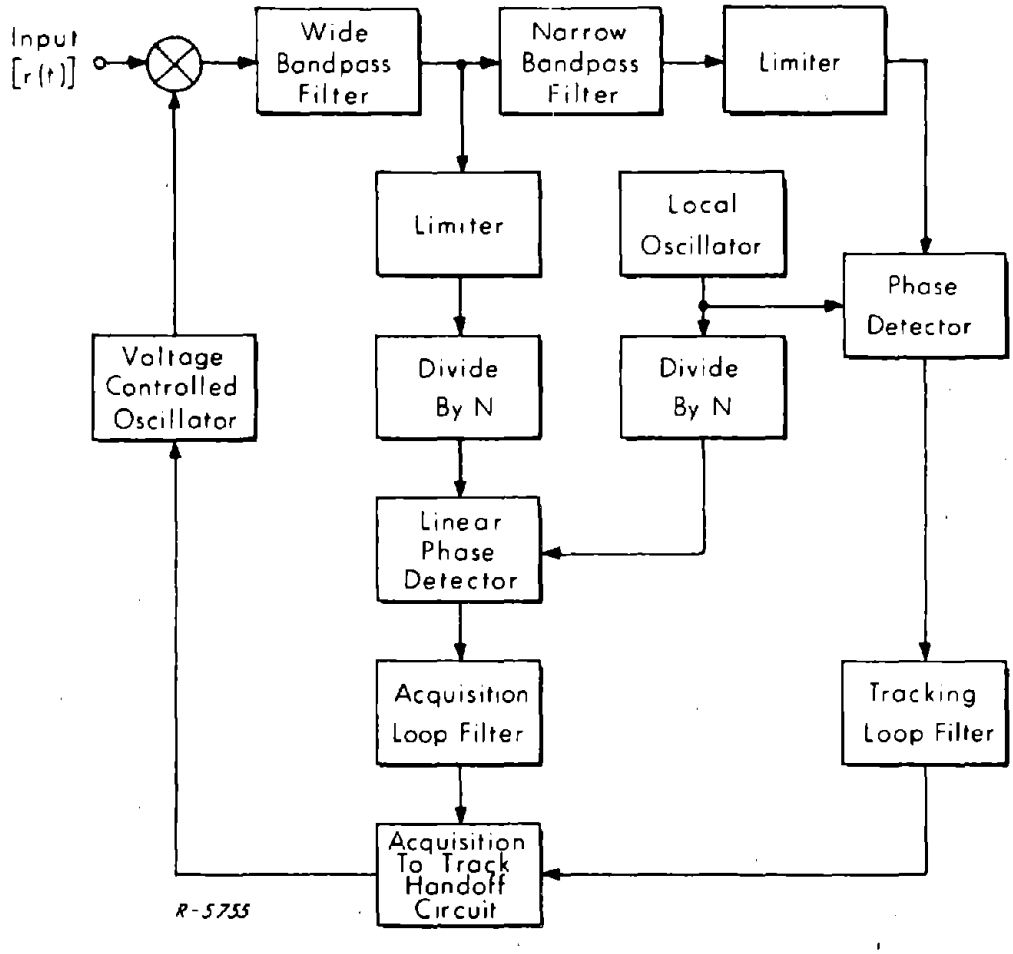

Fig. 20 Block Diagram of PLL with Divide-Down Acquisition Aiding

It is assumed that the input signal, r(t), is the transmitted signal plus noise:

$$r(t) = s(t) + n(t) \tag{236}$$

where n(t) is a sample function from a white, Gaussian process of spectral height No/2, doubled sided.

A phase model of the loop is shown in Fig. 22. It is derived in the following manner. The transmitted signal is taken as

$$s(t) = A \cos (\omega_o t + \theta(t)) \tag{237}$$

and

$$r(t) = A \cos (\omega_o t + \theta\ (t)) + n(t) \tag{238}$$

The input signal, r(t), is mixed with the VCO output to derive the IF signal. Since a low-pass phase model is desired, all operations will be performed using the complex envelope components of the IF signal. Thus, assuming that the output of the VCO is $\sin (\omega_V t + \hat{\theta}\ (t))$, the complex envelope components going into the bandpass filter are

$$e_q = \sin (\theta(t) - \hat{\theta}\ (t)) + n_1(t) \tag{239}$$

and

$$e_i = \cos (\theta(t) - \hat{\theta}\ (t)) + n_2\ (t) \tag{240}$$

where $n_1(t)$ and $n_2(t)$ are independent sample functions from a white, gaussian process of spectral height $N_o/2A^2$. The two envelope components are each filtered with low-pass equivalents of the bandpass filter. The limiter, divider, and linear phase detector are modeled as an arctangent function, modulo $2N\pi$. The arctangent function has unity gain, whereas the divider, phase detector in the loop has a phase attenuation of N. This is accounted for by introducing an attenuation of N in the gain of the loop filter. The rest of the phase model is equivalent to the actual loop implementation. This low-pass phase model will be used in subsequent discussions.

5.3 Acquisition Loop Design

The next step is the derivation of criteria for the design of the acquisition PLL. In particular, the parameter N and the loop filter characteristic G(s) must be determined. As an aid in making the

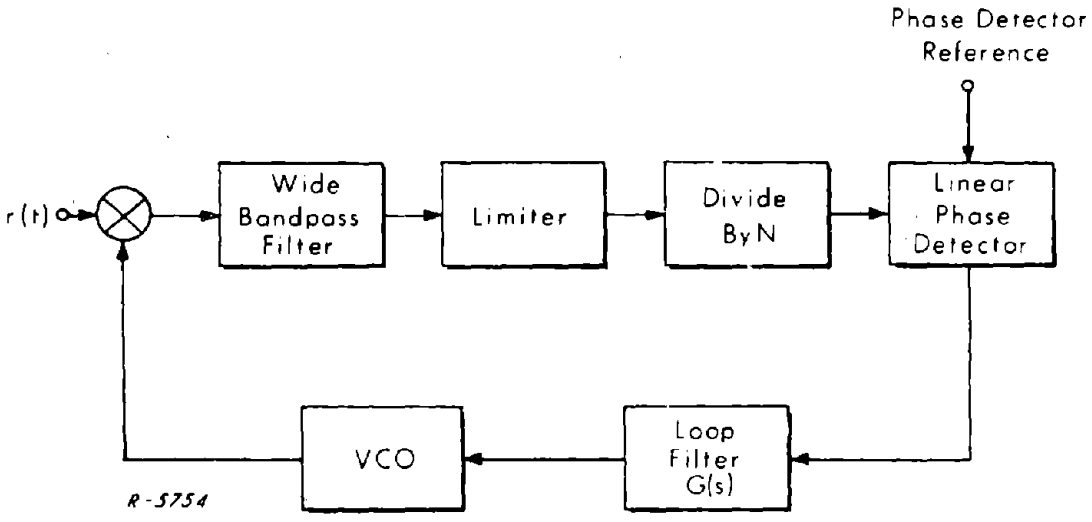

Fig. 21 Divide Down PLL

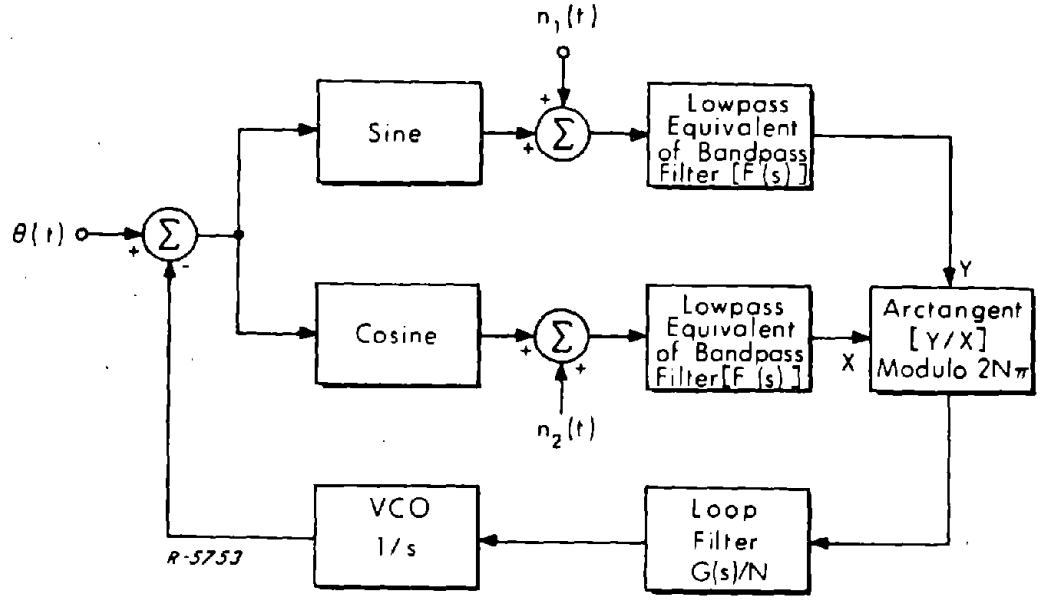

Fig. 22 Equivalent Phase Model of Loop

mathematics tractable, a linear PLL model shown in Fig. 23 will be used. The limiter suppresses the signal when the input signal-to-noise ratio is less than unity. This introduces an attenuation inside the loop which is dependent upon the SNR. This attenuation will be designated k. In addition, the noise introduces cycle skips at the output of the limiter. Every time a cycle skip occurs, the phase undergoes a step change of 2π radians. The cycle skip events are Poisson distributed and equally likely, positive and negative. For the purpose of the linear model, an additional phase noise contribution due to cycle skips, CS(t), is introduced. CS(t) is a random walk, staircase function with step height 2π. It is important to remember that the variance of such a function approaches infinity as time approaches infinity. Thus, it is important that acquisition occur before too many cycle skips occur. This criterion will establish the loop bandwidth. In particular, the characteristics of CS(t) will dictate the form for G(s).

By inspection of Fig. 23, the transient frequency error (as observed at the VCO input) due to a cycle skip step is expressible as

$$E_f(s) = \frac{s}{k}\left[\frac{K_v k G(s)}{1 + K_v k G(s)}\right] \times \frac{1}{s}$$

For the purpose of this discussion, it is assumed that G(s) will either result in a first order or second order PLL. If a second order PLL with half damping is desired (for k = 1) then

$$G(s) = 1 + \frac{\omega_n}{s} \qquad (241)$$

Since the bandwidth of the bandpass filter will be wide compared with the loop bandwidth, F(s) will be ignored. Figure 24 shows plots of the frequency error in the loop for a single cycle skip step, parametric in the suppression attenuation factor k. Note that for small k, disastrous errors can result. This particular characteristic makes a second order loop unacceptable, since, in fact, k will be minimum during maximum cycle skip activity.

The first order implementation is considered next. For a first order loop, the frequency error produced by a cycle skip never exceeds ω_n, and the damping is a function of the suppression factor k. This is definitely superior to the performance of a second order loop. But, a first order loop has a phase error proportional to the carrier frequency offset. If the loop bandwidth is relatively narrow, the resulting phase error can be hundreds of degrees. To avoid difficulty at large offset frequencies, the divider ratio N is selected so that the total phase error at the phase detector never exceeds the linear range of the phase detector which is $\pm 180^\circ$. To permit ample safety margin, the loop should be designed not to exceed $\pm 90^\circ$.

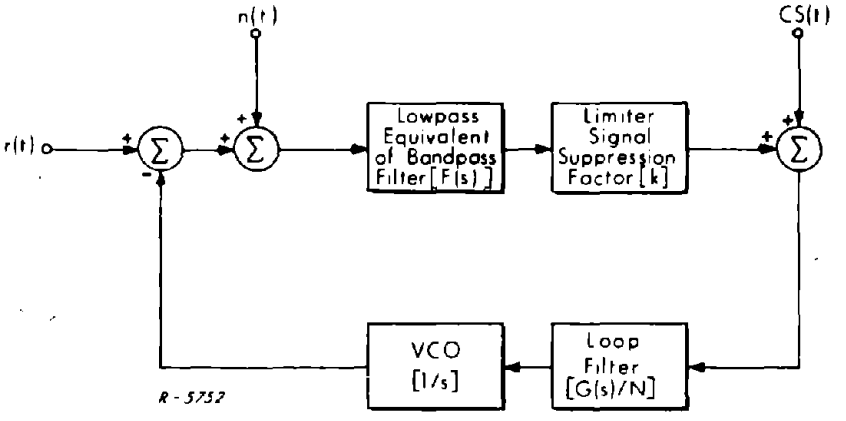

Fig. 23 Linear PLL Model

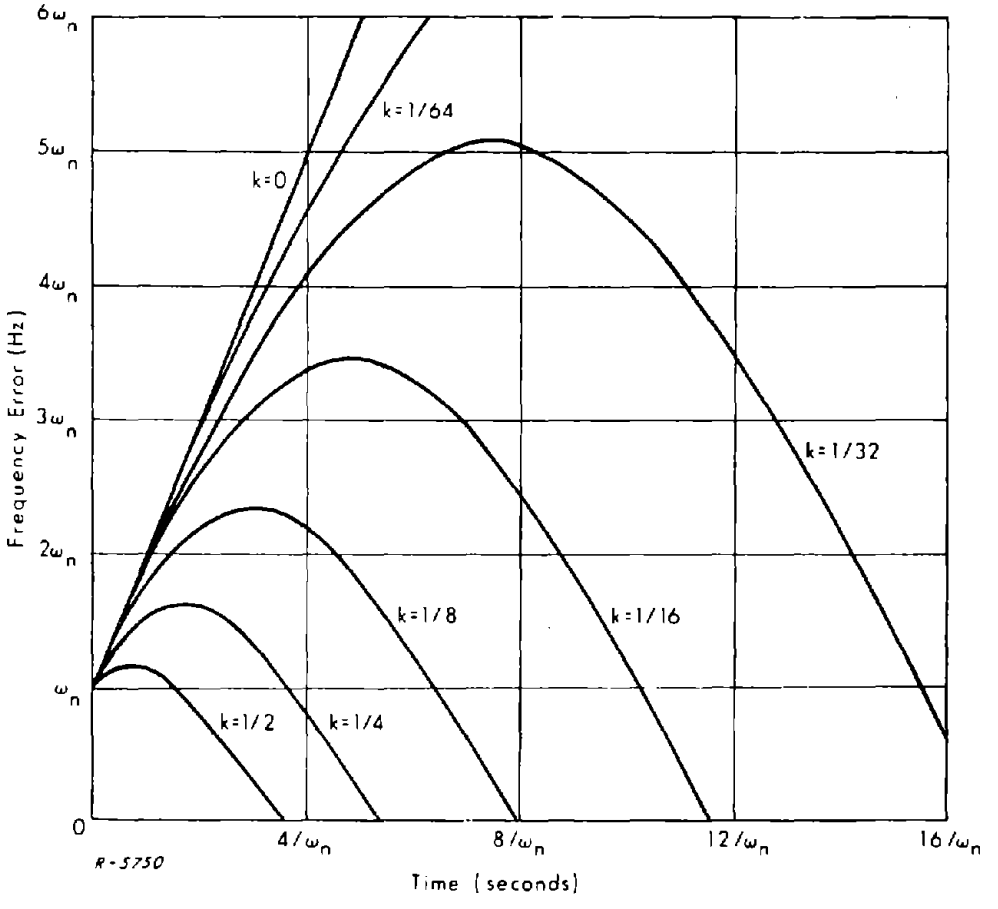

Fig. 24 Frequency Error in Loop for a Single Cycle Skip Step at t = 0

Summarizing, G(s) is determined to be a pure gain, thus producing a first order PLL. The gain will be $K_V k$ and the loop bandwidth will be $K_V/2$. The maximum carrier frequency offset in Hertz is equivalent to the single-sided bandwidth of the bandpass filter, BW/2. Thus, the maximum phase error in the loop will be

$$\text{Phase Error} = \pi BW/K_V k \text{ radians} \qquad (242)$$

The divider ratio N should be selected with a significant safety margin. In particular,

$$N \geq 2\,(\text{Phase Error})/\pi \qquad (243)$$

where N is assumed to be an integer power of 2. $K_V k$ is selected so that a small number of cycle skips (less than 10) occur within the expected loop time constant, $1/K_V k$. The suppression factor k and the average rate of cycle skips is determined from the worst case expected SNR.

5.4 Computer Simulation

As a means of verifying the expected performance of the divide-down acquisition technique, a digital computer simulation was performed. The simulation included one additional effect not previously discussed. In particular, it was assumed that the center frequency of the bandpass filter was offset from the nominal IF frequency. This would introduce a frequency offset noise bias. The block diagram used for the simulation, including this offset effect, is shown in Fig. 25. The frequency offset is simulated low-pass. This is accomplished by performing a frequency offset operation on e_q and e_i, to produce the offset quantities e_q' and e_i'.

$$e_q' = e_q \cos \omega_{of} t + e_i \sin \omega_{of} t \qquad (244)$$

$$e_i' = e_i \cos \omega_{of} t - e_q \sin \omega_{of} t \qquad (245)$$

where ω_{of} is the offset in the filter. After the filtering operation, the offset is removed by performing a complementary operation. These operations are depicted on the figure. The simulation program is listed in Appendix K. It is a straightforward implementation of the operations shown in Fig. 25.

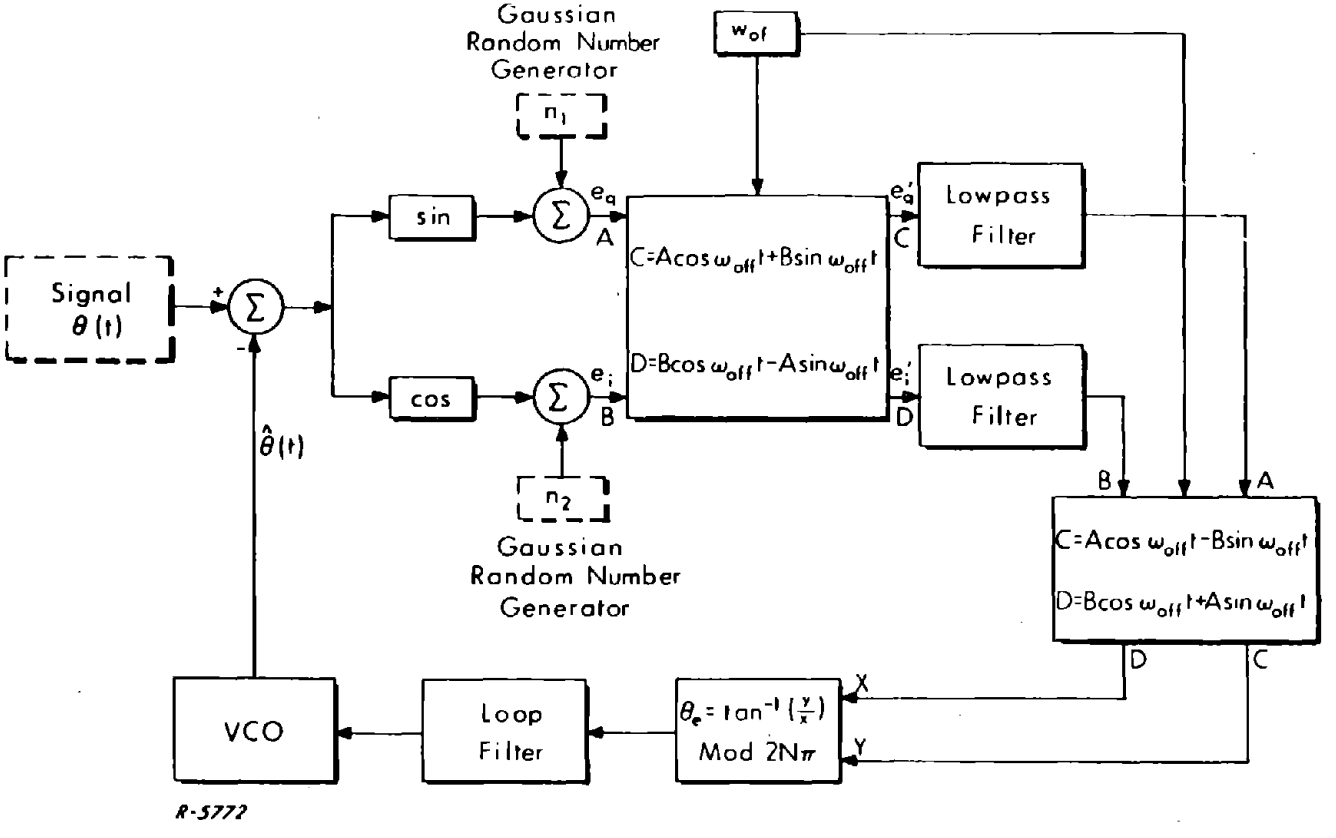

Fig. 25 Phase-Lock Loop Simulation Block Diagram

The first simulation performed was to verify the expected failure of the second order loop. The bandpass filter implemented was a single pole filter with noise bandwidth of 20 kHz, double sided. The divider ratio, N, was 16 and the double-sided loop bandwidth was 500 Hz. The loop would not acquire for signal-to-noise ratios less than unity in a 20 kHz bandwidth.

The second simulation performed was to verify the expected performance of the first order loop. At each noise level several different noise sample functions were employed. This was accomplished by initializing the random number generator with different starting numbers. Acquisition was achieved within less than 10 milliseconds for signal-to-noise ratios down to -10 dB in the 20 kHz IF bandpass filter. It was also found that the loop would acquire for signal-to-noise ratios down to -30 dB. This excellent performance is caused by the nature of the first order loop. The loop always tends to reduce the frequency error and eventually, the random noise, in combination with the action of the loop, produces a condition where the IF signal lies within the bandwidth of the narrow tracking loop bandpass filter. The hand-off to track is then immediately accomplished. For all simulation runs, the loop bandwidth was set to 1000 radians/sec. This is consistent with a reasonable narrow bandpass filter design for the track loop.

6. STEERABLE NULL CONTROL FOR THE DIFFUSE MULTIPATH CASE

6.1 Introduction

In the Interim Report*, ADCOM demonstrated how specular multipath interference in an aircraft-navigational satellite link could be reduced by the use of a steerable null control system. The major results of that problem are reviewed briefly in the following section, and the modifications required for the inclusion of both coherently fading and incoherently fading diffuse multipath are indicated. ADCOM'S conclusions concerning the effectiveness of the steerable null control system for combatting multipath interference at 1.6 GHz in a NAV/SAT application are summarized as follows:

1) Since diffuse multipath interference arises from scattering off a much larger area of the sea surface than for the case of specular scattering, the multipath interference in the diffuse case arrives at the aircraft from a range of different directions centered on the specular direction. Consequently, placing a sharp null in the direction of the specular point will not eliminate all of the multipath interference. In addition, slight variations of antenna gains with directions of arrival of the diffuse multipath components will preclude the possibility of achieving the required amplitude gain balancing necessary for achieving a true null. At best, only the coherently fading diffuse multipath component can be nulled, with the incoherently fading diffuse multipath interference being simply reduced somewhat.

2) The presence of incoherently fading diffuse multipath interference interferes with proper operation of the steerable null control system and may prevent the null from being placed on the direction of arrival of the coherently fading diffuse multipath component.

---

* Study of a Multipath Rejection Technique applied to Aircraft Navigation by Satellite, 15 April 1968.

3) Steerable null control at 1.6 GHz does not work as well at low grazing angles as at intermediate grazing angles (i.e., around 30^{o}), even for the case of specular scattering. For the 1.6 GHz NAV/SAT channel grazing angles as low as 10^{o} are being considered.

4) Steerable null control may not be needed at 1.6 GHz, since antennas can be built at these frequencies which may adequately discriminate against the multipath if the angular separation between the directions of arrival of the direct path and multipath signals at the aircraft is greater than about 20^{o}.

A modification of the steerable null simulator (constructed previously under this contract) to simulate the randomly fluctuating carrier phase of a coherently fading diffuse multipath component was carried out. The results indicated that the steerable null system could work well under such circumstances in that the rapidly fluctuating multipath carrier phase prevented the phase of the multipath carrier from dwelling too long in a region where operation of the steerable null control system became ineffective.

6.2 Review of Steerable Null Control for the Case of Specular Multipath Interferences

Specular multipath interference implies a mirror-like reflection of the transmitted signal off the sea surface. Such is the case for VHF frequencies at grazing angles below about 30^{o} and for normal seas.

In the Interim Report, a direct-path signal of the form

$$e_d(t) = \cos\left(\omega_c t + \theta(t)\right) \tag{246}$$

was considered. The received multipath signal was written as

$$e_m(t) = a \cos\left(\omega_c t - \omega_c \tau_d + \theta\ (t - \tau_d)\right) \tag{247}$$

for the case of pure specular scattering, and as

$$e_m(t) \tilde{=} a(t) \cos\left(\omega_c t + \theta\ (t-\tau_d) + \phi_c(t)\right) \tag{248}$$

for pure diffuse scattering. Here ω_c is the direct-path carrier frequency, including Doppler, and τ_d is the relative multipath time delay, and is time varying. The signal in Eq.(248) is actually a coherently

fading diffuse multipath component in that only a single relative multipath time delay was considered. If the range of relative multipath delays received at any given instant is a significant fraction of a period of the highest modulating frequency in $\theta(t)$, it may no longer be appropriate to consider only a single modulation delay. In this case, the received multipath interference may be represented by the sum of a coherently fading diffuse multipath component, as in Eq. (248), and an incoherently fading diffuse multipath component involving the sum over a range of relative multipath time delays. The received multipath signal then may be written as

$$e_m(t) = a(t)\cos\left(\omega_c t + \theta(t-\tau_d) + \phi_c(t)\right) + \sum_k a_k(t)\cos\left(\omega_c t + \theta(t-\tau_k) + \phi_k(t)\right) \tag{249}$$

In the steerable null system two essentially omnidirectional antennas, which are vertically separated by one-half wavelength, are used to receive the direct path and multipath signals. The separation of the two antennas results in phase shifts between the carrier-phases of the received direct path and multipath signals in the upper and lower antennas. An additional controlled phase shift between the signals received by the upper and lower antenna is introduced at IF so as to result in the multipath components of the signals received by the two antennas being 180° out of phase, and the direct path components being approximately in phase. Summation of the signals from the upper and lower antennas at this point can result, if the multipath component amplitudes are equalized, in a nulling of the multipath components and an enhancement of the direct path components. The purpose of the steerable null control system is to electronically maintain the proper phasing and amplitude balance required for multipath null as the aircraft flies along its course and the directions of arrival of the multipath and direct path signals change.

To do this, use is made of the fact that the presence of a residual multipath component at the output of the summer will result in amplitude as well as phase fluctuations in the resultant signal. If these amplitude fluctuations are detected by a square law detector followed by a high-pass filter, a signal fluctuating at the modulation rate and containing two components results. One of these components

is proportional to the phasing imbalance and the other to the amplitude imbalance. Since the fluctuating signals multiplying the two error signals are approximately orthogonal under certain circumstances, extraction of the error signals with negligible cross-talk error can be achieved if the fluctuating signals multiplying the error signals could be generated from the signals at the inputs to the summer and used as reference signals in a coherent detection scheme. Appropriate reference signal extractors for obtaining these fluctuating signals can produce good reference signals for the case where the errors are already small.

An experimental simulation of the multipath signals, the antennas, and the steerable null control system for phasing control was built which demonstrated the basic operation of the steerable null system.

The pertinent equations for description of the operation of the phase control portion of the steerable null system are now reviewed in order that the modifications required for the case where incoherently fading diffuse multipath components are present can be more easily understood. The multipath signal is assumed to be a coherently fading diffuse multipath interference.

The signals at the inputs to the summer are written as indicated below. The subscripts "u" and "ℓ" refer to "upper" and "lower" antenna received signals, while "d" and "m" refer to the "direct path" and "multipath" components.

Upper antenna direct path signal component:

$$e_{ud}(t) = \cos\left(\omega_o t + \theta\,(t)\right) \tag{250}$$

Lower antenna direct path signal component:

$$e_{\ell d}(t) = (1 + \Gamma_d)\cos\left(\omega_o t - \beta_{\ell d} + \delta + \theta\,(t)\right) \tag{251}$$

Lower antenna multipath signal component:

$$e_{\ell m}(t) = (1 + \Gamma_m)\, a\,(t) \cos\left(\omega_o t - \phi_c(t) + \delta + \theta\ (t - \tau_d)\right) \tag{252}$$

Upper antenna multipath signal component:

$$e_{um}(t) = a(t) \cos\left(\omega_o t - \phi_c(t) - \beta_{um} + \theta\ (t - \tau_d)\right) \tag{253}$$

Here Γ_d and Γ_m are amplitude imbalances in the direct path and multipath components respectively, $\beta_{\ell d}$ and β_{um} are the carrier phase shifts introduced by the antennas, and δ is the carrier phase shift introduced by the electronic phase shifter. The phase shift δ is written as the sum of the value required for null, δ_n, and an error component, δ_ϵ. The value of δ_n may readily be seen to be

$$\delta_n = \pi - \beta_{um} \tag{254}$$

Defining the carrier phase difference between the direct path components at null, γ_d, by

$$\gamma_d = \delta_n - \beta_{\ell d} \tag{255}$$

The output of the summer becomes

$$\begin{aligned} e_{sum}(t) &= e_{sum,\,d}(t) + e_{sum,\,m}(t) \\ &= A_d \cos\left(\omega_o t + \phi_o + \theta\,(t)\right) \\ &- \left\{\Gamma_m\right\} a(t) \cos\left(\omega_o t + \phi_o + \theta\,(t) - (\xi(t) + \Delta\theta\ (t, \tau_d))\right) \\ &+ \left\{\delta_\epsilon\right\} a(t)\, \sin\left(\omega_o t + \phi_o + \theta(t) - (\xi(t) + \Delta\theta\,(t, \tau_d))\right) \end{aligned} \tag{256}$$

where

$$A_d = \left\{(2 + \Gamma_d)^2 \cos^2\left[\frac{1}{2}(\gamma_d + \delta_\epsilon)\right] + \Gamma_d^2 \sin^2\left[\frac{1}{2}(\gamma_d + \delta_\epsilon)\right]\right\} \quad (257)$$

$$\phi_o = \frac{1}{2}(\gamma_d + \delta_\epsilon) + \zeta_d \quad (258)$$

$$\tan \zeta_d = \frac{\Gamma_d}{(2 + \Gamma_d)} \tan\left[\frac{1}{2}(\gamma_d + \delta_\epsilon)\right] \quad (259)$$

$$\left\{\Gamma_m\right\} = \cos\left(\frac{1}{2}\delta_\epsilon\right)\Gamma_m \quad (260)$$

$$\left\{\delta_\epsilon\right\} = (2 + \Gamma_m)\sin\left(\frac{1}{2}\delta_\epsilon\right) \quad (261)$$

$$\zeta(t) = \frac{1}{2}\gamma_d + \phi_c(t) + \beta_{um} + \zeta_d \quad (262)$$

and $$\Delta\theta(t, \tau_d) = \theta(t) - \theta(t - \tau_d) \quad (263)$$

These results are obtained by straightforward vector addition and trigonometric manipulation.

If this signal is square-law detected and high-pass filtered, the resulting signal is

$$e_{iAM}(t) = -\left\{\Gamma_m\right\} a(t) A_d \left(\cos\left[\xi(t) + \Delta\theta(t, \tau_d)\right]\right)_{HP} - \left\{\delta_\epsilon\right\} a(t) A_d \left(\sin\left[\xi(t) + \Delta\theta(t, \tau_d)\right]\right)_{HP} \quad (264)$$

where the subscript "HP" denotes high-pass filtering of the bracketed expression. If the delay τ_d is large enough to produce a sufficiently large fluctuating signal $\Delta\theta(t, \tau_d)$, the fluctuating signals

$$\left(\cos\left[\xi(t) + \Delta\theta\ (t, \tau_d)\right]\right)_{HP} \text{ and } \left(\sin\left[\xi(t) + \Delta\theta\ (t, \tau_d)\right]\right)_{HP}$$

will be approximately orthogonal. This will be particularly true if $\theta(t)$ is a narrowband signal process, such as a cluster of range tones. In this case, generation of signals proportional to these fluctuating signals can permit coherent detection techniques to be used to recover the error signals $\{\Gamma_m\}$ and $\{\delta_\epsilon\}$. Appropriate signal processing of the input signals to the summer (as described in the Interim Report) result in the generation of a phase error reference signal $e_\delta(t)$ given by

$$e_\delta(t) = -\,a(t)\,A_\delta\left(\sin\left[(\phi_\delta - \zeta_d) + \xi(t) + \Delta\theta(t, \tau_d)\right]\right)_{HP} \tag{265}$$

where

$$A_\delta = (2 + \Gamma_d + \Gamma_m)\cos\left[\frac{1}{2}\gamma_d + \delta_\epsilon\right]\left\{1 + \tan^2\phi_\delta\right\}^{1/2} \tag{266}$$

$$\tan\phi_\delta = \frac{(\Gamma_d - \Gamma_m)}{(2 + \Gamma_d + \Gamma_m)}\ \tan\left[\frac{1}{2}\ \gamma_d + \delta_\epsilon\right] \tag{267}$$

and $\tan\zeta_d$ was given in Eq. (14). Note that as $\Gamma_m \to 0$, $\tan\phi_\delta$ approaches $\tan\zeta_d$ and $(\phi_\delta - \zeta_d)$ approach zero. The quantity $(\phi_\delta - \zeta_d)$ is also reduced as $\delta_\epsilon \to 0$ and $1/2\ \gamma_d$ becomes small. That is, if the amplitude and phase imbalances are small, and the direct path signals add approximately in phase at the summer, the phase $(\phi_\delta - \zeta_d)$ will become small and the phase error reference signal will be precisely what is required for coherent detection of the phase error signal $\{\delta_\epsilon\}$. The steerable null system works best therefore when the errors are already small.

6.3 Modifications in Steerable Null Operation for the Case of Incoherently Fading Diffuse Multipath

For the case where the multipath interference contains significant incoherently fading diffuse multipath components, the multipath components at the input to the summer must be modified to include both the range of relative multipath time delays that may be present and the fact that even for components having the same relative multipath time delays different directions of arrival may produce

different antenna phase shifts and gain imbalances. In this case then Eq. (252) becomes

$$e_{\ell m}(t) = (1 + \Gamma_m)\, a(t) \cos\left(\omega_o t - \phi_o(t) + \delta + \theta\ (t - \tau_d)\right)$$

$$+ \sum_{k,j} a_{kj}(t)\,(1 + \Gamma_{kj}) \cos\left(\omega_o t - \phi_{kj}(t) + \delta + \theta\ (t - \tau_k)\right) \quad (268)$$

$$e_{um}(t) = a(t) \cos\left(\omega_o t - \phi_o(t) - \beta_{um} + \theta\ (t - \tau_d)\right)$$

$$+ \sum_{k,j} a_{kj}(t) \cos\left(\omega_o t - \phi_{kj}(t) - \beta_{kj} + \theta\ (t - \tau_k)\right) \quad (269)$$

If $\Delta\beta_{kj}$ is the additional carrier phase shift caused by the antenna from the kj incoherently fading diffuse multipath component, i.e.,

$$\Delta\beta_{kj} = \beta_{kj} - \beta_{um} \quad (270)$$

Then the output of the summer is modified to

$$e_{sum}(t) = A_d \cos\left(\omega_o t + \phi_o + \theta(t)\right)$$

$$-a(t)\left\{\Gamma_m\right\}\cos\left(\omega_o t + \phi_o + \theta(t) - (\xi(t) + \Delta\theta\ (t, \tau_d))\right)$$

$$+ a(t)\left\{\delta_\epsilon\right\}\sin\left(\omega_o t + \phi_o + \theta\ (t) - (\xi(t) + \Delta\theta\ (t, \tau_d))\right)$$

$$-\sum_{k,j} a_{kj}(t)\left[\cos\left(\frac{1}{2}\delta_\epsilon + \frac{1}{2}\Delta\beta_{kj}\right)\Gamma_{kj}\right]\cos\left(\omega_o t + \phi_o + \theta\ (t) - \left(\xi_{kj}(t) + \Delta\theta\,(t, \tau_k)\right)\right) \quad (271)$$

$$+\sum_{k,j} a_{kj}(t)\left[(2 + \Gamma_{kj})\sin\left(\frac{1}{2}\delta_\epsilon + \frac{1}{2}\Delta\beta_{kj}\right)\right]\sin\left(\omega_o t + \phi_o + \theta\ (t) - \left(\xi_{kj}(t) + \Delta\theta(t, \tau_k)\right)\right)$$

where

$$\xi_{kj}(t) = \frac{1}{2}\gamma_d + \phi_{kj}(t) + \frac{1}{2}\Delta\beta_{kj} + \beta_{um} + \xi_d \qquad (272)$$

and

$$\Delta\theta(t, \tau_k) = \theta(t) - \theta(t-\tau_k) \qquad (273)$$

The terms in square brackets in Eq. (271) may be expanded as

$$\left[\cos\left(\frac{1}{2}\delta_\epsilon + \frac{1}{2}\Delta\beta_{kj}\right)\Gamma_{kj}\right] = \cos\left(\frac{1}{2}\delta_\epsilon\right)\cos\left(\frac{1}{2}\Delta\beta_{kj}\right)\Gamma_{kj} - \sin\left(\frac{1}{2}\delta_\epsilon\right)\sin\left(\frac{1}{2}\Delta\beta_{kj}\right)\Gamma_{kj} \qquad (274)$$

and

$$\left[\left(2+\Gamma_{kj}\right)\sin\left(\frac{1}{2}\delta_\epsilon + \frac{1}{2}\Delta\beta_{kj}\right)\right] = \left(2+\Gamma_{kj}\right)\cos\left(\frac{1}{2}\Delta\beta_{kj}\right)\sin\left(\frac{1}{2}\delta_\epsilon\right) + \left(2+\Gamma_{kj}\right)\cos\left(\frac{1}{2}\delta_\epsilon\right)\sin\left(\frac{1}{2}\Delta\beta_{kj}\right) \qquad (275)$$

With $\Delta\beta_{kj}$ and Γ_{kj} small for all kj, the second term in Eq.(274) may be neglected compared to the first term. These terms may be written in abbreviated form as

$$\left[\cos\left(\frac{1}{2}\delta_\epsilon + \frac{1}{2}\Delta\beta_{kj}\right)\Gamma_{kj}\right] = \left|\Gamma_{kj}\right| \qquad (276)$$

and

$$\left[\left(2+\Gamma_{kj}\right)\sin\left(\frac{1}{2}\delta_\epsilon + \frac{1}{2}\Delta\beta_{kj}\right)\right] = \left|\delta_{\epsilon k_j}\right| + \left|\Delta\beta_{kj}\right| \qquad (277)$$

With the above notation the output of the square-law detector and high-pass filter combination becomes to first approximation

$$e_{iAM}(t) \approx -\left\{\Gamma_m\right\} a(t) A_d \left(\cos\left[\xi(t) + \Delta\theta\left(t, \tau_m\right)\right]\right)_{HP} - \left\{\delta_\epsilon\right\} a(t) A_d \left(\sin\left[\xi(t) + \Delta\theta\left(t, \tau_m\right)\right]\right)_{HP}$$

$$- \sum_{k,j} \left\{\Gamma_{kj}\right\} a_{kj}(t) A_d \left(\cos\left[\xi_{kj}(t) + \Delta\theta\left(t, \tau_k\right)\right]\right)_{HP}$$

$$- \sum_{k,j} \left\{\delta_{\epsilon_{kj}}\right\} a_{kj}(t) A_d \left(\sin\left[\xi_{kj}(t) + \Delta\theta\left(t, \tau_k\right)\right]\right)_{HP}$$

$$- \sum_{k,j} \left\{\Delta\beta_{kj}\right\} a_{kj}(t) A_d \left(\sin\left[\xi_{kj}(t) + \Delta\theta\left(t, \tau_k\right)\right]\right)_{HP} \qquad (278)$$

The approximation involves neglecting products of incoherently fading diffuse multipath components with each other and with the coherently fading multipath components. In the above note that when δ_ϵ and $\Gamma_m \to 0$, $\left\{\delta_{\epsilon_{kj}}\right\}$ goes to zero, but $\left\{\Gamma_{kj}\right\}$ and $\left\{\Delta\beta_{kj}\right\}$ do not. These represent the amplitude and phase imbalances of the kj incoherently fading diffuse multipath component. Also note that the presence of these components will prevent δ_ϵ and Γ_m from going to zero when the loop is closed. Since the rms value of any $a_{kj}(t)$ is much less than that of a(t), the coherently fading diffuse multipath component should dominate, with the incoherently fading diffuse multipath components acting more or less like noise.

As might be expected, the phase error reference signal is also corrupted by the presence of incoherently fading diffuse multipath components. This may cause the system to fail more readily than the presence of these components in the output of the square-law detector high-pass filter combination in that a good reference signal is necessary for proper system operation. The phase error reference signal is to a first approximation

$$e_\delta(t) \tilde{=} -a(t)\, A_\delta \left(\sin\left[\left(\phi_\delta - \tau_d \right) + \xi(t) + \Delta\theta\left(t, \tau_d\right) \right] \right)_{HP}$$

$$- \sum_{k,j} a_{kj}(t)\, A_{kj} \left(\sin\left[\left(\phi_{kj} - \tau_d \right) + \xi_{kj}(t) + \Delta\theta\left(t, \tau_k\right) \right] \right)_{HP} \qquad (279)$$

where

$$A_{kj} = \left(2 + \Gamma_d + \Gamma_{kj}\right) \cos\left[\frac{1}{2}\gamma_d + \delta_\epsilon\right] \left| 1 + \tan^2 \phi_{kj} \right|^{1/2} \qquad (280)$$

and

$$\tan \phi_{kj} = \frac{\Gamma_d - \Gamma_{kj}}{(2 + \Gamma_d + \Gamma_{kj})} \tan\left[\frac{1}{2}\gamma_d + \delta_\epsilon\right] \qquad (281)$$

Again products of incoherently fading diffuse multipath components with each other and with the coherently fading multipath components have been neglected.

If most of the received multipath power is in the coherently fading diffuse multipath component, the steerable null control system may function to place the null in the direction of arrival of the coherently fading diffuse multipath component. On the other hand, if the incoherently fading diffuse multipath component dominates the coherently fading multipath component, the steerable null control system will probably not function properly. The non-linear nature of the steerable null control system and the complex nature of the various signals precludes an exact analysis of the behavior of the steerable null control system in the presence of large incoherently fading diffuse multipath interference in much the same way as a phase -locked loop becomes difficult to analyze near and below threshold. However, since incoherently fading diffuse multipath interference is much more noise-like than specular or coherently fading diffuse multipath insofar as its effects on range tone phase errors are concerned, an antenna which suppresses the multipath sufficiently so that only first order interference effects are significant, may be all that is needed to insure acceptable ranging performance.

In summary, if the incoherently fading diffuse multipath component can be made smaller than the direct path signal by the use of a single directive antenna, that is all that may be needed for acceptable ranging performance. Whereas for proper steerable null control system performance, the incoherently fading diffuse multipath component must be smaller than the coherently fading diffuse multipath component. This is so because in this control system the coherently fading diffuse multipath component plays the role of the desired signal and the incoherently fading diffuse multipath signal plays the role of interference. The expression for the phase error reference signal $e_\delta(t)$, demonstrates this point quite nicely.

6.4 Simulation Experiment for the Steerable Null Phase Control System for the Case of Coherently Fading Diffuse Multipath

The steerable null phase control system simulator described in the Interim Report was modified to simulate one of the major effects of a coherently fading diffuse multipath interference. As indicated previously, the difference between the specular and coherently fading diffuse multipath signals was that the amplitude and carrier phase of the coherently fading diffuse multipath signal are time varying random processes. The randomly varying amplitude and phase results from the fact that the scattering area from which multipath radiation is received by the aircraft is much larger for the diffuse case than for the specular case. Although all the multipath components received from this area have essentially the same modulation delay (this is the definition of coherent fading), their carrier phases may differ by many radians. The fading of the resultant multipath signal occurs primarily as a result of the differential doppler across the scattering area.

The randomly varying carrier phase is by far the more important difference so far as steerable null performance is concerned. This is so because fluctuations in the amplitude are readily compensated for by the AGC system. If the multipath amplitude gets too small for the steerable null control system to track properly, the multipath will be too small to cause any problems anyway. On the other hand, as the multipath amplitude gets larger, the easier it is for the steerable null control system to track and null the multipath. The behavior of the multipath carrier phase has a much more significant effect on the behavior of the steerable null control system, since if this phase

dwells too long at an unfavorable value the steerable null system may lose lock momentarily. This effect was noticed with the simulator when specular multipath interference at 136 MHz was being simulated. With a randomly varying multipath carrier phase, as would be experienced for a coherently fading diffuse multipath component at 1.6 GHz, the likelihood that the phase will dwell for too long at an unfavorable value is much reduced. This was indeed found to be the case.

In the simulation experiment conducted under Task V of the present contract, the phase of the multipath interference was randomly varied by driving a General Radio Frequency Synthesizer (GR1164-A) by Gaussian random noise of 20-200 Hz bandwidth in a VCO mode. The output frequency of this synthesizer was set at 1 MHz (nominal) and the synthesizer was used to drive the multipath multiplier chain. The phasing in the antenna simulator was adjusted so that the multipath would cancel and the direct path would add in phase at the output of the summer. The phasing of the multipath component in the antenna simulator was then changed so that the multipath components at the input to the summer would be approximately 30° away from their null phasing. This was done with the loop open and closed and the waveform of the signal at the output of the summer observed on the scope. Scope photographs of this signal are shown in Fig. 26. The upper waveforms in both photographs are for the case where the multipath is nulled by adjustment of the phasing in the antenna simulator, and the lower waveforms in both photographs are for the case where the multipath phase is shifted away from null in the antenna simulator as indicated above. The effect of the steerable null control system is the nulling of the multipath component at the output of the summer by a feedback compensation for the improper phasing at the inputs to the summer. This is evidenced by the greatly reduced ripple on the signal at the output of the summer when the loop is closed compared with that when the loop is open. For convenience and facility in interpretting the various waveforms in the system, a simple 100 kHz sinusoidal signal was utilized as the modulation.

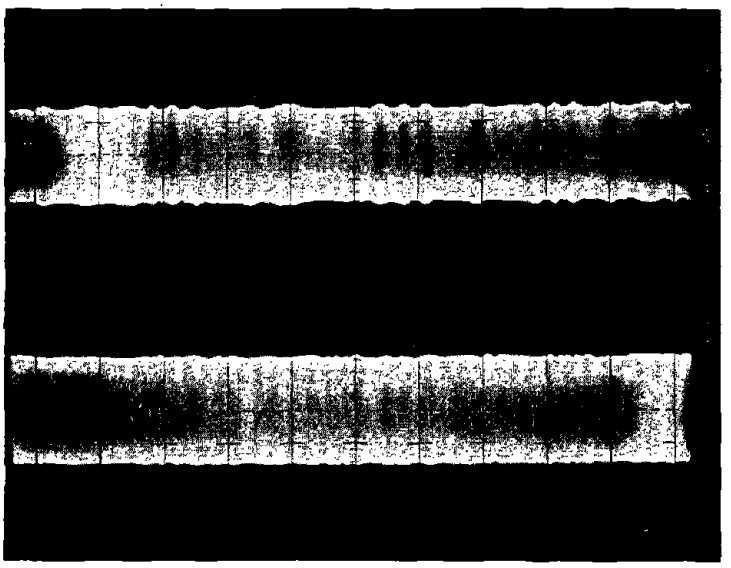

Fig. 26(a) Input Signal to Summer (upper) and Output Signal of Summer (lower) for the Antenna Simulator Adjusted for Multipath Cancellation (Loop is Closed).

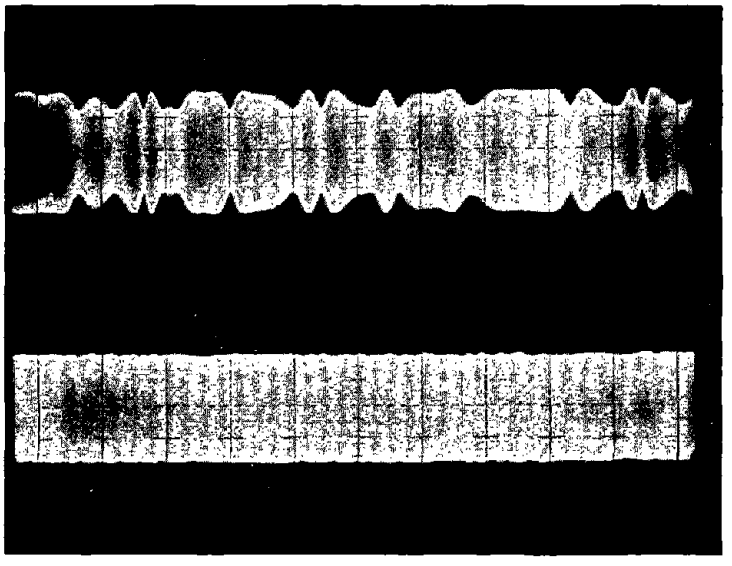

Fig. 26(b) Same as 26(a), but for the Antenna Simulator Adjusted so that Phases of the Multipath Component at the Input to the Summer are 30° Away from Null.

REFERENCES

1. Beckmann and Spizzichino, The Scattering of Electromagnetic Waves from Rough Surfaces, p 9, Pergamon Press, 1963.

2. Blair Kinsman, Wind Waves, pp 343-344, Prentice-Hall, 1963.

3. Beckmann and Spizzichino, The Scattering of Electromagnetic Waves from Rough Surfaces, p 248 Table 12.1 and p 319, Pergamon Press, 1963.

4. ibid, chapter 7.

5. R.H. Clarke and G.O. Hendry, "Prediction and Measurement of the Coherent and Incoherent Power Reflected from a Rough Surface," IEEE Transactions on Antennas and Propagation, pp 353-363, May 1964.

6. Beckmann and Spizzichino, The Scattering of Electromagnetic Waves from Rough Surfaces, p 246, Pergamon Press, 1963.

7. ibid. p 220.

8. ibid. chapter 8.

9. ibid. p 224.

10. Durrani and Staras, "Multipath Problems in Communications Between Low Altitude Spacecraft and Stationary Satellites," RCA Review, pp 77-105, March 1968.

11. Beckmann and Spizzichino, The Scattering of Electromagnetic Waves from Rough Surfaces, pp 20, 28, 29, Pergamon Press, 1963.

12. ibid., p 320.

13. "Phase Difference Navigation Study," Interim Scientific Report, Prepared for: Electronics Research Center, National Aeronautics and Space Administration, Cambridge, Massachusetts, under Contract NAS12-509, Fig. 6-33, p 6-66, June 1967.

14. Schwartz, Bennett, and Stein, Communications Systems and Techniques, chapter 9, McGraw-Hill, 1966.

REFERENCES (Continued)

15. Gary G. Wong, "Wide Angular Coverage Circularly Polarized Antenna for NAV/SAT Application," NAECOM Proceedings 1968, Dayton, Ohio, May 6-8, 1968.

16. M. W. Almutt, C. H. King, C. D. Lunden, "Aircraft Antennas for Communication with Spacecraft."

17. TRW Report, Vol. 3.

18. Dorne and Margolin, Inc., Bohemia, N. Y., Type DM C33-2.

19. Julius A. Kaiser, "The Archimedean Two-Wire Spiral Antenna," IRE Transactions on Antennas and Propagation. Vol. AP-8, May 1960.

Addendum

Computation of Relative Multipath Carrier Doppler for an Aircraft - NAV/SAT Link

The following addendum contains a revised derivation of the differential carrier doppler f_{ms} which avoids a potentially invalid approximation in Sec. 2.2.1. This is so, because the approximations used to compute τ_{ms}, the relative specular multipath time delay would, in fact, yield zero differential carrier doppler.

Conditions:

1) Aircraft is at altitude h.

2) Multipath grazing angle is γ.

3) Component of aircraft velocity parallel to the earth's surface and in the plane of the plane of incidence of the NAV/SAT signal is v_ϕ.

4) Component of aircraft velocity along the local vertical is v_h.

Find: The relative contributions of v_ϕ and v_h to the relative multipath doppler.

Geometry: See Fig.1. (Note that the notation used for certain quantities differs somewhat from that used previously.)

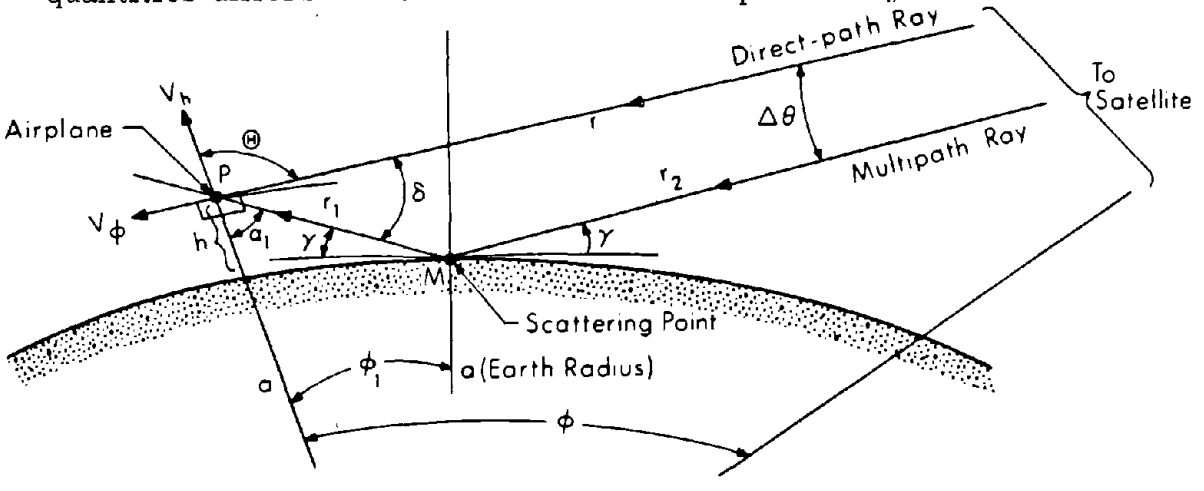

R-5959

The phase of the received direct-path signal is

$$\phi_d = \omega_c t - \omega_c \frac{r(t)}{c} \tag{1}$$

whereas, the phase of the received multipath signal is

$$\phi_{ms} = \omega_c t - \omega_c \frac{r_1(t)}{c} - \omega_c \frac{r_2(t)}{c} \tag{2}$$

where r, r_1 and r_2 are the direct-path range and the range segments of the multipath range. The relative multipath doppler is taken to be

$$(\dot{r} - \dot{r}_1) \qquad (\dot{r}_2 \text{ does not enter into the problem as may be verified by direct calculation}) \tag{3}$$

This is equal to the difference between the projections of the aircraft's velocity vector along r and along r_1. (The satellite is presumed stationary with respect to the earth, although for completeness, the effects of satellite motion should be computed.)

In terms of v_h and v_ϕ, $(\dot{r} - \dot{r}_1)$ is

$$v_h (-\cos\textcircled{H} - \cos\alpha_1) + v_\phi (\cos(\frac{\pi}{2} - \textcircled{H}) - \cos(\frac{\pi}{2} - \alpha_1))$$

or

$$(\dot{r} - \dot{r}_1) = - v_h (\cos\textcircled{H} + \cos\alpha_1) + v_\phi (\sin\textcircled{H} - \sin\alpha_1) \tag{4}$$

where $\textcircled{H}$ is the angle between the local vertical and r, and α_1 is the angle between the local vertical and r_1. We wish to express this in terms of the aircraft altitude h and the grazing angle γ.

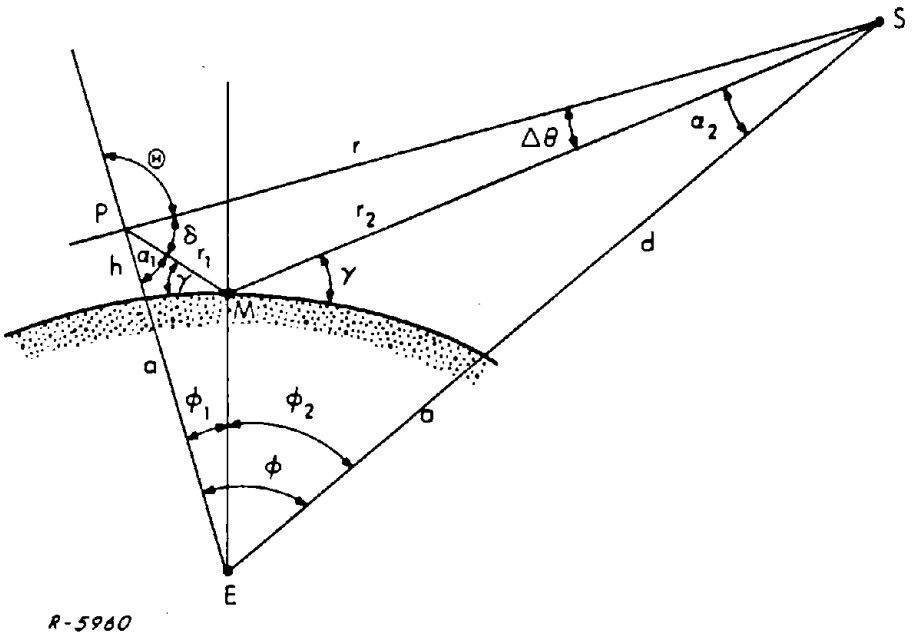

The following relationships may be derived from Fig. 2.

$$\sin \alpha_1 = \frac{a}{a + h} \cos \gamma \tag{5}$$

$$\sin \alpha_2 = \frac{a}{a + d} \cos \gamma \tag{6}$$

$$\phi_1 = \frac{\pi}{2} - \alpha_1 - \gamma \tag{7}$$

$$\phi_2 = \frac{\pi}{2} - \alpha_2 - \gamma \tag{8}$$

$$\phi = \phi_1 + \phi_2 \tag{9}$$

$$r_1 = (a + h) \frac{\sin \phi_1}{\cos \gamma} \tag{10}$$

$$r_2 = (a + d) \frac{\sin \phi_2}{\cos \gamma} \tag{11}$$

$$r = \sqrt{(a + h)^2 + (a + d)^2 - 2 (a + h) (a + d) \cos \phi} \tag{12}$$

$$r = \sqrt{r_1^2 + r_2^2 + 2 r_1 r_2 \cos 2 \gamma} \tag{13}$$

$$\sin \Delta\theta = \frac{r_1}{r} \sin 2\gamma \tag{14}$$

$$\sin \delta = \frac{r_2}{r} \sin 2\gamma \tag{15}$$

$$\delta + \Delta \theta - 2 \gamma = 0 \tag{16}$$

$$\text{(H)} = \pi - \delta - \alpha_1 = \pi - 2 \gamma - \alpha_1 + \Delta \theta \tag{17}$$

Let us examine the factor

$$(\sin \text{(H)} - \sin \alpha_1)$$

use $$\text{(H)} = \pi - 2 \gamma - \alpha_1 + \Delta \theta$$

and $$\alpha_1 = \frac{\pi}{2} - \gamma - \phi_1$$

$$\sin \text{(H)} = \sin (\alpha_1 + 2 \gamma - \Delta\theta) = \cos (\gamma - \phi_1 - \Delta\theta)$$

$$\sin \alpha_1 = \cos (\gamma + \phi_1)$$

so that

$$(\sin \textcircled{H} - \sin \alpha) = \cos (\gamma - \phi_1 - \Delta\theta) - \cos (\gamma + \phi_1) \qquad (18)$$

If γ is not <u>too</u> small, and h/a is small, then ϕ_1 (the angle at the center of the earth between the scattering point and the airplane) will be small. In the flat earth approximation, $\phi_1 \equiv 0$.

If the satellite is very far away (synchronous orbit), and if h is small, $\Delta\theta$ (the angle between the directions of propagation of the direct-path and multipath signals from the satellite) will be small. In the parallel ray approximation, $\Delta\theta \equiv 0$.

If ϕ_1 is very small, and $\Delta\theta$ is very small (compared to γ), $(\sin \textcircled{H} - \sin \alpha_1)$ will be small, and will be zero in the parallel ray, flat earth approximation. In previous work, the parallel ray, flat earth approximations were made in order to relate the relative multipath delay τ_{ms}, to h and γ. The real spherical earth, non-parallel ray situation was used to express γ in terms of h and the angle ϕ (see Figs. 1 and 2) (and the earth radius, a, and the NAV/SAT altitude, d). The time delay τ_{ms} was then differentiated with respect to time, and expressed in terms of $\dot{\phi}$ ($v_\phi = (a + h)\,\dot{\phi}$) and the other pertinent parameters. Since the expression for γ in terms of h and ϕ was only approximate, the validity of the value of $\dot{\tau}_{ms}$ must be questioned, particularly, since τ_{ms} was expressed in terms of γ and h using the flat earth, parallel ray approximation. The correct (exact) derivation $(\sin \textcircled{H} - \sin \alpha_1)$ reveals that the contribution to the relative multipath doppler from the horizontal aircraft velocity component v_ϕ is non-zero only because the values of ϕ_1 and $\Delta\theta$ deviate slightly from zero. Consequently we shall examine $(\sin \textcircled{H} - \sin \alpha)$ more carefully.

$$\cos(\gamma - \phi_1 - \Delta\theta) - \cos(\gamma + \phi_1) = \cos\left(\gamma - \frac{\Delta\theta}{2} - \left(\phi_1 + \frac{\Delta\theta}{2}\right)\right)$$

$$- \cos\left(\gamma - \frac{\Delta\theta}{2} + \left(\phi_1 + \frac{\Delta\theta}{2}\right)\right)$$

$$= 2 \sin\left(\gamma - \frac{\Delta\theta}{2}\right) \sin\left(\phi_1 + \frac{\Delta\theta}{2}\right) \tag{19}$$

$$= 2\left[\sin\gamma \cos\left(\frac{\Delta\theta}{2}\right) - \cos\gamma \sin\left(\frac{\Delta\theta}{2}\right)\right]\left[\sin\phi_1 \cos\left(\frac{\Delta\theta}{2}\right)\right.$$

$$\left. + \cos\phi_1 \sin\left(\frac{\Delta\theta}{2}\right)\right] \tag{20}$$

$$= 2\left[\sin\gamma \sin\phi_1 \cos^2\left(\frac{\Delta\theta}{2}\right)\right] + \sin\gamma \cos\phi_1 \sin(\Delta\theta)$$

$$- \cos\gamma \sin\phi_1 \sin(\Delta\theta) - 2\cos\gamma \cos\phi_1 \sin^2\left(\frac{\Delta\theta}{2}\right) \tag{21}$$

$$= 2 \sin\gamma \sin\phi_1 + \sin\gamma \cos\phi_1 \sin(\Delta\theta)$$

$$- \cos\gamma \sin\phi_1 \sin(\Delta\theta) - 2\cos\gamma \cos\phi_1 \sin^2\left(\frac{\Delta\theta}{2}\right)$$

$$- 2 \sin\gamma \sin\phi_1 \sin^2\left(\frac{\Delta\theta}{2}\right) \tag{22}$$

For γ not too small, the above is written in order of decreasing importance (i.e., $\sin\Delta\theta < \sin\phi_1$).

To show that $\sin\Delta\theta < \sin\phi_1$, express $\sin\Delta\theta$ and $\sin\phi_1$ as

$$\sin\Delta\theta = \frac{r_1}{r} \sin 2\gamma = \frac{2r_1}{r} \cos\gamma \sin\gamma \tag{23}$$

$$\sin \phi_1 = \frac{r_1}{(a+h)} \cos \gamma \tag{24}$$

or

$$\sin \Delta\theta = \left[\frac{r_1}{(a+h)} \cos \gamma \right] \left(\frac{2(a+h)}{r} \sin \gamma \right) \tag{25}$$

which is

$$\sin \Delta\theta = \sin \phi_1 \left(\frac{2(a+h)}{r} \sin \gamma \right) \tag{26}$$

since for γ not too small,

$$\frac{2(a+h)}{r} \sin \gamma < 1 \tag{27}$$

Consequently, the first two terms in the expansion of $(\sin \textcircled{H} - \sin \alpha_1)$ are most important.

$$\text{With } \cos \phi_1 = 1 - 2 \sin^2 \left(\frac{\phi_1}{2} \right) \tag{28}$$

$$(\sin \textcircled{H} - \sin \alpha_1) = 2 \sin \gamma \left(\sin \phi_1 + \frac{1}{2} \sin \Delta\theta \right)$$

$$- \cos \gamma \sin \phi_1 \sin (\Delta\theta) - 2 \cos \gamma \cos \phi_1 \sin^2 \left(\frac{\Delta\theta}{2} \right)$$

$$- 2 \sin \gamma \sin \phi_1 \sin^2 \left(\frac{\Delta\theta}{2} \right) - 2 \sin \gamma \sin (\Delta\theta) \sin^2 \left(\frac{\phi_1}{2} \right) \tag{29}$$

$$\approx 2 \sin \gamma \left(\sin \phi_1 + \frac{1}{2} \sin \Delta\theta \right) \tag{30}$$

Now $\sin \phi_1 = \sin\left(\frac{\pi}{2} - \alpha_1 - \gamma\right) = \cos(\alpha_1 + \gamma) =$

$$\cos\alpha_1 \cos\gamma - \sin\alpha_1 \sin\gamma = \sqrt{1 - \sin^2\alpha_1}\cos\gamma - \sin\alpha_1 \sin\gamma$$

$$= \left[\sqrt{1 - \left(\frac{a}{a+h}\right)^2 \cos^2\gamma}\ \cos\gamma - \left(\frac{a}{a+h}\right)\cos\gamma \sin\gamma\right] \qquad (31)$$

$$\sin\Delta\theta = 2 \sin\phi_1 \left(\frac{a+h}{r}\sin\gamma\right) \qquad (32)$$

$$(\sin \text{(H)} - \sin\alpha_1) \approx 2 \sin\gamma \sin\phi_1 \left[1 + \left(\frac{a+h}{r}\right)\sin\gamma\right] \qquad (33)$$

Now

$$\sqrt{1 - \left(\frac{a}{a+h}\right)^2 \cos^2\gamma} = \sqrt{\left(\frac{a+h}{a+h}\right)^2 - \left(\frac{a}{a+h}\right)^2 \cos^2\gamma}$$

$$= \sqrt{\left(\frac{a}{a+h}\right)^2 \sin^2\gamma + \frac{2ah}{(a+h)^2} + \frac{h^2}{(a+h)^2}}$$

$$= \left(\frac{a}{a+h}\right)\sin\gamma\sqrt{1 + \frac{2h}{a}\frac{1}{\sin^2\gamma} + \left(\frac{h}{a}\right)^2 \frac{1}{\sin^2\gamma}} \qquad (34)$$

$$\sin\phi_1 = \left(\frac{a}{a+h}\right)\sin\gamma\cos\gamma\left[\sqrt{1 + \frac{2(h/a) + (h/a)^2}{\sin^2\gamma}} - 1\right] \qquad (35)$$

If $(2h/a) << \sin^2\gamma$,

(For example: If h = 5 miles

$a \approx 4000$ miles

$\frac{2h}{a} = \frac{1}{400}$

$\sin\gamma >> \frac{1}{20}$, or $\gamma >> .05$ radians)

then the square root may be expanded in a Taylor series to obtain

$$(\sin \textcircled{H} - \sin\alpha_1) \approx 2 \sin\gamma \left[1 + \left(\frac{a+h}{r}\right) \sin\gamma\right]\left(\frac{a}{a+h}\right) \sin\gamma\cos\gamma \times \left\{\left(\frac{h}{a}\right) \frac{1}{\sin^2\gamma} \left[1 + \frac{1}{2}\left(\frac{h}{a}\right)\left[1 - \frac{1}{\sin^2\gamma}\right]\right]\right.$$

$$\approx 2\left(\frac{h}{a+h}\right) \cos\gamma\left[1 - \frac{1}{2}\left(\frac{h}{a}\right)\cot^2\gamma\right]\left[1 + \left(\frac{a+h}{r}\right) \sin\gamma\right] \qquad (36)$$

which for $h/a << 1$ may be further approximated by

$$(\sin \textcircled{H} - \sin\alpha_1) \approx 2\left(\frac{h}{a}\right) \cos\gamma\left[1 - \frac{1}{2}\left(\frac{h}{a}\right) \cot^2\gamma\right]\left[1 + \frac{a}{r} \sin\gamma\right] \qquad (37)$$

Additional algebraic manipulation or automatic computation may be used to reduce this result still further. Computation of $(\cos \textcircled{H} + \cos\alpha_1)$ follows similar lines, except that this factor will not be small. Consequently, the relative multipath doppler is much more sensitive to vertical aircraft motion than to horizontal aircraft motion. Because of this unanticipated result, the effects of satellite motion should also be considered, since it may contribute an unexpectedly large proportion to the total relative multipath doppler. Both changes in ϕ and in d should be considered. Note also that r_2 will not be zero in this case.

Appendix A

CALCULATION OF σ_k^2 FOR CASE (b)

$$\sigma_k^2 = \left\langle n_k^2 \right\rangle = \int_o^{\ell T} dt_1 \int_o^{\ell T} dt_2 \, E_{\phi_{c\ell_n}} \left(c\ell_k \left(t_1 - t_o + \frac{\phi_{c\ell_n}(t_1)}{\omega_{c\ell}} \right) c\ell_k \left(t_2 - t_o + \frac{\phi_{c\ell_n}(t_2)}{\omega_{c\ell}} \right) \right)$$

$$\times E_{n_v} \left(\left(n_v \otimes h_{LP} \right)_{t_1} \left(n_v \otimes h_{LP} \right)_{t_2} \right) \qquad \text{(A-1)}$$

where $E_{\phi_{c\ell_n}}$ and E_{n_v} denote statistical averaging over the clock phase jitter and the video Gaussian noise.

Now, since n_v is assumed to be "white" (i.e., much larger bandwidth than the bandwidth for h_{LP}) and of double-sided noise power density $\Phi/2$, $E_{n_v} \left(\left(n_v \otimes h_{LP} \right)_{t_1} \left(n_v \otimes h_{LP} \right)_{t_2} \right)$ is

$$E_{n_v} \left(\left(n_v \otimes h_{LP} \right)_{t_1} \left(n_v \otimes h_{LP} \right)_{t_2} \right) = \frac{\Phi}{2} \psi_{h_{LP}}(t_2 - t_1) \qquad \text{(A-2)}$$

where

$$\psi_{h_{LP}}(\tau) = \int_{-\infty}^{\infty} h_{LP}(t) h_{LP}(t + \tau) dt \qquad \text{(A-3)}$$

Introducing the function $P_{\ell T}(t)$ defined by

$$P_{\ell T}(t) = \begin{cases} 1 & 0 < t < \ell T \\ 0 & \text{elsewhere} \end{cases} \qquad \text{(A-4)}$$

σ_k^2 may be written as

$$\sigma_k^2 = \sigma^2 \int_{-\infty}^{\infty} d\tau \, \psi_{h_{LP}}(\tau) \psi_k(\tau) = \sigma^2 \gamma_k^2 \qquad \text{(A-5)}$$

where

$$\sigma^2 = \frac{\Phi}{2} \ell T \qquad \text{(A-6)}$$

and

$$\psi_k(\tau) = E_{\phi_{c\ell_n}}\left(\frac{1}{\ell T}\int_{-\infty}^{\infty} dt\; c\ell_k\left(t - t_o + \frac{\phi_{c\ell_n}(t)}{\omega_{c\ell}}\right)P_{\ell T}(t)\right.$$

$$\left.\times\, c\ell_k\left(t - t_o + \tau + \frac{\phi_{c\ell_n}(t+\tau)}{\omega_{c\ell}}\right)P_{\ell T}(t+\tau)\right) \qquad (A\text{-}7)$$

To proceed further, a specific lowpass filter function is chosen. For the sake of simplicity, a single-pole lowpass filter impulse response is chosen. The 3 dB filter bandwidth is taken to be equal to five times the clock frequency. That is

$$h_{LP}(t) = \alpha e^{-\alpha t}\, u_{-1}(t) \qquad (A\text{-}8)$$

where

$$\alpha = 5\omega_{c\ell}$$

In this case, $\psi_{h_{LP}}(\tau)$ is

$$\psi_{h_{LP}}(\tau) = \frac{\alpha}{2} e^{-\alpha|\tau|} \qquad (A\text{-}9)$$

Since $\psi_{h_{LP}}(\tau)$ is a very narrow pulse compared with the pulse width of $\psi_k(\tau)$, which is $2\ell T$, it is only necessary to determine $\psi_k(\tau)$ for small τ. To determine just how small a range of $|\tau|$ need be considered, notice that for $|\tau| = T_{c\ell} = 2\pi/\omega_{c\ell}$,

$$\frac{\psi_{h_{LP}}(T_{c\ell})}{\psi_{h_{LP}}(0)} = e^{-10\pi} \cong 2.27 \times 10^{-14} \qquad (A\text{-}10)$$

which is entirely negligible. Consequently $\psi_k(\tau)$ need only be considered in the range $|\tau| < T_{c\ell}$. In this range $\psi_k(\tau)$ may be shown, for the case of no clock jitter, to be given by

$$\psi_k(\tau) = 1 - \left(2 - \frac{T_k}{2\ell T}\right)\frac{|\tau|}{(T_k/2)} \qquad \text{for } |\tau| < \frac{T_k}{2} \qquad (A\text{-}11)$$

where

$$T_k = 2^k T_{c\ell}, \qquad T = 2^N T_{c\ell} \qquad (N=12)$$

The factor $T_k/\ell T$ is

$$\frac{T_k}{\ell T} = \frac{2^k}{2^N \ell} = \frac{2^k}{4,096\,\ell} \tag{A-12}$$

which is much less than 2 for k small compared to N.

For $\phi_{c\ell_n} \neq 0$, $\psi_k(0) = 1$, but $|\psi_k(\tau)|$ will be slightly less than $|\psi_k(\tau)|$ for $\phi_{c\ell_n}(t) = 0$, since the effect of the clock jitter is to further decorrelate the functions

$$c\ell_k\left(t - t_o + \frac{\phi_{c\ell_n}(t)}{\omega_{c\ell}}\right) \text{ and } c\ell_k\left(t - t_o + \tau + \frac{\phi_{c\ell_n}(t+\tau)}{\omega_{c\ell}}\right).$$

The amount of decorrelation increases as the ratio of the bandwidth of the clock loop to the frequency of the clock increases. Since this ratio is approximately 6.4 to 320,000, the amount of decorrelation, as a result of a small non-zero clock phase jitter, in the range of $|\tau| < T_{c\ell}$ is entirely negligible.

Consequently σ_k^2 is approximately

$$\sigma_k^2 \approx \sigma^2 \int_{-T_{c\ell}}^{T_{c\ell}} \frac{\alpha}{2} e^{-\alpha|\tau|}\left(1 - \left(2 - \frac{T_k}{2\ell T}\right)\frac{|\tau|}{(T_k/2)}\right) d\tau$$

$$= \sigma^2 \int_o^{\alpha T_{c\ell}} dx\, e^{-x}\left(1 - \left(\frac{4}{\alpha T_k} - \frac{1}{\alpha \ell T}\right) x\right) \tag{A-13}$$

$$\approx \sigma^2\left(1 + \frac{1}{5\pi\ell 2^{13}} - \frac{1}{5\pi 2^{(k-1)}}\right) = \sigma^2\gamma_k^2$$

Since $5\pi\ell 2^{13} >> 1$, the function γ_k^2 is approximately

$$\gamma_k^2 \approx 1 - \frac{1}{5\pi}\left(\frac{1}{2^{(k-1)}}\right) \tag{A-14}$$

A table of values of γ_k^2 for $k = 1, 2, \cdots, 12$ is given below in Table A.1.

Table A.1

k	γ_k^2
1	0.936338
2	0.968169
3	0.984085
4	0.992042
5	0.996021
6	0.998011
7	0.999005
8	0.999503
9	0.999751
10	0.999876
11	0.999938
12	0.999969

Appendix B

COMPUTATION OF $\langle s_k \rangle$ FOR CASE (b)

For case (b) s_k is given by

$$s_k = \int_o^{\ell T} (C)^{1/2} \sin\beta \cos\phi_c(t) \left(b_{13} \otimes h_{LP}\right)_t c\ell_k\left(t - t_o + \frac{\phi_{c\ell_n}(t)}{\omega_{c\ell}}\right) dt \qquad \text{(B-1)}$$

$$= \mu\rho_{13}^{-1} \int_{-\infty}^{\infty} d\xi\, h_{LP}(\xi) \frac{1}{\ell T} \int_o^{\ell T} b_{13}(t-\xi) c\ell_k\left(t - t_o + \frac{\phi_{c\ell_n}(t)}{\omega_{c\ell}}\right) \cos\phi_c(t) dt \qquad \text{(B-2)}$$

where

$$\mu = (C)^{1/2} \sin\beta\, (\ell T) \rho_{13} \qquad \text{(B-3)}$$

and use has been made of

$$\left(b_{13} \otimes h_{LP}\right)_t = \int_{-\infty}^{\infty} d\xi\, h_{LP}(\xi) b_{13}(t-\xi) \qquad \text{(B-4)}$$

The expectation value of s_k is

$$\langle s_k \rangle = \mu \left\{ \frac{1}{\rho_{13}} \int_{-\infty}^{\infty} d\xi\, h_{LP}(\xi) \frac{1}{\ell T} \int_o^{\ell T} b_{13}(t-\xi) \right.$$

$$\left. \times E_{\phi_{c\ell_n}} \left(c\ell_k\left(t - t_o + \frac{\phi_{c\ell_n}}{\omega_{c\ell}}\right)\right) E_{\phi_c}(\cos\phi_c) dt \right\} \qquad \text{(B-5)}$$

The expectation value $E_{\phi_c}(\cos\phi_c)$ is

$$E_{\phi_c}(\cos\phi_c) = E_{\phi_c}\left(\cos(\phi_{ct} + \phi_{cn})\right) = \cos\phi_{ct} E_{\phi_{cn}}(\cos\phi_{cn})$$

$$= \cos\phi_{ct}\, e^{-\frac{1}{2}\sigma_{cn}^2} \qquad \text{(B-6)}$$

where $\sigma_{cn}^2 = \langle \phi_{cn}^2 \rangle$.

The cross-correlation function between $b_{13}(t)$ and $c\ell_k(t)$ is defined as

$$\psi_{c\ell_k b_{13}}(\tau) = \frac{1}{T}\int_o^T b_{13}(t)c\ell_k(t+\tau)dt \tag{B-7}$$

It is a property of BINOR codes that

$$\psi_{c\ell_k b_{13}}(\tau) = \psi_{c\ell_k b_{13}}(-\tau) \tag{B-8}$$

Interchanging the order of statistical averaging over $\phi_{c\ell_n}$ and integration over t, $\langle s_k \rangle$ becomes

$$\langle s_k \rangle = \mu e^{-\frac{1}{2}\sigma_{cn}^2} \cos\phi_{ct} E_{\phi_{c\ell_n}}\left\{\frac{1}{\rho_{13}}\int_{-\infty}^{\infty} d\xi\, h_{LP}(\xi)\psi_{c\ell_k b_{13}}\left(t_o - \frac{\phi_{c\ell_n}}{\omega_{c\ell}} - \xi\right)\right\} \tag{B-9}$$

where use has been made of Eqs. (B-6), (B-7), and (B-8). Now

$$\int_{-\infty}^{\infty} d\xi\, h_{LP}(\xi)\psi_{c\ell_k b_{13}}\left(t_o - \frac{\phi_{c\ell_n}}{\omega_{c\ell}} - \xi\right) = \left(h_{LP} \otimes \psi_{c\ell_k b_{13}}\right)_{t_o - \frac{\phi_{c\ell_n}}{\omega_{c\ell}}} \tag{B-10}$$

is the convolution of $\psi_{c\ell_k b_{13}}$ and h_{LP} evaluated at $\left(t_o - \phi_{c\ell_n}/\omega_{c\ell}\right)$. Defining $\chi_k\left(t_o - \frac{\phi_{c\ell_n}}{\omega_{c\ell}}\right)$ by

$$\chi_k\left(t_o - \frac{\phi_{c\ell_n}}{\omega_{c\ell}}\right) \equiv \frac{1}{\rho_{13}}\left(h_{LP} \otimes \psi_{c\ell_k b_{13}}\right)_{t_o - \frac{\phi_{c\ell_n}}{\omega_{c\ell}}} \tag{B-11}$$

$\langle s_k \rangle$ may finally be written as

$$\langle s_k \rangle = \mu e^{-\frac{1}{2}\sigma_{cn}^2} \cos\phi_{ct} E_{\phi_{c\ell_n}}\left(\chi_k\left(t_o - \frac{\phi_{c\ell_n}}{\omega_{c\ell}}\right)\right) \tag{B-12}$$

Appendix C

COMPUTATION OF $E_{\phi_{c\ell_n}}\left(\chi_k\left(\frac{\phi_{c\ell_n}}{\omega_{c\ell}} - t_o\right)\right)$

The expectation value of $\chi_k\left(\frac{\phi_{c\ell_n}}{\omega_{c\ell}} - t_o\right)$ is given by

$$E_{\phi_{c\ell_n}}\left(\chi_k\left(\frac{\phi_{c\ell_n}}{\omega_{c\ell}} - t_o\right)\right) = \int_{-\infty}^{\infty} d\phi_{c\ell_n} P\left(\phi_{c\ell_n}\right)\left[1 - \epsilon_k(1 - \ell n2) - \epsilon_k 5\phi_{c\ell_n}\right]$$

$$+ \int_{-\infty}^{\frac{1}{5}\ell n2} P\left(\phi_{c\ell_n}\right)\left[2\epsilon_k(1 - \ell n2)\right.$$

$$\left. - \epsilon_k e^{5\phi_{c\ell_n}} + 2\epsilon_k 5\phi_{c\ell_n}\right] \qquad (C-1)$$

with

$$P\left(\phi_{c\ell_n}\right) = \frac{1}{\sqrt{2\pi}\,\sigma_{c\ell_n}} e^{-\phi^2_{c\ell_n}/2\sigma^2_{c\ell_n}} \qquad (C-2)$$

The first integral in Eq. (C-1) is simply

$$I_1 = 1 - \epsilon_k(1 - \ell n2) - 5\epsilon_k\sigma_{c\ell_n} \qquad (C-3)$$

The second integral may be evaluated by using the following trick. Consider the integral

$$G(\alpha) = \int_{-\infty}^{\phi_{c\ell_o}} e^{5\alpha\phi_{c\ell_n}} P\left(\phi_{c\ell_n}\right) d\phi_{c\ell_n} \qquad (C-4)$$

In terms of this integral, the second integral in Eq. (C-1) is

$$I_2 = \left[2\epsilon_k(1 - \ell n2)G(0) - \epsilon_k G(1) + 2\epsilon_k \frac{dG}{d\alpha}\right]_{\alpha=0} \qquad (C-5)$$

Consequently, we need only evaluate $G(\alpha)$ and specialize the variable α to obtain the various terms in I_2.

$$G(\alpha) = \int_{-\infty}^{\phi_{c\ell_o}} e^{5\alpha\phi_{c\ell_n}} \frac{1}{\sqrt{2\pi}\,\sigma_{c\ell_n}} e^{-\phi_{c\ell_n}^2 \Big/ 2\sigma_{c\ell_n}^2} d\phi_{c\ell_n} \tag{C-6}$$

Completing the square in the exponent,

$$\frac{\phi_{c\ell_n}^2}{2\sigma_{c\ell_n}^2} - 5\alpha\phi_{c\ell_n} = \frac{1}{2\sigma_{c\ell_n}^2}\left(\phi_{c\ell_n}^2 - 2\left(5\alpha\sigma_{c\ell_n}^2\right)\phi_{c\ell_n} + \left(5\alpha\sigma_{c\ell_n}^2\right)^2 - \left(5\alpha\sigma_{c\ell_n}^2\right)^2\right)$$

$$= \frac{1}{2\sigma_{c\ell_n}^2}\left(\left(\phi_{c\ell_n} - \left(5\alpha\sigma_{c\ell_n}^2\right)\right)^2 - \left(5\alpha\sigma_{c\ell_n}^2\right)^2\right)$$

$$= \frac{1}{2\sigma_{c\ell_n}^2}\left(\xi^2 - \left(5\alpha\sigma_{c\ell_n}^2\right)^2\right) \tag{C-7}$$

$G(\alpha)$ becomes

$$G(\alpha) = \int_{-\infty}^{\left(\phi_{c\ell_o} - 5\alpha\sigma_{c\ell_n}^2\right)} \frac{1}{\sqrt{2\pi}\,\sigma_{c\ell_n}} e^{-\xi^2 \Big/ 2\sigma_{c\ell_n}^2} d\xi\, e^{\frac{1}{2}\left(5\alpha\sigma_{c\ell_n}\right)^2} \tag{C-8}$$

$$G(\alpha) = e^{\frac{1}{2}\left(5\alpha\sigma_{c\ell_n}\right)^2} \frac{1}{2}\left[1 + \operatorname{erf}\left(\frac{\phi_{c\ell_o} - 5\alpha\sigma_{c\ell_n}^2}{\sqrt{2}\,\sigma_{c\ell_n}}\right)\right] \tag{C-9}$$

$$G(0) = \frac{1}{2}\left[1 + \operatorname{erf}\left(\frac{\ell n 2}{\sqrt{2}\,5\sigma_{c\ell_n}}\right)\right] \tag{C-10}$$

$$G(1) = e^{\left(\frac{5\sigma_{c\ell_n}}{\sqrt{2}}\right)^2} \frac{1}{2}\left[1 - \operatorname{erf}\left(\frac{5\sigma_{c\ell_n}}{\sqrt{2}} - \frac{\ell n 2}{\sqrt{2}\,5\sigma_{c\ell_n}}\right)\right] \tag{C-11}$$

$$\left.\frac{dG}{d\alpha}\right]_{\alpha=0} = -\frac{1}{2}\left(\frac{5\sigma_{c\ell_n}}{\sqrt{2}}\right)\frac{2}{\sqrt{\pi}}\, e^{-\left(\frac{\ell n 2}{\sqrt{2}\,5\sigma_{c\ell_n}}\right)^2} \tag{C-12}$$

Introducing the above into (C-5) and rearranging terms, $E_{\phi_{c\ell_n}}\left(\chi_k\left(\frac{\phi_{c\ell_n}}{\omega_{c\ell}} - t_o\right)\right)$ becomes

$$E_{\phi_{c\ell_n}}\left(\chi_k\left(\frac{\phi_{c\ell_n}}{\omega_{c\ell}} - t_o\right)\right) = 1 - \epsilon_k\left\{-(1 - \ell n)\operatorname{erf}\left(\frac{\ell n 2}{\sqrt{2}\,5\sigma_{c\ell_n}}\right)\right.$$

$$+ \frac{5\sigma_{c\ell_n}}{\sqrt{2}}\frac{2}{\sqrt{\pi}}\, e^{-\left(\frac{\ell n 2}{\sqrt{2}\,5\sigma_{c\ell_n}}\right)^2}$$

$$\left. + e^{\left(\frac{5\sigma_{c\ell_n}}{\sqrt{2}}\right)^2} \frac{1}{2}\left[1 - \operatorname{erf}\left(\frac{5\sigma_{c\ell_n}}{\sqrt{2}} - \frac{\ell n 2}{\sqrt{2}\,5\sigma_{c\ell_n}}\right)\right]\right\} \tag{C-13}$$

where

$$\epsilon_k = \frac{1}{5\pi}(1 - a_k)$$

Appendix D

COMPUTATION OF $E_{\phi_{c\ell}}\left(\chi_k\left(t_o - \frac{\phi_{c\ell}}{\omega_{c\ell}}\right)\right)$

Starting with Eqs. (86),

$$E_{\phi_{c\ell}}\left(\chi_k\left(t_o - \frac{\phi_{c\ell}}{\omega_{c\ell}}\right)\right) = E_{\phi_{c\ell_s}}\left(1 - \epsilon_k\left\{-\left(1 - \ell n2 + 5\phi_{c\ell_s}\right)\operatorname{erf}\left(\frac{\ell n2}{\sqrt{2}\,5\sigma_{c\ell}} - \frac{\phi_{c\ell_s}}{\sqrt{2}\sigma_{c\ell}}\right)\right.\right.$$

$$+\left(\frac{5\sigma_{c\ell}}{\sqrt{2}}\right)\frac{2}{\sqrt{\pi}}\, e^{-\left(\frac{\ell n2}{\sqrt{2}\,5\sigma_{c\ell}} - \frac{\phi_{c\ell_s}}{\sqrt{2}\sigma_{c\ell}}\right)^2}$$

$$\left.\left. + e^{5\phi_{c\ell_s}}\, e^{\left(\frac{5\sigma_{c\ell}}{\sqrt{2}}\right)^2}\,\frac{1}{2}\left[1 + \operatorname{erf}\left(\frac{\ell n2}{\sqrt{2}\,5\sigma_{c\ell}} - \frac{5\sigma_{c\ell}}{\sqrt{2}} - \frac{\phi_{c\ell_s}}{\sqrt{2}\sigma_{c\ell}}\right)\right]\right\}\right) \quad \text{(D-1)}$$

This is expanded in a power series about $\phi_{c\ell_s} = 0$. To do this the following Taylor series expansions are used:

$$\operatorname{erf}\left(\frac{\ell n2}{\sqrt{2}\,5\sigma_{c\ell}} - \frac{\phi_{c\ell_s}}{\sqrt{2}\sigma_{c\ell}}\right) = \operatorname{erf}\left(\frac{\ell n2}{\sqrt{2}\,5\sigma_{c\ell}}\right) - \frac{2}{\sqrt{\pi}}\, e^{-\left(\frac{\ell n2}{\sqrt{2}\,5\sigma_{c\ell}}\right)^2}\,\frac{\phi_{c\ell_s}}{\sqrt{2}\sigma_{c\ell}}$$

$$- \frac{2}{\sqrt{\pi}}\left(2\,\frac{\ell n2}{\sqrt{2}\,5\sigma_{c\ell}}\right) e^{-\left(\frac{\ell n2}{\sqrt{2}\,5\sigma_{c\ell}}\right)^2}\,\frac{1}{2}\,\frac{\phi_{c\ell_s}^2}{2\sigma_{c\ell}^2} + \cdots \quad \text{(D-2)}$$

$$\frac{2}{\sqrt{\pi}}\, e^{-\left(\frac{\ell n2}{\sqrt{2}\,5\sigma_{c\ell}} - \frac{\phi_{c\ell_s}}{\sqrt{2}\sigma_{c\ell}}\right)^2} = \frac{2}{\sqrt{\pi}}\, e^{-\left(\frac{\ell n2}{\sqrt{2}\,5\sigma_{c\ell}}\right)^2} + \frac{2}{\sqrt{\pi}}\left(2\,\frac{\ell n2}{\sqrt{2}\,5\sigma_{c\ell}}\right) e^{-\left(\frac{\ell n2}{\sqrt{2}\,5\sigma_{c\ell}}\right)^2}\,\frac{\phi_{c\ell_s}}{\sqrt{2}\sigma_{c\ell}}$$

$$+ \frac{2}{\sqrt{\pi}}\,\frac{1}{2}\left[-2 + 4\left(\frac{\ell n2}{\sqrt{2}\,5\sigma_{c\ell}}\right)^2\right] e^{-\left(\frac{\ell n2}{\sqrt{2}\,5\sigma_{c\ell}}\right)^2}\,\frac{\phi_{c\ell_s}^2}{2\sigma_{c\ell}^2} + \cdots \quad \text{(D-3)}$$

$$e^{5\phi_{c\ell_s}} = 1 + 5\phi_{c\ell_s} + \frac{1}{2}(5)^2 \phi^2_{c\ell_s} + \cdots \tag{D-4}$$

$$e^{\left(\frac{5\sigma_{c\ell}}{\sqrt{2}}\right)^2} \frac{1}{2}\left[1 + \operatorname{erf}\left(\frac{\ell n 2}{\sqrt{2}\,5\sigma_{c\ell}} - \frac{5\sigma_{c\ell}}{\sqrt{2}} - \frac{\phi_{c\ell_s}}{\sqrt{2}\sigma_{c\ell}}\right)\right] =$$

$$= e^{\left(\frac{5\sigma_{c\ell}}{\sqrt{2}}\right)^2} \frac{1}{2}\left[1 + \operatorname{erf}\left(\frac{\ell n 2}{\sqrt{2}\,5\sigma_{c\ell}} - \frac{5\sigma_{c\ell}}{\sqrt{2}}\right)\right] - \frac{2}{\sqrt{\pi}} e^{-\left(\frac{\ell n 2}{\sqrt{2}\,5\sigma_{c\ell}}\right)^2} \frac{\phi_{c\ell_s}}{\sqrt{2}\sigma_{c\ell}}$$

$$- \frac{2}{\sqrt{\pi}}\left(\frac{\ell n 2}{\sqrt{2}\,5\sigma_{c\ell}} - \frac{5\sigma_{c\ell}}{\sqrt{2}}\right) e^{-\left(\frac{\ell n 2}{\sqrt{2}\,5\sigma_{c\ell}}\right)^2} \frac{\phi^2_{c\ell_s}}{2\sigma^2_{c\ell}} + \cdots \tag{D-5}$$

In Eq. (D-5) use has been made of the fact that

$$e^{\left(\frac{5\sigma_{c\ell}}{\sqrt{2}}\right)^2} e^{-\left(\frac{\ell n 2}{\sqrt{2}\,5\sigma_{c\ell}} - \frac{5\sigma_{c\ell}}{\sqrt{2}}\right)^2} = e^{-\left(\frac{\ell n 2}{\sqrt{2}\,5\sigma_{c\ell}}\right)^2} e^{-\ell n 2}$$

$$= 2e^{-\left(\frac{\ell n 2}{\sqrt{2}\,5\sigma_{c\ell}}\right)^2} \tag{D-6}$$

Introducing the above series in Eq. (D-1), and grouping terms of like powers of $\phi_{c\ell_s}$, and realizing that $E_{\phi_{c\ell_s}}(\phi_{c\ell_s}) = 0$, Eq. (D-1) becomes to second order in $\phi^2_{c\ell_s}$

$$E_{\phi_{c\ell}}\left(X_k\left(t_o - \frac{\phi_{c\ell}}{\omega_{c\ell}}\right)\right) = 1 - \epsilon_k \left\{ - (1 - \ell n 2)\operatorname{erf}\left(\frac{\ell n 2}{\sqrt{2}\,5\sigma_{c\ell}}\right)\right.$$

$$\left. + \left(\frac{5\sigma_{c\ell}}{\sqrt{2}}\right)\frac{2}{\sqrt{\pi}} e^{-\left(\frac{\ell n 2}{\sqrt{2}\,5\sigma_{c\ell}}\right)^2}\right.$$

$$+ e^{\left(\frac{5\sigma_{c\ell}}{\sqrt{2}}\right)^2} \frac{1}{2}\left[1 + \mathrm{erf}\left(\frac{\ell n 2}{\sqrt{2}\,5\sigma_{c\ell}} - \frac{5\sigma_{c\ell}}{\sqrt{2}}\right)\right]\Bigg\}$$

$$- \epsilon_k E_{\phi_{c\ell_s}}\left(\phi^2_{c\ell_s}\right)\Bigg\{(-5)\left(-\frac{2}{\sqrt{\pi}}\, e^{-\left(\frac{\ell n 2}{\sqrt{2}\,5\sigma_{c\ell}}\right)^2} \frac{1}{\sqrt{2}\sigma_{c\ell}}\right)$$

$$- (1 - \ell n 2)\left(-\frac{2}{\sqrt{\pi}}\,\frac{2\ell n 2}{\sqrt{2}\,5\sigma_{c\ell}}\right) e^{-\left(\frac{\ell n 2}{\sqrt{2}\,5\sigma_{c\ell}}\right)^2} \frac{1}{2\sigma^2_{c\ell}}\,\frac{1}{2}$$

$$+ \left(\frac{5\sigma_{c\ell}}{\sqrt{2}}\right)\frac{2}{\sqrt{\pi}}\,\frac{1}{2}\left[-2 + 4\left(\frac{\ell n 2}{\sqrt{2}\,5\sigma_{c\ell}}\right)^2\right] e^{-\left(\frac{\ell n 2}{\sqrt{2}\,5\sigma_{c\ell}}\right)^2} \frac{1}{2\sigma^2_{c\ell}}$$

$$+ \frac{1}{5}(5)^2\, e^{\left(\frac{5\sigma_{c\ell}}{\sqrt{2}}\right)^2} \frac{1}{2}\left[1 + \mathrm{erf}\left(\frac{\ell n 2}{\sqrt{2}\,5\sigma_{c\ell}} - \frac{5\sigma_{c\ell}}{\sqrt{2}}\right)\right]$$

$$+ (5)\left(-\frac{2}{\sqrt{\pi}}\, e^{-\left(\frac{\ell n 2}{\sqrt{2}\,5\sigma_{c\ell}}\right)^2} \frac{1}{\sqrt{2}\sigma_{c\ell}}\right)$$

$$- \frac{2}{\sqrt{\pi}}\left(\frac{\ell n 2}{\sqrt{2}\,5\sigma_{c\ell}} - \frac{5\sigma_{c\ell}}{\sqrt{2}}\right) e^{-\left(\frac{\ell n 2}{\sqrt{2}\,5\sigma_{c\ell}}\right)^2} \frac{1}{2\sigma^2_{c\ell}}\Bigg\} \qquad \text{(D-7)}$$

Examination of Eq. (D-7) shows that in the expression multiplying $E_{\phi_{c\ell_s}}(\phi^2_{c\ell_s})$, the first and fifth terms cancel, the first parts of the second

and sixth terms cancel, the second part of the second term and the second part of the third term cancel, and the first part of the third term and the second part of the sixth term cancel. This leaves only the fourth term. Consequently Eq. (D-7) becomes

$$E_{\phi_{c\ell}}\left(\chi_k\left(t_o - \frac{\phi_{c\ell}}{\omega_{c\ell}}\right)\right) = (\chi_k)_{max} - \epsilon_k \Gamma(\sigma_{c\ell})$$

$$- \epsilon_k \left|H_{c\ell}(\omega_{ms})\right|^2 \frac{1}{2} a_{ms}^2 \sin^2[\omega_{c\ell}\tau_{ms}] \frac{1}{2}(5)^2 \qquad \text{(D-8)}$$

$$\times e^{\left(\frac{5\sigma_{c\ell}}{\sqrt{2}}\right)^2} \frac{1}{2}\left[1 + \text{erf}\left(\frac{\ell n 2}{\sqrt{2}\,5\sigma_{c\ell}} - \frac{5\sigma_{c\ell}}{\sqrt{2}}\right)\right]$$

where use has been made of Eq. (50), which defines $\Gamma(\sigma_{c\ell})$, and of the relation

$$E_{\phi_{c\ell_s}}\left(\phi_{c\ell_s}^2\right) = \left|H_{c\ell}(\omega_{ms})\right|^2 \frac{1}{2} a_{ms}^2 \sin^2[\omega_{c\ell}\tau_{ms}] \qquad \text{(D-9)}$$

Appendix E

COMPUTATION OF $\langle s_k^2 \rangle_{ms}$

In estimating $\langle s_k^2 \rangle_{ms}$, the small effects of ϕ_c and $\phi_{c\ell}$ may be neglected. That is

$$\langle s_k^2 \rangle_{ms} \cong a_{ms}^2 \, C \sin^2\beta \, E_{d_{ms}} \left\{ \int_o^{\ell T} dt_1 \int_o^{\ell T} dt_2 \cos d_{ms}(t_1) \cos d_{ms}(t_2) \right.$$
$$\left. \times \left(b_{13} \otimes h_{LP} \right)_{t_1 - \tau_{ms}} \left(b_{13} \otimes h_{LP} \right)_{t_2 - \tau_{ms}} c\ell_k(t_1 - t_o) c\ell_k(t_2 - t_o) \right\} \tag{E-1}$$

To proceed, we write

$$\cos[d_{ms}(t)] \approx \cos[\omega_{ms} t + d_{ms}(0)] \tag{E-2}$$

for $0 < t < \ell T$. That is, it is assumed that ω_{ms}, the relative carrier Doppler frequency of the specular multipath component, is essentially constant over a time interval on the order of ℓT. Then, averaging over d_{ms} corresponds to averaging over $d_{ms}(0)$ which is assumed to be uniformly distributed over 2π. When this is done it is found that

$$E_{d_{ms}} \left(\cos[d_{ms}(t_1)] \cos[d_{ms}(t_2)] \right) = \frac{1}{2} \cos[\omega_{ms}(t_2 - t_1)]$$
$$= \frac{1}{2} - \sin^2 \left[\frac{\omega_{ms}(t_2 - t_1)}{2} \right] \tag{E-3}$$

Then $\langle s_k^2 \rangle_{ms}$ is approximately

$$\langle s_k^2 \rangle_{ms} \cong a_{ms}^2 C \sin^2\beta \, \frac{1}{2} \left(\int_o^{\ell T} dt \left(b_{13} \otimes h_{LP} \right)_{t_1 - \tau_{ms}} c\ell_k(t - t_o) \right)^2$$
$$- a_{ms}^2 C \sin^2\beta \int_{-2\ell T}^{2\ell T} \sin^2 \left[\frac{\omega_{ms}\tau}{2} \right] \int_{-\infty}^{\infty} dt_1 \left(b_{13} \otimes h_{LP} \right)_{t_1 - \tau_{ms}} c\ell_k(t_1 - t_o) P_{\ell T}(t_1)$$
$$\times \left(b_{13} \otimes h_{LP} \right)_{t_1 - \tau_{ms} + \tau} c\ell_k(t_1 - t_o + \tau) P_{\ell T}(t_1 + \tau) \tag{E-4}$$

where $P_{\ell T}(t)$ is defined by

$$P_{\ell T}(t) = \begin{cases} 1 & 0 < t < \ell T \\ 0 & \text{elsewhere} \end{cases} \qquad \text{(E-5)}$$

An upper bound on $\langle s_k^2 \rangle_{ms}$ is obtained by neglecting the second portion of Eq. (E-4). If ω_{ms} is small compared to $2\pi/2\ell T$, this term will be much smaller than the first term. The first term is simply

$$\langle s_k^2 \rangle_{ms} \approx \frac{1}{2} a_{ms}^2 \left(C \sin^2 \beta (\ell T)^2 \rho_{13}^2 \right) \chi_k^2 (t_o - \tau_{ms})$$

$$= \frac{1}{2} a_{ms}^2 \mu^2 \chi_k^2 (t_o - \tau_{ms}) \qquad \text{(E-6)}$$

which is less than or equal to

$$\langle s_k^2 \rangle_{ms} \leq \frac{1}{2} a_{ms}^2 \mu^2 \qquad \text{(E-7)}$$

Appendix F

COMPUTATION OF $\langle n_k^2 \rangle_d$

The properties of $x_c(t)$ and $x_q(t)$ discussed in the beginning of Sec. 6 may be used to write $\langle n_k^2 \rangle_d$ approximately as

$$\langle n_k^2 \rangle_d = C \sin^2\beta \, E_{d_{ms}} \Bigg\{ \int_o^{\ell T} dt_1 \int_o^{\ell T} dt_2 \, \phi_m(t_2 - t_1) \times \Big[\cos[d_{ms}(t_1)] \cos[d_{ms}(t_2)] + \sin[d_{ms}(t_1)] \sin[d_{ms}(t_2)] \Big] \times \Big(b_{13} \otimes h_{LP} \Big)_{t_1 - \tau_{ms}} c\ell_k(t_1 - t_o) \Big(b_{13} \otimes h_{LP} \Big)_{t_2 - \tau_{ms}} c\ell_k(t_2 - t_o) \Bigg\} \tag{F-1}$$

Now

$$\cos[d_{ms}(t_1)] \cos[d_{ms}(t_2)] + \sin[d_{ms}(t_1)] \sin[d_{ms}(t_2)] = \cos[d_{ms}(t_2) - d_{ms}(t_1)] \tag{F-2}$$

so that if

$$d_{ms}(t) \approx \omega_{ms} t + d_{ms}(0)$$

over the range $0 < t < \ell T$, $\langle n_k^2 \rangle_d$ becomes

$$\langle n_k^2 \rangle_d = C \sin^2\beta \int_o^{\ell T} dt_1 \int_o^{\ell T} dt_2 \, \phi_m(t_2 - t_1) \cos[\omega_{ms}(t_2 - t_1)] \times \Big(b_{13} \otimes h_{LP} \Big)_{t_1 - \tau_{ms}} c\ell_k(t_1 - t_o) \Big(b_{13} \otimes h_{LP} \Big)_{t_2 - \tau_{ms}} c\ell_k(t_2 - t_o) \tag{F-3}$$

To proceed further, the effects of the lowpass video filter and the phase shifter time delay are neglected as being of only minor importance. In this case $\langle n_{k\ d}^2 \rangle$ becomes

$$\langle n_k^2 \rangle_d \approx C \sin^2\beta \int_o^{\ell T} dt_1 \int_o^{\ell T} dt_2 \, \phi_m(t_2 - t_1) \cos[\omega_{ms}(t_2 - t_1)] \times b_{13}(t_1 - \tau_{ms}) c\ell_k(t_1) b_{13}(t_2 - \tau_{ms}) c\ell_k(t_2) \tag{F-4}$$

The autocorrelation function $\phi_m(t_2 - t_1)$ is now expressed in terms of its Fourier transform

$$\phi_m(t_2 - t_1) = \int_{-\infty}^{\infty} \frac{d\omega}{2\pi} \Phi_m(\omega) e^{j\omega(t_2-t_1)} \qquad \text{(F-5)}$$

where $\Phi_m(\omega)$ is the power spectrum of $x_c(t)$ and $x_q(t)$. It is useful to work with $\Phi_m(\omega)$ since, although its precise form may not be known, an estimate of its bandwidth can be made. Writing $\cos[\omega_{ms}(t_2 - t_1)]$ as

$$\cos[\omega_{ms}(t_2 - t_1)] = \frac{1}{2}\left\{e^{j\omega_{ms}(t_2-t_1)} + e^{-j\omega_{ms}(t_2-t_1)}\right\} \qquad \text{(F-6)}$$

and making use of Eq. (F-5), $\left\langle n_k^2 \right\rangle_d$ may be written as

$$\left\langle n_k^2 \right\rangle_d \approx C \sin^2\beta \int_{-\infty}^{\infty} \frac{d\omega}{2\pi} \Phi_m(\omega) \int_o^{\ell T} dt_1 \int_o^{\ell T} dt_2 \, e^{j\omega(t_2-t_1)}$$

$$\times \frac{1}{2}\left\{e^{j\omega_{ms}(t_2-t_1)} + e^{-j\omega_{ms}(t_2-t_1)}\right\} b_{13}(t_1 - \tau_{ms}) c\ell_k(t_1) b_{13}(t_2 - \tau_{ms}) c\ell_k(t_2) \qquad \text{(F-7)}$$

The usefulness of this procedure may now be more fully appreciated in that examination of Eq. (F-7) reveals that the variables t_1 and t_2 may now be separated as follows.

$$\left\langle n_k^2 \right\rangle_d \approx \frac{1}{2} C \sin^2\beta (\ell T)^2 \rho_{13}^2 \int_{-\infty}^{\infty} \frac{d\omega}{2\pi} \Phi_m(\omega)$$

$$\times \left\{ \left[\frac{1}{\rho_{13}} \frac{1}{\ell T} \int_o^{\ell T} b_{13}(t_1 - \tau_{ms}) c\ell_k(t_1) e^{-j(\omega+\omega_{ms})t_1} \right] \right.$$

$$\times \left[\frac{1}{\rho_{13}} \frac{1}{\ell T} \int_o^{\ell T} b_{13}(t_2 - \tau_{ms}) c\ell_k(t_2) e^{j(\omega+\omega_{ms})t_2} \right]$$

$$+ \left[\frac{1}{\rho_{13}} \frac{1}{\ell T} \int_o^{\ell T} b_{13}(t_1 - \tau_{ms}) c\ell_k(t_1) e^{-j(\omega-\omega_{ms})t_1} \right]$$

$$\left. \times \left[\frac{1}{\rho_{13}} \frac{1}{\ell T} \int_o^{\ell T} b_{13}(t_2 - \tau_{ms}) c\ell_k(t_2) e^{j(\omega-\omega_{ms})t_2} \right] \right\} \qquad \text{(F-8)}$$

Since $b_{13}(t - \tau_{ms})c\ell_k(t)$ is periodic with the period of the BINOR code, T, it may be expanded in a Fourier series as

$$b_{13}(t - \tau_{ms})c\ell_k(t) = \sum_{p=-\infty}^{\infty} \alpha_p(\tau_{ms})e^{jp\omega_{13}t} \qquad (F\text{-}9)$$

$$\alpha_p(\tau_{ms}) = \frac{1}{\ell T}\int_o^{\ell T} b_{13}(t - \tau_{ms})c\ell_k(t)e^{-jp\omega_{13}t}\,dt \qquad (F\text{-}10)$$

Since $b_{13}(t - \tau_{ms})c\ell_k(t)$ is real, $\alpha_{-p}(\tau_{ms}) = \alpha_p^*(\tau_{ms})$. In particular, $\alpha_o(\tau_{ms})$ is

$$\alpha_o(\tau_{ms}) = \frac{1}{\ell T}\int_o^{\ell T} b_{13}(t - \tau_{ms})c\ell_k(t)dt$$

$$= \phi_{c\ell_k b_{13}}(-\tau_{ms}) = \phi_{c\ell_k b_{13}}(\tau_{ms}) = \rho_{13}\chi_k^o(\tau_{ms}) \qquad (F\text{-}11)$$

The superscript "o" in $\chi_k^o(\tau_{ms})$ indicates that there is no video filtering being considered. The effects of the other coefficients $\alpha_p(\tau_{ms})$ for $p \neq 0$ are shown in Appendix G to be of negligible consequence.

Introducing Eq. (F-9) into Eq. (F-8), and making use of the relationship

$$\frac{1}{\ell T}\int_o^{\ell T} dt\, e^{j\omega_o t} b_{13}(t - \tau_{ms})c\ell_k(t) = \sum_{p=-\infty}^{\infty} \alpha_p(\tau_{ms})\frac{1}{\ell T}\int_o^{\ell T} dt\, e^{j(\omega_o+\omega_p)t}$$

$$= \sum_{p=-\infty}^{\infty} \alpha_p(\tau_{ms})e^{j(\omega_o+\omega_p)\frac{\ell T}{2}}$$

$$\cdot\ \mathrm{sinc}\left[(\omega_o + \omega_p)\frac{\ell T}{2}\right] \qquad (F\text{-}12)$$

where $\omega_p = p\omega_{13}$, and

$$\mathrm{sinc}\ x \equiv \frac{\sin x}{x} \qquad (F\text{-}13)$$

$\left\langle n_k^2 \right\rangle_d$ becomes

$$\left\langle n_k^2 \right\rangle_d \approx \frac{1}{2}\mu^2 \int_{-\infty}^{\infty} \frac{d\omega}{2\pi} \Phi_m(\omega)$$

$$\times \left\{ \left[\frac{1}{\rho_{13}} \sum_{p=-\infty}^{\infty} \alpha_p(\tau_{ms}) e^{j(\omega_p - \omega - \omega_{ms})\frac{\ell T}{2}} \operatorname{sinc}\left[(\omega_p - \omega - \omega_{ms})\frac{\ell T}{2}\right] \right] \right.$$

$$\times \left[\frac{1}{\rho_{13}} \sum_{r=-\infty}^{\infty} \alpha_r(\tau_{ms}) e^{j(\omega_r + \omega + \omega_{ms})\frac{\ell T}{2}} \operatorname{sinc}\left[(\omega_r + \omega + \omega_{ms})\frac{\ell T}{2}\right] \right]$$

$$+ \left[\frac{1}{\rho_{13}} \sum_{p=-\infty}^{\infty} \alpha_p(\tau_{ms}) e^{j(\omega_p - \omega + \omega_{ms})\frac{\ell T}{2}} \operatorname{sinc}\left[(\omega_p - \omega + \omega_{ms})\frac{\ell T}{2}\right] \right]$$

$$\left. \times \left[\frac{1}{\overline{\rho_{13}}} \sum_{r=-\infty}^{\infty} \alpha_r(\tau_{ms}) e^{j(\omega_r + \omega - \omega_{ms})\frac{\ell T}{2}} \operatorname{sinc}\left[(\omega_r + \omega - \omega_{ms})\frac{\ell T}{2}\right] \right] \right\} \tag{F-14}$$

Examination of the products

$$\operatorname{sinc}\left(\omega_p - \omega - \omega_{ms}\right)\frac{\ell T}{2}\right] \operatorname{sinc}\left[(\omega_r + \omega + \omega_{ms})\frac{\ell T}{2}\right]$$

$$= \operatorname{sinc}\left[(\omega + \omega_{ms} - \omega_p)\frac{\ell T}{2}\right] \operatorname{sinc}\left[(\omega + \omega_{ms} + \omega_r)\frac{\ell T}{2}\right] \tag{F-15}$$

and

$$\operatorname{sinc}\left[(\omega_p - \omega + \omega_{ms})\frac{\ell T}{2}\right] \operatorname{sinc}\left[(\omega_r + \omega - \omega_{ms})\frac{\ell T}{2}\right]$$

$$= \operatorname{sinc}\left[(\omega - \omega_{ms} - \omega_p)\frac{\ell T}{2}\right] \operatorname{sinc}\left[(\omega - \omega_{ms} + \omega_r)\frac{\ell T}{2}\right] \tag{F-16}$$

indicates that they are essentially negligible except for r = -p. Retaining only the r = -p terms, Eq. (F-14) becomes

$$\left\langle n_k^2 \right\rangle_d \approx \frac{1}{2}\mu^2 \int_{-\infty}^{\infty} \frac{d\omega}{2\pi} \Phi_m(\omega)$$

$$\times \sum_{p=-\infty}^{\infty} \frac{1}{2\rho_{13}} \alpha_p(\tau_{ms}) \alpha_{-p}(\tau_{ms}) \left\{ \operatorname{sinc}^2\left[(\omega - \omega_p + \omega_{ms})\frac{\ell T}{2}\right] \right.$$

$$\left. + \operatorname{sinc}^2\left[(\omega - \omega_p - \omega_{ms})\frac{\ell T}{2}\right] \right\} \qquad \text{(F-17)}$$

This may be written as

$$\left\langle n_k^2 \right\rangle_d \approx \frac{1}{2}\mu^2 \frac{1}{2\rho_{13}} \alpha_o^2(\tau_{ms}) \int_{-\infty}^{\infty} \frac{d\omega}{2\pi} \Phi_m(\omega)$$

$$\times \left\{ \operatorname{sinc}^2\left[(\omega + \omega_m)\frac{\ell T}{2}\right] + \operatorname{sinc}^2\left[(\omega - \omega_m)\frac{\ell T}{2}\right] \right\}$$

$$+ \mu^2 \sum_{p=1}^{\infty} \frac{1}{2\rho_{13}} \alpha_p(\tau_{ms}) \alpha_{-1}(\tau_{ms}) \int_o^{\infty} \frac{d\omega}{2\pi} \Phi_m(\omega)$$

$$\times \left\{ \operatorname{sinc}^2\left[(\omega - p\omega_{13} + \omega_{ms})\frac{\ell T}{2}\right] + \operatorname{sinc}^2\left[(\omega - p\omega_{13} - \omega_{ms})\frac{\ell T}{2}\right] \right\}$$

(F-18)

Assuming a Gaussian shaped spectrum for $\Phi_m(\omega)$

$$\Phi_m(\omega) = \frac{\sigma_m^2}{\sqrt{\pi}\, B_m} e^{-(f/B_m)^2} \qquad \text{(F-19)}$$

where σ_m^2 is the total power associated with the spectrum $\Phi_m(\omega)$,

$$\sigma_m^2 = \phi_m(0) = \int_{-\infty}^{\infty} \frac{d\omega}{2\pi} \Phi_m(\omega) \qquad \text{(F-20)}$$

it is assumed that B_m is sufficiently large so that over the bandwidth of the functions

$$\left\{\text{sinc}^2\left[(\omega + \omega_{ms})\frac{\ell T}{2}\right] + \text{sinc}^2\left[(\omega - \omega_{ms})\frac{\ell T}{2}\right]\right\}$$

$\Phi_m(\omega)$ may be replaced by $\Phi_m(0)$. The p = 0 term in $\left\langle n_k^2 \right\rangle_d$ is then

$$\left\langle n_k^2 \right\rangle_d (p = 0) = \frac{1}{2}\mu^2 \frac{1}{\rho_{13}^2} \alpha_o^2(\tau_{ms}) \frac{1}{2\pi} \frac{\sigma_m^2}{\sqrt{\pi} B_m} (2)(\frac{2}{\ell T})\pi \qquad \text{(F-21)}$$

where use has been made of the definite integral

$$\int_{-\infty}^{\infty} \frac{\sin^2 x}{x^2} dx = \pi = \int_{-\infty}^{\infty} \text{sinc}^2 x \, dx \qquad \text{(F-22)}$$

Introducing the expression for $\alpha_o^2(\tau_{ms})$ into Eq. (F-21), $\left\langle n_k^2 \right\rangle_d$ (p = 0) becomes

$$\left\langle n_k^2 \right\rangle_d (p = 0) = \mu^2 \sigma_m^2 \frac{1}{\sqrt{\pi} B_m \ell T} \left(\chi_k^o(\tau_{ms})\right)^2 \qquad \text{(F-23)}$$

This is by far the most important contribution to $\left\langle n_k^2 \right\rangle_d$, and is the only one which will be considered in the computation of $(P_c)_T$.

Appendix G

ESTIMATE OF EFFECTS OF $\alpha_p(\tau_{ms})\,\alpha_{-p}(\tau_{ms})$ FOR $p \neq 0$

In Appendix F $\alpha_p(\tau_{ms})$ for the k^{th} frequency-divided down square-wave was defined as

$$\alpha_p(\tau_{ms}) = \frac{1}{\ell T} \int_0^{\ell T} b_{13}(t - \tau_{ms}) c\ell_k(t) e^{-jp\omega_{13}t}\, dt \qquad \text{(G-1)}$$

Now $b_{13}(t - \tau_{ms})$ and $c\ell_k(t)$ were written as

$$b_{13}(t - \tau_{ms}) = \sum_{n=-\infty}^{\infty} \beta_n e^{jn\omega_{13}t} e^{-jn\omega_{13}\tau_{ms}} \qquad \text{(G-2)}$$

and

$$c\ell_k(t) = \frac{4}{\pi} \sum_{q=0}^{\infty} \frac{1}{(2q+1)} \sin[(2q+1)\,\omega_k t]$$

$$= \frac{4}{\pi} \sum_{q=0}^{\infty} \frac{1}{(2q+1)} \frac{1}{2j} \left[e^{j(2q+1)\omega_k t} - e^{-j(2q+1)\omega_k t} \right] \qquad \text{(G-3)}$$

Introducing these expressions into Eq. (G-1), $\alpha_p(\tau_m)$ may be shown to be

$$\alpha_p(\tau_{ms}) = \frac{4}{\pi} e^{-jp\omega_{13}\tau_{ms}} \sum_{q=0}^{\infty} \frac{1}{(2q+1)} \frac{1}{2j}$$

$$\times \left[\beta_{-\left[(2q+1)\frac{\omega_k}{\omega_{13}} - p\right]} e^{j(2q+1)\omega_k \tau_{ms}} - \beta_{\left[(2q+1)\frac{\omega_k}{\omega_{13}} + p\right]} e^{-j(2q+1)\omega_k \tau_{ms}} \right] \qquad \text{(G-4)}$$

Now β_n is

$$\beta_n = \frac{1}{T}\int_0^T b_{13}(t)e^{-jn\omega_{13}t}dt$$

$$= -j\frac{1}{T}\int_0^T b_{13}(t)\sin(n\omega_{13}t)dt = -j\frac{\delta_n}{2} \qquad \text{(G-5)}$$

since $b_{13}(-t) = -b_{13}(t)$. From Eq. (G-5) it is also seen that $\beta_{-n} = -\beta_n$, so that $\alpha_p(\tau_{ms})$ is

$$\alpha_p(\tau_{ms}) = \frac{4}{\pi}e^{-jp\omega_{13}\tau_{ms}}\left(\frac{1}{4}\right)\sum_{q=0}^{\infty}\frac{1}{(2q+1)}$$

$$\times\left[\beta_{\left[(2q+1)\frac{\omega_k}{\omega_{13}}-p\right]}e^{j(2q+1)\omega_k\tau_{ms}} + \beta_{\left[(2q+1)\frac{\omega_k}{\omega_{13}}+p\right]}e^{-j(2q+1)\omega_k\tau_{ms}}\right] \qquad \text{(G-6)}$$

and $\alpha_p(\tau_{ms})\alpha_{-p}(\tau_{ms}) = \alpha_p(\tau'_{ms})\alpha^*_p(\tau_{ms})$ is

$$\alpha_p(\tau_{ms})\alpha_{-p}(\tau_{ms}) = \frac{1}{\pi^2}\sum_{q=0}^{\infty}\sum_{s=0}^{\infty}\frac{1}{(2q+1)}\frac{1}{(2s+1)}$$

$$\times\left\{\left[\beta_{\left[(2q+1)\frac{\omega_k}{\omega_{13}}-p\right]}e^{j(2q+1)\omega_k\tau_{ms}} + \beta_{\left[(2q+1)\frac{\omega_k}{\omega_{13}}+p\right]}e^{-j(2q+1)\omega_k\tau_{ms}}\right]\right.$$

$$\left.\times\left[\beta^*_{\left[(2s+1)\frac{\omega_k}{\omega_{13}}-p\right]}e^{-j(2s+1)\omega_k\tau_{ms}} + \beta^*_{\left[(2s+1)\frac{\omega_k}{\omega_{13}}+p\right]}e^{+j(2s+1)\omega_k\tau_{ms}}\right]\right\}$$

which is

$$\alpha_p(\tau_{ms})\alpha_p^*(\tau_{ms}) = \frac{1}{4}\frac{1}{\pi^2}\sum_{q=0}^{\infty}\sum_{s=0}^{\infty}\frac{1}{(2q+1)}\frac{1}{(2s+1)}$$

$$\times\left\{\left[\left[\delta\left[(2q+1)\frac{\omega_k}{\omega_{13}}-p\right]e^{j(2q+1)\omega_k\tau_{ms}}+\delta\left[(2q+1)\frac{\omega_k}{\omega_{13}}+p\right]e^{-j(2q+1)\omega_k\tau_{ms}}\right]\right.\right.$$

$$\left.\left.\times\left[\delta\left[(2s+1)\frac{\omega_k}{\omega_{13}}-p\right]e^{-j(2s+1)\omega_k\tau_{ms}}+\delta\left[(2s+1)\frac{\omega_k}{\omega_{13}}+p\right]e^{j(2s+1)\omega_k\tau_{ms}}\right]\right\} \quad \text{(G-8)}$$

$$=\frac{1}{4\pi^2}\left\{\left[\left(\delta\left[\frac{\omega_k}{\omega_{13}}-p\right]+\delta\left[\frac{\omega_k}{\omega_{13}}+p\right]\right)^2-4\delta\left[\frac{\omega_k}{\omega_{13}}-p\right]\delta\left[\frac{\omega_k}{\omega_{13}}+p\right]\sin^2(\omega_k\tau_{ms})\right]\right.$$

$$+\frac{2}{3}\left[\left(\delta\left[\frac{3\omega_k}{\omega_{13}}-p\right]\delta\left[\frac{\omega_k}{\omega_{13}}-p\right]+\delta\left[\frac{3\omega_k}{\omega_{13}}+p\right]\delta\left[\frac{\omega_k}{\omega_{13}}+p\right]\right)\cos(2\omega_k\tau_{ms})\right.$$

$$\left.+\left(\delta\left[\frac{3\omega_k}{\omega_{13}}-p\right]\delta\left[\frac{\omega_k}{\omega_{13}}+p\right]+\delta\left[\frac{3\omega_k}{\omega_{13}}+p\right]\delta\left[\frac{\omega_k}{\omega_{13}}-p\right]\right)\cos(4\omega_k\tau_{ms})\right]$$

$$\left.+\frac{1}{9}\left[\left(\delta\left[\frac{3\omega_k}{\omega_{13}}-p\right]+\delta\left[\frac{3\omega_k}{\omega_{13}}+p\right]\right)^2-4\delta\left[\frac{3\omega_k}{\omega_{13}}-p\right]\delta\left[\frac{3\omega_k}{\omega_{13}}+p\right]\sin^2(3\omega_k\tau_{ms})\right]+\cdots\right\} \quad \text{(G-9)}$$

The dominant contribution to $\alpha_p(\tau_{ms})\alpha_p^*(\tau_{ms})$ comes from the $q = 0$, $s = 0$ term. This is the only term which will be considered. From Eq. (G-5),

$$\delta\left[\frac{\omega_k}{\omega_{13}} \pm p\right] = \frac{2}{T}\int_0^T b_{13}(t)\sin\left[\omega_k t \pm p\omega_{13}t\right]dt$$

$$= \frac{4}{T}\int_0^{T/2} b_{13}(t)\sin\left[\omega_k t \pm p\omega_{13}t\right]dt \qquad \text{(G-10)}$$

since $b_{13}(-t) = -b_{13}(t)$.

By utilizing the relationships

$$b_{13}(t) = \sum_{n=1}^{\infty} \delta_n \sin[n\omega_{13}t] \qquad \text{(G-11)}$$

and

$$b'_{13}(t) = \sum_{n=1}^{\infty} \delta_n (n\omega_{13})\cos[n\omega_{13}t]$$

Eq. (G-10) may be written

$$\delta\left[\frac{\omega_k}{\omega_{13}} \pm p\right] = \frac{4}{\left[\frac{\omega_k}{\omega_{13}} \pm p\right]\omega_{13}T}\int_0^{T/2} b'_{13}(t)\cos[\omega_k t \pm p\omega_{13}t]dt \qquad \text{(G-12)}$$

$$= \frac{2}{\pi}\frac{1}{\left[\frac{\omega_k}{\omega_{13}} \pm p\right]}\left\{\int_0^{T/2} b'_{13}(t)\cos[p\omega_{13}t]dt\right.$$

$$\left. \mp \int_0^{T/2} b'_{13}(t)\sin[\omega_k t]\sin[p\omega_{13}t]dt\right\} \qquad \text{(G-13)}$$

This is convenient because $b'_{13}(t)$ consists only of impulses of areas + or - 2 at the zero-crossings of $b_{13}(t)$, and this greatly simplifies the evaluation of the integrals in Eq. (G-13). The sum

$$\left(\delta\left[\frac{\omega_k}{\omega_{13}} - p\right] + \delta\left[\frac{\omega_k}{\omega_{13}} + p\right]\right) = \frac{4}{\pi}\,\frac{1}{\left[\frac{\omega_k}{\omega_{13}} \pm p\right]}\int_0^{T/2} b'_{13}(t)\cos[\omega_k t]\cos[p\omega_{13}t]\,dt \qquad \text{(G-14)}$$

For those values of k less than about 4, the above is quite negligible because ω_k/ω_{13} is equal to or greater than 256, and the integral is much smaller than that. For values of k above about 8, $\sin^2(\omega_k \tau_{ms})$ is quite small for the values of τ_{ms} which would be encountered in the NAV/SAT application (see Eq. (G-9)), so that for these values of k the dependence of $\alpha_p(\tau_{ms})\alpha_p^*(\tau_{ms})$ on τ_{ms} is essentially negligible. The largest values of Eq. (G-14) occurs for values of k and p for which $[\omega_k/\omega_{13} \pm p]$ is a small integer. Since only small integer values of p are of interest, the values of k for which $[\omega_k/\omega_{13} \pm p]$ is small are approximately k = 9, 10, 11, and 12. Since $\alpha_p \alpha_p^*(p\neq 0)$ is negligible for all but the largest values of k, only the values of $(P_c)_k$ for these k are affected by the terms involving $\alpha_p \alpha_p^*(p\neq 0)$. Since the effects of these few values of $(P_c)_k$ are small, the total effect on $(P_c)_T$ may be assumed to be quite negligible in relation to the effects of the p = 0 component.

Appendix H

TABLES OF FACTORS INVOLVED IN THE COMPUTATION OF THE PROBABILITY OF CORRECT BINOR ACQUISITION, $(P_c)_T$

Table H.1 Factors in f_k Which are Independent of k

Situation	$J_o(a_{ms})$	$e^{-\frac{1}{2}\sigma_{cn}^2\left(1+\left(\frac{\sigma_{cd}^2}{\sigma_{cn}^2}\right)_{max.}\right)}$	$\left[1+\frac{\langle n_k^2\rangle_d}{\sigma^2}\right]_{max}^{-\frac{1}{2}}$
1	0.984	0.9582	0.8826
2	0.984	0.9786	1.0000
3	1.000	0.9745	0.9357
4	0.984	0.9582	0.8826

Table H.2 Factors in f_k Which are Dependent on k

Situation	$(\chi_k)_{max}-\epsilon_k\Gamma(\sigma_{c\ell})$						
	k=1	2	3	4	5	6	7-12
1	0.9210	0.9636	0.9855	0.9953	0.9987	0.9999	1.0000
2	0.9255	0.9660	0.9865	0.9955	0.9988	0.9999	1.0000
3	0.9242	0.9655	0.9862	0.9955	0.9988	0.9999	1.0000
4	0.9210	0.9636	0.9855	0.9953	0.9987	0.9999	1.0000

Table H. 2 (Continued)

Situation $\epsilon_k \frac{1}{2} a_{ms}^2 \left(\frac{5}{\sqrt{2}}\right)^2 e^{\left(\frac{5\sigma_{c\ell}}{\sqrt{2}}\right)^2} \frac{1}{2}\left[1 - \text{erf}\left(\frac{5\sigma_{c\ell}}{\sqrt{2}} - \frac{\ell n 2}{\sqrt{2}\, 5\sigma_{c\ell}}\right)\right]$

	k=1	2	3	4	5	6	7-12
1	0.0137	0.0062	0.0025	0.0008	0.0002	0.0000	0
2	0.0148	0.0067	0.0027	0.0009	0.0002	0.0000	0
3	0	0	0	0	0	0	0
4	0.0137	0.0062	0.0025	0.0008	0.0002	0.0000	0

Situation $E_{\phi_{c\ell}}\left(\chi_k(t_o - \phi_{c\ell}/\omega_{c\ell})\right) \approx \left(\chi_k\right)_{max} - \epsilon_k \Gamma(\sigma_{c\ell}) - \left(\epsilon_k \frac{1}{2} a_{ms}^2 \left(\frac{5}{\sqrt{2}}\right)^2 e^{\left(\frac{5_{c\ell}}{\sqrt{2}}\right)^2} \times \frac{1}{2}\left[1 - \text{erf}\left(\frac{5\sigma_{c\ell}}{\sqrt{2}} - \frac{\ell n 2}{\sqrt{2}\, 5\sigma_{c\ell}}\right)\right]\right)$

	k=1	2	3	4	5	6	7-12
1	0.9073	0.9574	0.9830	0.9945	0.9985	0.9999	1.000
2	0.9107	0.9593	0.9838	0.9946	0.9986	0.9999	1.000
3	0.9242	0.9655	0.9862	0.9955	0.9988	0.9999	1.000
4	0.9073	0.9574	0.9830	0.9945	0.9985	0.9999	1.000

Table H.3 Factors in $\left(P_c\right)_k$

Situation	f_k ($\cos \phi_{ct}$ is between 0.989 and 1.0 for $\lvert \ddot{r}/g \rvert < 1$, so it is assumed approximately equal to 1.)						
	k=1	2	3	4	5	6	7-12
1	0.7550	0.7967	0.8180	0.8276	0.8309	0.8321	0.8322
2	0.8770	0.9238	0.9474	0.9578	0.9616	0.9629	0.9630
3	0.8428	0.8804	0.8993	0.9078	0.9108	0.9118	0.9119
4	0.7550	0.7967	0.8180	0.8276	0.8309	0.8321	0.8322

Situation	$\left(\frac{\mu}{\Sigma \sigma}\right) f_k$						
	k=1	2	3	4	5	6	7-12
1	2.144	2.263	2.323	2.350	2.360	2.363	2.363
2	2.491	2.624	2.691	2.720	2.731	2.735	2.735
3	2.394	2.500	2.526	2.578	2.587	2.590	2.590
4	2.397	2.530	2.597	2.627	2.639	2.642	2.642

Table H.3 (Continued)

Situation $\frac{1}{2}\left[1 + \operatorname{erf}\left(\frac{\mu}{\sqrt{2}\,\sigma} f_k\right)\right]$

	k=1	2	3	4	5	6	7-12
1	0.998786	0.999314	0.999490	0.999555	0.999577	0.999584	0.999584
2	0.999786	0.999897	0.999929	0.999940	0.999944	0.999945	0.999945
3	0.999645	0.999796	0.999823	0.999867	0.999873	0.999875	0.999875
4	0.999650	0.999827	0.999880	0.999898	0.999905	0.999907	0.999907

Situation $\frac{1}{2}\left(\frac{1}{2} a_{ms}^2\right)\left(\frac{\mu}{\sqrt{2}\,\sigma} f_k\right)^3 \frac{2}{\sqrt{\pi}} e^{-\left(\frac{\mu}{\sqrt{2}\,\sigma} f_k\right)^2} \frac{1}{g_k^2}$

	k=1	2	3	4	5	6	7-12
1	0.002395	0.001497	0.001167	0.001040	0.000997	0.000984	0.000984
2	0.000716	0.000382	0.000274	0.000237	0.000224	0.000220	0.000220
3	0	0	0	0	0	0	0
4	0.001061	0.000582	0.00424	0.000366	0.000346	0.000340	0.000340

Table H.4 Conditional Probabilities $\left(P_c\right)_k$

Situation	$\left(P_c\right)_k$						
	k=1	2	3	4	5	6	7-12
1	0.996391	0.997817	0.998323	0.998515	0.998580	0.998600	0.998600
2	0.999070	0.999515	0.999655	0.999703	0.999720	0.999725	0.999725
3	0.999645	0.999796	0.999823	0.999867	0.999873	0.999875	0.999875
4	0.998589	0.999245	0.999456	0.999532	0.999559	0.999567	0.999567

Table H.5 Total Average Probability of Correct BINOR Acquisition

Situation	$\left(P_c\right)_T = \prod_{k=1}^{12} \left(P_c\right)_k$
1	0.980 or 98.0%
2	0.996 or 99.6%

Appendix I

EXPANSION of cos ($\beta_2 b(t)$ and sin ($\beta_2 b(t)$)

The expansion of

$$\cos\left(\beta_2\, b(t)\right) = \cos\left[\frac{\beta_2}{4} \quad b_1(t)+b_2(t)+b_3(t)+b_4(t)\right] \tag{I. 1}$$

where

$b_1(t)$, $b_2(t)$, $b_3(t)$ and $b_4(t)$ are unity amplitude square waves i. e.,

$b_i(t) = \pm 1$ and β_2 is the maximum deviation.

$$\cos\left[\frac{\beta_2}{4}\left(b_1(t)+b_2(t)+b_3(t)+b_4(t)\right)\right] =$$

$$\cos\left[\frac{\beta_2}{4}\left(b_1(t)+b_2(t)\right)\right] \cos\left[\frac{\beta_2}{4}\left(b_3(t)+b_4(t)\right)\right]$$

$$- \sin\left[\frac{\beta_2}{4}\left(b_1(t)+b_2(t)\right)\right] \left[\sin\frac{\beta_2}{4}\left(b_3(t)+b_4(t)\right)\right]$$

$$= \left\{\cos\left[\frac{\beta_2}{4}\, b_1(t)\right] \cos\left[\frac{\beta_2}{4}\, b_2(t)\right] - \sin\left[\frac{\beta_2}{4}\, b_1(t)\right] \sin\left[\frac{\beta_2}{4}\, b_2(t)\right]\right\}$$

$$\times \left\{\cos\left[\frac{\beta_2}{4}\, b_3(t)\right] \cos\left[\frac{\beta_2}{4}\, b_4(t)\right] - \sin\left[\frac{\beta_2}{4}\, b_3(t)\right] \sin\left[\frac{\beta_2}{4}\, b_4(t)\right]\right\}$$

$$- \left\{\sin\left[\frac{\beta_2}{4}\, b_1(t)\right] \cos\left[\frac{\beta_2}{4}\, b_2(t)\right] + \cos\left[\frac{\beta_2}{4}\, b_1(t)\right] \sin\left[\frac{\beta_2}{4}\, b_2(t)\right]\right\}$$

$$\times \left\{\sin\left[\frac{\beta_2}{4}\, b_3(t)\right] \cos\left[\frac{\beta_2}{4}\, b_4(t)\right] + \cos\left[\frac{\beta_2}{4}\, b_3(t)\right] \sin\left[\frac{\beta_2}{4}\, b_4(t)\right]\right\}$$

(I. 2)

collecting terms and recognizing that $b_i(t) = \pm 1$, yields

$$\cos^4 \frac{\beta_2}{4} - \left[b_1(t)b_2(t)+b_1(t)b_3(t)+b_2(t)b_4(t)+b_2(t)b_3(t)+b_2(t)b_4(t) + b_3(t)b_4(t) \right] \cos^2 \frac{\beta_2}{4} \sin^2 \frac{\beta_2}{4} + b_1(t)b_2(t)b_3(t)b_4(t) \sin^4 \frac{\beta_2}{4}$$

$$\approx \cos^4 \frac{\beta_2}{4} \approx 1 \qquad \text{(I. 3)}$$

for $\beta_2/4 \ll 1$

The expansion of

$$\sin\left(\beta_2\, b(t)\right) = \sin\left[\frac{\beta_2}{4} \left(b_1(t)+b_2(t)+b_3(t)+b_4(t) \right) \right] \qquad \text{(I. 4)}$$

is performed similarly

$$\sin\left[\frac{\beta_2}{4} \left(b_1(t)+b_2(t)+b_3(t)+b_4(t) \right) \right] =$$

$$\sin\left[\frac{\beta_2}{4} \left(b_1(t)+b_2(t) \right)\right] \cos\left[\left(\frac{\beta_2}{4} \left(b_3(t)+b_4(t)\right)\right)\right] \qquad \text{(I. 5)}$$

$$+ \cos\left[\left(\frac{\beta_2}{4} \; b_1(t)+b_2(t)\right)\right] \sin\left[\left(\frac{\beta_2}{4} \; b_3(t)+b_4(t)\right)\right]$$

$$= \left\{ \sin\left[\frac{\beta_2}{4} b_1(t)\right] \cos\left[\frac{\beta_2}{4} \, b_2(t)\right] + \cos\left[\frac{\beta_2}{4} \, b_1(t)\right] \sin\left[\frac{\beta_2}{4} \, b_2(t)\right] \right\}$$

$$\times \left\{ \cos\left[\frac{\beta_2}{4} \, b_3(t)\right] \cos\left[\frac{\beta_2}{4} \, b_4(t)\right] - \sin\left[\frac{\beta_2}{4} \, b_3(t)\right] \sin\left[\frac{\beta_2}{4} \, b_4(t)\right] \right\}$$

$$+ \left\{ \cos\left[\frac{\beta_2}{4} \, b_1(t)\right] \cos\left[\frac{\beta_2}{4} \, b_2(t)\right] - \sin\left[\frac{\beta_2}{4} \, b_1(t)\right] \sin\left[\frac{\beta_2}{4} b_2(t)\right] \right\}$$

$$\times \left\{ \sin\left[\frac{\beta_2}{4} \, b_3(t)\right] \cos\left[\frac{\beta_2}{4} \, b_4(t)\right] + \cos\left[\frac{\beta_2}{4} \, b_3(t)\right] \sin\left[\frac{\beta_2}{4} \, b_4(t)\right] \right\}$$

collecting terms and recognizing that $b_i(t) = \pm 1$, yields

$$\left(b_1(t)+b_2(t)+b_3(t)+b_4(t) \right) \sin\frac{\beta_2}{4} \cos^3 \frac{\beta_2}{4}$$

$$-\left(b_1(t)b_3(t)b_4(t)+b_2(t)b_3(t)b_4(t)+b_1(t)b_2(t)b_3(t) \right.$$

$$\left. +b_1(t)b_2(t)b_4(t) \right) \sin^3 \frac{\beta_2}{4} \cos \frac{\beta_2}{4} \qquad \text{(I. 6)}$$

$$\approx \left[\sum_i b_i(t) \right] \sin \frac{\beta_2}{4}$$

for $\beta_2/4 \ll 1$

Appendix J

COMPARISON OF A 3-TONE BINOR CODE WITH A 3-TONE LINEAR SUM

For the 3 tone case, equal subcarrier amplitudes are achieved when

$$\cos \beta_b = \cos^3 \frac{\beta_2}{3} \tag{J-1}$$

but from Equation 45 modified for 3 tones

$$\tan \frac{\beta_2}{3} = .221 \tag{J-2}$$

or

$$\frac{\beta_2}{3} = 12.5^\circ \tag{J-3}$$

as before substituting (J-3) into (J-1) yields

$$\cos \beta_b = .93$$

and

$$\beta_b = 21.5^\circ \tag{J-4}$$

Assuming optimum demodulation of the BINOR code, the BINOR system performance will be superior if

$$\rho_3 \tan \beta_b \geq \frac{4}{\pi\sqrt{2}} \sin \frac{\beta_2}{3} \cos^2 \frac{\beta_2}{3} \tag{J-5}$$

where $\rho_2 = \frac{1}{2}$ is the BINOR coefficient. Substituting from (J-1) and noting that

$$\rho_3 \tan \beta_b = (.5)(.3939) = .197$$

and (J-6)

$$\frac{4}{\pi\sqrt{2}} \tan \frac{\beta_2}{3} = (.9)(.221) = .1989$$

it is concluded that the BINOR is not superior in performance to the sum of square waves for this case.

Appendix K

COMPUTER SIMULATION PROGRAM

```
C      PHASE LOCK LOOP SIMULATION G-106
C
C
       TYPE 20
 20    FORMAT(1H/,'INPUT THE FOLLOWING PARAMETERS'/
      1' N-ZERO,OMEGA,SINT,BDWIDTH,DIV N,TGC,TGD,A,VCO',/)
       ACCEPT 12,STDIV,OMOFF,FO,BW,EN,TGC,TGD,A,TI
 12    FORMAT (9F)
       THETA=0
       IRANIT=30883623
       CALL GAUSS(IRANIT,STDIV,0.0,RANDOM)
       WOFT=0
       FOO=O
       A3=0
       B3=1.0
       TI=TI*FO
       PHI2=0
       PHO=0
       DPHIN=0
       INDEX=0
       T2=TI
       ENP=0
       ENM=0
       ATCOS=0
       ATSIN=0
       TYPE 23
 23    FORMAT (1H ,'STEP',2X,'VCO FREQ',4X,'VCO OUTPUT',2X,
      1'DIV OUTPUT',2X,'N/PLUS',6X,'N/MINUS')
       STDIV=SQRT(STDIV/FO)
       BW=1.0-EXP(-BW*FO)
 1     THETA=(-T2+DPHIN+THETA)
       THETA=AMOD(THETA,6.28318)
       IF(THETA-3.14159) 10,5,5
 5     THETA=THETA-6.28318
       GO TO 15
 10    IF(THETA+3.14159) 11,15,15
 11    THETA=THETA+6.28318
 15    CONTINUE
       TSIN=SIN(THETA)
       TCOS=COS(THETA)
       ATCOS=(TCOS-ATCOS)*A+ATCOS
       ATSIN=(TSIN-ATSIN)*A+ATSIN
       CALL GAUSS(IRANIT,STDIV,0.0,RANDOM)
       ACOMP=TSIN+RANDOM
       CALL GAUSS(IRANIT,STDIV,0.0,RANDOM)
       BCOMP=TCOS+RANDOM
       WOFT=OMOFF*FO+WOFT
       COWT=COS(WOFT)
       SIWT=SIN(WOFT)
       A2COMP=ACOMP*COWT+BCOMP*SIWT
       B2COMP=BCOMP*COWT-ACOMP*SIWT
```

```
      A3=(A2COMP-A3)*BW+A3
      B3=(B2COMP-B3)*BW+B3
      A4=A3*COWT-B3*SIWT
      B4=B3*COWT+A3*SIWT
      PHI=ATAN2(A4,B4)
      IF(ABS(PHI-PHI2)-3.1415926) 100,100,101
101   IF(PHI-PHI2) 102,100,103
102   PHO=PHO+6.28318
      GO TO 100
103   PHO=PHO-6.28318
100   PHI2=PHI
      PHA=(PHI+PHO)/EN
      PHA=AMOD(PHA,6.28318)
      IF(PHA-3.14159) 105,104,104
104   PHA=PHA-6.28318
      PHO=PHO-6.28318*EN
      GO TO 107
105   IF(PHA+3.14159) 106,107,107
106   PHA=PHA+6.28318
      PHO=PHO+6.28318*EN
107   PHA=PHA*EN
      GOO=PHA-FOO
      IF(GOO-3.14159*EN) 25,30,30
30    GOO=GOO-6.28318*EN
      GO TO 35
25    IF (GOO+3.14159*EN) 26,35,35
26    GOO=GOO+6.28318*EN
35    IF(GOO-AMOD(GOO,6.28318)) 36,39,38
36    ENM=ENM+1.0
      GO TO 37
38    ENP=ENP+1.0
37    FOO=PHA-AMOD(PHA,6.28318)
39    CONTINUE
      T1=(PHA*TGC)+T1
      T2=T1+PHA*TGD
      LIP=MOD(INDEX,100)
      IF(LIP .EQ. 0) GO TO 500
      INDEX=INDEX+1
      GO TO 1
500   T3=T2/FO
      PHA=PHA/EN
      TYPE 501,INDEX,T3,THETA,PHA,ENP,ENM
501   FORMAT(1H ,I4,5(2X,1PE10.3))
      INDEX=INDEX+1
      IF(((ATCOS*ATCOS)+(ATSIN*ATSIN)) .GT. 0.6) GO TO 50
      GO TO 1
50    TYPE 502
502   FORMAT(1H-,'HANDOFF TO TRACK')
      END
```

Appendix L

NEW TECHNOLOGY APPENDIX

After a diligent review of the work performed under this contract, no new innovation, discovery, improvement or invention was made.